

December 2017

# Design and Implementation of a Multi-port Solid State Transformer for Flexible Der Integration

Mohammad Rashidi

*University of Wisconsin-Milwaukee*

Follow this and additional works at: <https://dc.uwm.edu/etd>



Part of the [Electrical and Electronics Commons](#), and the [Oil, Gas, and Energy Commons](#)

---

## Recommended Citation

Rashidi, Mohammad, "Design and Implementation of a Multi-port Solid State Transformer for Flexible Der Integration" (2017).  
*Theses and Dissertations*. 1681.  
<https://dc.uwm.edu/etd/1681>

This Dissertation is brought to you for free and open access by UWM Digital Commons. It has been accepted for inclusion in Theses and Dissertations by an authorized administrator of UWM Digital Commons. For more information, please contact [open-access@uwm.edu](mailto:open-access@uwm.edu).

# DESIGN AND IMPLEMENTATION OF A MILTI-PORT SOLID STATE TRANSFORMRE FOR FLEXIBLE DER INTEGRATION

by

Mohammad Rashidi

A Dissertation Submitted in  
Partial Fulfillment of the  
Requirements for the Degree of  
Doctor of Philosophy  
in Engineering

at

The University of Wisconsin-Milwaukee

December 2017

# ABSTRACT

## DESIGN AND IMPLEMENTATION OF A MULTI-PORT SOLID STATE TRANSFORMER FOR FLEXIBLE DER INTEGRATION

by

Mohammad Rashidi

The University of Wisconsin-Milwaukee, 2017  
Under the Supervision of Professor Adel Nasiri

Conventional power system includes four major sections, bulk generation, transmission network, distribution network, and loads. The main converter in the conventional electric grid is the low-frequency passive transformer providing galvanic isolation and voltage regulation for various voltage zones. In this configuration, small-scale renewable energy resources are connected to the power system at low voltage zones or inside microgrids.

Recent developments in the design of power electronic elements with higher voltage and power ratings and medium/high frequency enable making use of solid state transformer at different voltage levels in the distribution system and microgrid design. In this work, the concept of a Multi-Port Solid State Transformer (MPSST) for distribution network application is introduced. MPSST provides a compact, integrated and galvanically isolated multi-port node for microgrid and distribution applications and reduces the number and size of the converters in the concept of efficient smart distribution systems.

A new architecture for distribution systems integrating distributed generation (DG) at different voltage zones using MPSST is proposed, studied and simulated. The developed concept interconnects different voltage types and levels using one compact converter with a centralized

control logic. Also, a general method is developed and mathematically analyzed to provide active and reactive power support using the local alternative power sources through MPSST.

MPSST is a combination of high-frequency power electronic converters and a multi-winding high-frequency transformer. The total size of the MPSST is dramatically smaller than the conventional transformers with the same voltage and power rating. MPSST also enables online measurement and data collection and active control of the parameters at all connected ports. A two-layer control technique, which is a combination of duty cycle control and a modified phase shift control is used to regulate the voltage and power flow of the different ports. Since the converter has several independent and dependent variables, a transfer matrix between variables of the converter is calculated and used in system control.

Finally, the implementation process of the converter including, component selection, modeling, software development, and transformer design is presented, and the first prototype of the MPSST is developed and tested in the lab. Chapter five includes the hardware test results and the discussion and comparison of the results with the design expectations.

*Dedicated to my MOTHER for her endless love and support*

© Copyright by Mohammad Rashidi, 2017  
All Rights Reserved

# TABLE OF CONTENTS

<b>ABSTRACT.....</b>	<b>II</b>
<b>TABLE OF CONTENTS .....</b>	<b>VI</b>
<b>LIST OF FIGURES .....</b>	<b>IX</b>
<b>LIST OF TABLES .....</b>	<b>XIII</b>
<b>LIST OF ACRONYMS .....</b>	<b>XIV</b>
<b>ACKNOWLEDGMENTS .....</b>	<b>XVI</b>
<b>CHAPTER 1 INTRODUCTION.....</b>	<b>1</b>
1.1 Background .....	5
1.2 Problem Statement .....	8
<b>CHAPTER 2 MULTI PORT SOLID STATE TRANSFORMER .....</b>	<b>10</b>
2.1 Solid State Transformer .....	10
2.2 Analytical study of Multiport Solid State Transformer .....	13
2.2.1 Voltage polarity, Current direction and Power flow in MPSST .....	16
2.3 Advantages of MPSST in Comparison to the Regular SST.....	18
2.3.1 DC Bus Fault Analysis in a System Including MPSST .....	20
<b>CHAPTER 3 FUTURE CONFIGURATION OF ACTIVE EFFICIENT POWER</b>	
<b>DISTRIBUTION SYSTEM.....</b>	<b>26</b>
3.1 Conventional Power Distribution.....	26
3.2 SST Based Zonal Distribution System.....	29
3.3 MPSST Based Zonal Distribution System .....	33
3.4 MPSST Application for Grid Support.....	34

- 3.4.1 Active Power Management in a Power Network Which includes MPSST .. 35
- 3.4.2 Volt-VAR Control for Frequency Support in Electricity Grid including MPSST

44

**CHAPTER 4 MATHEMATICAL MODELING AND CONTROL OF MPSST ..... 51**

- 4.1 Power Sharing Control Logic..... 51
- 4.2 Multilayer Control for Voltage and Power Regulation in MPSST ..... 52
  - 4.2.1 Primary control..... 52
  - 4.2.2 Secondary control..... 54
  - 4.2.3 4-Port black-box method for calculation of MPSST transfer matrix ..... 57
- 4.3 State Space Modeling of MPSST..... 60
  - 4.3.1 Modeling in dq reference frame ..... 68

**CHAPTER 5 IMPLEMENTATION AND TESTING OF MPSST ..... 72**

- 5.1 Simulation and programming..... 74
- 5.2 Component Selection and Design Consideration..... 78
- IXYS DSEI 2x 61-10B X2 ..... 81
- 5.3 Transformer Design Consideration and Implementation ..... 82
  - 5.3.1 Core Material Selection and Design..... 82
  - 5.3.2 Cable Selection..... 85
  - 5.3.3 Winding Placement ..... 85
- 5.4 Running and Test Results..... 90
  - 5.4.1 Hardware Test Results ..... 92

**CHAPTER 6 CONCLUSION..... 96**

**REFERENCES..... 99**



<b>APPENDIX A PPM METHOD M-FILE CODE .....</b>	<b>110</b>
<b>APPENDIX B TRANSFER MATRIX ELEMENTS.....</b>	<b>112</b>
<b>CURRICULUM VITAE.....</b>	<b>114</b>

# LIST OF FIGURES

Figure 1-1. MPSST application for distribution system .....	8
Figure 2-1. AC-AC solid state configuration.....	10
Figure 2-2. Series resonant SST configuration [13] .....	13
Figure 2-3. General structure of a microgrid .....	15
Figure 2-4. Configuration of the Four Port SST .....	16
Figure 2-5 Standard Voltage polarity and current direction in the four port configuration .....	17
Figure 2-6. Feeding multiple loads with (a) SST based system and (b) MPSST bases system....	19
Figure 2-7 Power flow control in a system with multiple loads components (a) SST based system and (b) MPSST bases system .....	20
Figure 2-8 Line to Line fault on DC bus [51].....	21
Figure 2-9 Line to Ground fault on DC bus.....	22
Figure 2-10. DC side fault on a port with active H-Bridge .....	24
Figure 2-11. DC side fault on a port with full bridge diode rectifier .....	24
Figure 3-1. Conventional distribution system.....	28
Figure 3-2. Zonal AC-DC DG based distribution structure based on two port SST application .	30
Figure 3-3.AC DC zonal distribution system based on SST [2].....	31
Figure 3-4. Different levels of regulated DC voltage in an AC DC zonal distribution system based on SST, (a) 15kVDC, (b) 1kVDC, (c) 380VDC (d) 24VDC (e) 1kVrms (f) 208Vrms .....	32
Figure 3-5 Zonal AC-DC DG based distribution structure based on four-port SST application .	34
Figure 3-6. Simplified block diagram of the controller based on PPM for power-sharing .....	38

Figure 3-7. Equivalent circuit of MPSST for power-sharing analysis.....	39
Figure 3-8 Phase shift between the output voltages of three active converters and transformer voltage for very light load .....	41
Figure 3-9 Phase shift effect on the power-sharing between different ports and the response of the controller in load power change .....	41
Figure 3-10 Power sharing control of the converters using Phase Shift Control for mode 7 .....	42
Figure 3-11 Power sharing control of the converters using Phase Shift Control for mode 2 .....	42
Figure 3-12. Power sharing control of the converters using Phase Shift Control when the RER port does not generate power.....	43
Figure 3-13. Volt-VAR control Strategy [54].....	46
Figure 3-14. IEEE 14 Bust Test System. ....	47
Figure 3-15. Three-phase RMS voltage at bus #1 .....	49
Figure 3-16. Three-phase RMS voltage at bus #4 .....	49
Figure 3-17. Three-phase RMS voltage at bus #4 .....	50
Figure 3-18. Reactive power curves of the three feeders during transition .....	50
Figure 4-1 General architecture of MPSST control strategy .....	51
Figure 4-2 a) The configuration of an H-Bridge converter b)Duty cycle control for a single phase H-Bridge .....	53
Figure 4-3. Simulation results of applying duty cycle control to regulate DC voltage .....	54
Figure 4-4.Two AC voltage vectors with phase shift .....	55
Figure 4-5. Phase shift control.....	56
Figure 4-6. The general components of a four-port SST to calculate the transfer matrix of MPSST.....	57

Figure 4-7. Equivalent circuit of the internal elements of four-port SST for calculation of transfer matrix.....	58
Figure 4-8. Square shape AC output of each active H-Bridge .....	59
Figure 4-9. The equivalent circuit of general configuration of a four-port SST.....	61
Figure 4-10. Circuit simplifications to optimize the number of states .....	63
Figure 4-11. System step response considering V4 as the output and C=40nF.....	66
Figure 4-12. System step response considering V4 as the output and C=10nF.....	67
Figure 4-13. System step response considering V4 as the output and C=10nF.....	67
Figure 5-1. Design steps for building an isolated PE converter .....	72
Figure 5-2. 2-D design of component placement in the converter box .....	73
Figure 5-3. The control and sensing structure of the MPSST.....	75
Figure 5-4 MPSST interface board.....	76
Figure 5-5. AC/AC solid state transformer.....	77
Figure 5-6. Simulation results of different conversion steps of a solid state transformer .....	78
Figure 5-7. (a)The selected silicon carbide MOSFET module; (b) The selected fast recovery diode module .....	80
Figure 5-8. Core material comparison for HF design [61] .....	84
Figure 5-9. Test cases of MPSST windings placement: (1) Grid (red). (2) DG (blue). (3) ES (green). (4) Load (yellow). .....	87
Fig. 5-10. ANSYS Maxwell 3D simulation of the designed core .....	88
Figure 5-11. Final assembled multi-winding HF transformer .....	90
Figure 5-12. Implementation process of the MPSST.....	91
Figure 5-13. Final assembly of the four port solid state transformer.....	92

Figure 5-14. MPSST experimental result for $D=35\%$ and $f=100$ kHz .....	93
Figure 5-15. MPSST experimental result for $D=50\%$ and $f=100$ kHz .....	93
Figure 5-16. Shifted gate signals .....	94
Figure 5-17. Power flow control using phase shift control.....	94
Figure 5-18. Experimental test results by adding snubber circuit and DC capacitors .....	95

# LIST OF TABLES

Table 1-1. US Electricity generation shares by different fuel types [1] ..... 2

Table 3-1.PPM Modes of Operation..... 36

Table 3-2. Bus voltages during the transition period..... 47

Table 5-1. Selected switch module characteristics ..... 80

Table 5-2.The converter design parameter and components ..... 81

Table 5-3. Flux Density and Frequency Range of The Studied Materials [22], [23], [24], [61].. 84

Table 5-4. Coupling Coefficient between the windings for the different case studies ..... 89

# LIST OF ACRONYMS

<b>AC</b>	Alternating Current
<b>AVS</b>	Zero Voltage Switching
<b>DC</b>	Direct Current
<b>DER</b>	Distributed Energy Resources
<b>DG</b>	Distributed Generation
<b>DOE</b>	department of energy
<b>ES</b>	Energy Storage
<b>ESS</b>	Energy Storage System
<b>EV</b>	Electrical Vehicle
<b>FPGA</b>	Field Programmable Gate Array
<b>HF</b>	High Frequency
<b>IGBT</b>	Insulated-Gate Bipolar Transistor
<b>KVL</b>	Kirchhoff's Voltage Law
<b>KCL</b>	Kirchhoff's Current Law
<b>LF</b>	Low Frequency
<b>LV</b>	Low Voltage
<b>MOSFET</b>	Metal–Oxide–Semiconductor Field-Effect Transistor
<b>MPSST</b>	Multi Port Solid State Transformer
<b>MV</b>	Medium Voltage
<b>PCB</b>	Printed Circuit Board

<b>PPM</b>	Pool of Power Method
<b>PSC</b>	Phase Shift Control
<b>RER</b>	Renewable Energy Resource
<b>SiC</b>	Silicon Carbide
<b>SLR</b>	Series Load Resonant
<b>SoC</b>	State of Charge
<b>SST</b>	Solid State Transformer
<b>VFPSM</b>	Variable Frequency Phase Shift Modulation
<b>ZCS</b>	Zero Current Switching



# ACKNOWLEDGMENTS

I would like to express my sincere gratitude to my mentor and advisor Prof. Adel Nasiri. I thank him for his guidance, encouragement, and supports during the development of this project in the last four years.

I am indebted to my committee members: Prof. Rob Cuzner, Prof. Sevki Demirbas, Prof. Ilya Avdeev and Prof. David Yu. They have provided their insight and suggestions, which are precious to me. Each of the members of my dissertation committee has provided me extensive personal and professional guidance and taught me a great deal about scientific research.

This work is funded by GRAPES NSF I/UCRC. I would like to thank the academic and corporate members of GRAPES for their supports.

I also want to thank Prof. Mehrdad Abdi and Prof. Hesamoddin Sadeghi from Tehran Polytechnic for their support during my undergrad and masters.

I am grateful to all of those with whom I have had the pleasure to work during my Ph.D. project and other related projects; my amazing friends and colleagues in Eaton Corporation and Power Electronics and Electrical Drives Lab at UWM, Dr. Andrew Rockhill, Dr. Antonio Trojillo, Dr. Igor Stamenkovic, Mark Juds, Dr. Peng Wang, Ezana Mekonnon, Abedalsalam Bani-Ahmed, Mohammad Sabbah, and Jason Katcha.

I would like to thank my mother, brother and sisters whose love and guidance are with me in whatever I pursue in my personal and academic life. They are the ultimate role models. Nobody has been more important to me in the pursuit of Ph.D. than the members of my family.

Most importantly, I wish to thank my beloved wife, Fatima. She has been my best friend and great companion through this period in the most positive way.

# CHAPTER 1

## Introduction

The fast industry growth and the move toward electrical vehicles (EV) for transportation during the last decades have increased the demand for energy gradually. Several studies have investigated the relationship between industry growth and EV based transportation in different countries and consumption of electricity [27], [28], [29] which show the direct relationship between these factors. On the other hand, due to the environmental concerns about fossil fuels, a lot of attention has been paid from governments, investors and researchers all around the world to find and expand the new solutions for the world's growing needs for energy resources[3].

One of the solutions to tackle these problems is to use the alternative sources of energy to generate electricity. The technology improvements in utilizing renewable energy resources (RER) has decreased the operational price of RER and made it a compatible with the conventional sources of power. The renewable sources of energy could utilize into the power grid in the large scale as power plants [30] or as a small source of power which is connected directly to the distribution network or utilized in the grid inside the microgrid [4], [30]. Having distributed energy resources (DER) helps the power system by providing power for the increasing demand and improving the survivability of the important loads when they lose their tie to the utility. Also, the transmittance of a portion of energy generation to a position closer to the load by distributing the energy sources in the form of small-scale renewable and/or fuel-based generators decreases the transmission loss [2] and increases the total efficiency of the power system.

Application of sources of energy, especially wind and solar energy have become an important alternative for the conventional fossil fuel based source of electricity generation in the last decades and different countries are planning their future energy policies to rely more on these sources of energy [59].

Table 1-1 shows the US Department of Energy (DOE) prediction of the expansion of electricity generation using different sources by 2030. The table shows that the share of wind and solar energy which are the two biggest potentials and actively utilized alternative sources of power is raising from %6 to %15 by 2030.

Table 1-1. US Electricity generation shares by different fuel types [1]

Fuel Type	2015-Billion kWhr	2015-Percentage	2030-Billion kWhr	2030-Percentage
Nuclear	798	20	798	17
Coal	1355	33	972	21
Natural Gas	1348	33	1702	37
Wind/Solar	227	6	683	15
Other	362	9	443	10

However, there is some complexity for the wide application of DERs in the power grid. One major problem with the wind and solar power generation is the dependency of their output power to the weather situation. In another word, the generated power of the wind turbines and solar power generators change by changing wind speed and radiation of sunshine. This problem affects both programmability and the continuity factors of the RER power generation.

Several works have been done on modeling of wind and sun condition based on the analysis of past collected data and weather prediction [8], [9]. These methods help to improve the predictability factor of the wind and solar energy generation and enable more accurate planning on the power generation capability of these sources of power. To resolve the problem of the large variation of the output power of the wind/solar based power generation systems, they need to be integrated with the energy storages to deliver reliable power to the load [31], [32]. Combining ESS with RERs in the form of hybrid power generation improves the reliability of the DER based power generation and make it a programmable source of power.

The technological developments and research efforts in the field of application of small-scale distributed renewable energy resources (RER), along with the technology expansion in developing high power and efficient energy storage systems (ESS), have reduced the implementation cost the of hybrid renewable generation, and made it a reliable solution for providing electricity for commercial and residential loads.

In the new designs of the power grid, having power electronic converters seems to be an inseparable part of the system for two major reasons. First, the voltage type of the generated power of the majority of DERs is not compatible with the standard power grid, and they include a lot of fluctuations, power electronic converters are needed for voltage conversion to utilize the DERs in the conventional electricity grid. Also, the nature of loads and different components of the distribution system is changing toward the combination of AC and DC loads and smarter components which need power electronic converters to become compatible with the voltage type of the available electricity network.

In the conventional distribution systems, low-frequency transformers (LFT) are the main converters of the system. These transformers are mainly used to isolate voltage zones galvanically and regulate the AC voltage levels to match the voltage between their input and output sides [5]. These passive low-frequency transformers are simple, efficient, and reliable for long time service in the grid [4][6]. However, the main drawback of the conventional transformers is using the relatively large amount of metal for building the core of this type of transformers which consequently, makes their size and weight larger than the other components in the same power rating system. It makes the transportation, installation and maintenance process of these LFTs, complicated and expensive. Also, the conventional passive transformers are not compatible with some of the requirements of the new technologies, such as DC distribution systems, RER, and energy storage which are increasingly being utilized in the power grid [7].

New developments in the design of isolated power electronic components with high-frequency range, and medium/high voltage, and power rating enables the migration from conventional passive LFT as the main converters in the distribution systems to PE based solid state transformers.

Solid state transformer (SST) is a combination of power electronic converters and HF isolation transformer that offers a proper solution to the problems above. Using SST for utilizing DER and smart components in the power system provides galvanic isolation for the components while the total size of the system is minimized as the result of HF design of the isolation transformer. Furthermore, SST provides the regular functionality of the conventional transformers in a zonal distribution system to match the voltage between different zones which makes it a proper

candidate to replace the LFTs and redesign the whole system based on these active transformers. The future design of the distribution system is discussed in chapter 3.

The main drawback of using SST as the isolation transformer between voltage zones in the whole power grid is the need for integration of several PE converters for reconfiguring the whole system which increases the size, cost, failure rate, and control complexity of the system. One solution to tackle the technical problem of having several converters is to combine converters in the form of multi-port solid state transformer (MPSST).

MPSST is a type of SST which uses a multi-winding HF transformer to form a multi-port isolated connection point for different elements in the system. It combines the functionality of several converters in one converter, minimizes the number of components, and increases the power density in the system. The converter uses a centralized controller to regulate the voltages and control the power flow from and to each port.

## **1.1 Background**

Conventionally electricity grid structure includes power plants, transmission and distribution system, and AC loads. This nature of the power system is changing as the result of penetration of distributed energy resources, DC loads and smart components. Also, the whole power grid is moving toward the concept of smart grid which is a system with online monitoring and control and benefits from smart distribution and fault management.

The future configuration of distribution system has discussed in several articles, and different configurations are suggested and studies for the future generation of distribution systems [2]. In [33] the impact of the concept of smart grid on distribution grid is investigated while the growing implementation of the DG in the grid for the case study of Slovenia using statistical

analysis and future prediction numbers. The study in [34] discusses the local installation of energy storage as one of the main requirements of the future structure of the distribution for supporting the local demands. Some other researchers have studied the application of SSTs for the power distribution systems [35]. The common base in all of these designs and studies is having DER utilized in the power system. Higher efficiency, easier installation, and maintenance, survivability of the critical loads and better fault management are the main parameter in the different configurations which are improved in the different articles using software and hardware modification techniques.

Due to the vast capability of the PE converters in interfacing between components and voltage zones in the power system, and the controllability advantages for the system, power electronic converters are considered as the enabler components for the promised smart and efficient future distribution systems.

Also, one important requirement for connecting two voltage zones in any distribution system design is galvanic isolation between voltage zones. The transformer is the component which provides galvanic isolation in the available distribution by transferring power between two voltage zones through the electromagnetic field of the transformer without electrical connection.

Solid state transformer includes a combination of power electronic converters and high or medium-frequency transformers. Having SST in the distribution system, different voltage zones are galvanically isolated using the high-frequency transformer of the SST configuration which reduces the size and weight of the converter dramatically in comparison to the conventional transformers with the same voltage and power rating[10][11]. Also, the power electronic stages of SST enables online monitoring of the system.

There are two major factors which drive the research efforts on solid state transformers. The growing need for compact, controllable converters to utilize distributed energy resources within the electricity grid and the development of high power and high-frequency power electronic switches, which allows feeding the isolation transformer with very high frequency to optimize the size of converter [4][3][7].

The introduced configuration in this study is a four-port SST which is capable of utilizing hybrid RER/ESS in a system with two zones of voltage using one compact converter.

Figure 1-1 shows the topology of a four-port SST configuration. All of the ports in this topology are DC, and the shown components in the figure are the HF stages of the topology. The stages of this converter at each port could be extended by adding inverters for AC connection. The high-frequency stages of the converter include HF inverters (rectifiers) and an HF transformer. Multiport SST (MPSST) is a type of SST with more than two ports. The four-port MPSST is designed to utilize DG and ES in a system with load and grid connection or in a zonal distribution using a one controllable converter.

The multiport isolated power electronic topologies have been discussed and used for different application from traction machines [38], [55], [57] to the hybrid DG applications. In [36] for port SST topology is introduced based on a quad-active-bridge (QAB) to be used for utilizing DER in the grid. All of the converters of the ports in this topology are controllable switch based bi-directional PE converters, and the article derives a state space model for controlling the converter parameters. A three port SST with the capability of having a port to integrate energy storage directly into the power network for supporting the power flow is discussed in [37]. Also,



MPSST topology has been used vastly for electric traction application with MV busbar at the input and motor loads at the output side[38].

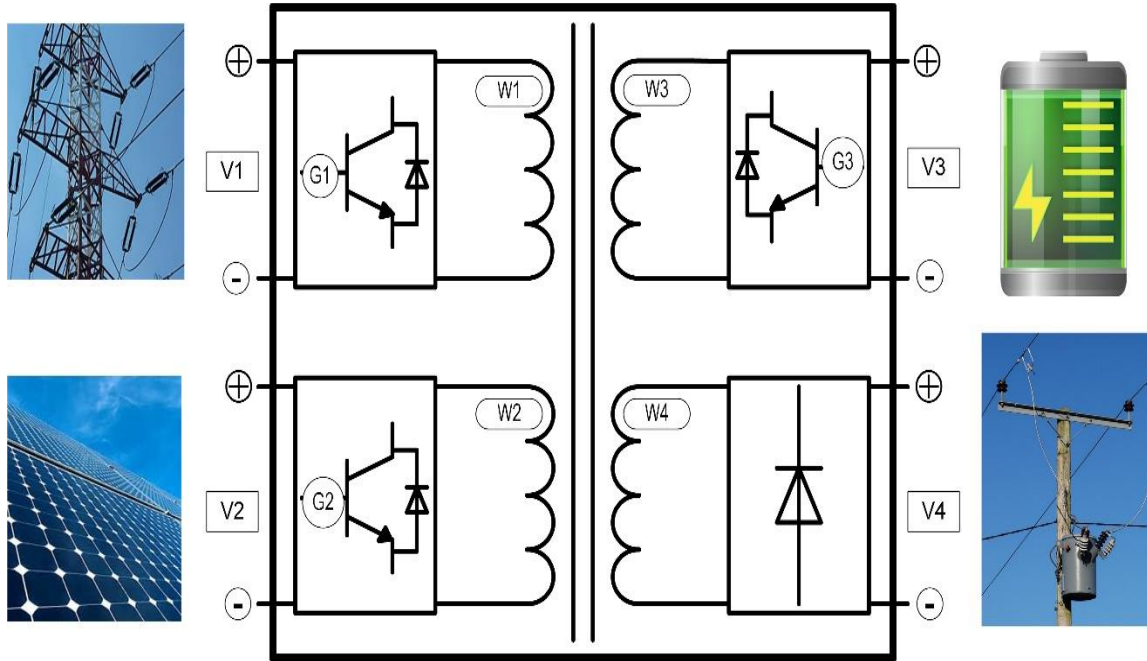


Figure 1-1. MPSST application for distribution system

MPSST offers several adjustable ports for the components to connect and exchange power with each other. The MPSST comprises a multi-winding HF transformer to isolate the ports galvanically. Using MPSST enables higher efficiency and reliable centralized control for all of the connected components in the system.

## 1.2 Problem Statement

The focus of this research is on simulation, modeling, design, and implementation of a Multi-Port Solid State Transformer (MPSST). Also, application of this converter in the new configurations of the distribution system for grid supporting is discussed and simulated.

The whole process of implementation of an isolated PE converter for the design of the MPSST of this project is illustrated. There are several complications in the design and running process of an HF multi-port converter.

A new control method is used to specify the optimal operation point for multiple converters of the system and regulate the expected parameters of the system based on the status of the other parameters of this multi-input, multi-output system.

# CHAPTER 2

## Multiport Solid State Transformer

Multi-port solid state transformer is a type of power electronic converter which uses multi-winding HF transformer to form a modular, isolated, adjustable and compact converter to utilize multiple elements in the power grid[60]. The converter could be used in the structure of power system as the isolation transformer between voltage zones, or it could be used to feed a single load from hybrid DER and grid using one converter[58].

### 2.1 Solid State Transformer

The concept of solid state transformer in different forms has been studied by several articles since the early 80s [12][13][14][39]. In this concept, a combination of power electronic converters and high or medium-frequency transformers form a controllable isolated converter.

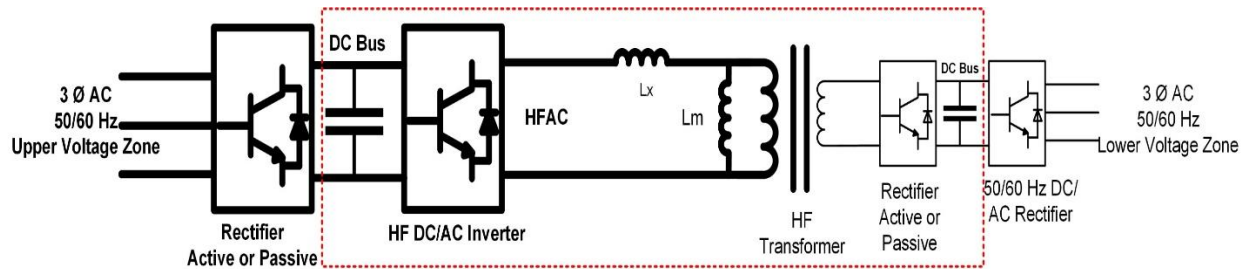


Figure 2-1. AC-AC solid state configuration

Besides the normal functionalities of the conventional transformers [50] like galvanic isolation and voltage matching between two AC voltage zones, the power electronic based transformer benefits the power distribution system by enabling active monitoring and control on the voltage and current flow of the ports of the SST. Also, due to the medium or high-frequency design of the transformer of the SST, the size of the converter is smaller than the conventional LF

isolated converters with the same voltage and power rating. This size and weight reduction which is enabled by involving power electronic converters to transfer power in high-frequency AC is the key motivation for designing high-frequency isolated power electronic converters. The relationship between transformer dimension and the characteristics of the core material and its nominal power can be calculated using equation (2-1)[10].

$$W_a A_c = \left( \frac{\Sigma S \times 10^4}{K_f K_{cu} K_j f B_{pk}} \right)^{1.16} \quad (2-1)$$

In (2-1)  $W_a$  is the window area,  $A_c$  is the cross-sectional core area,  $K_f$  relates RMS voltage to volt-seconds,  $K_j$  relates area product to current density,  $f$  is the switching frequency, and  $B_{pk}$  is the peak flux density in the core.

The red dot zone in Figure 2-1 which includes two AC/DC converter and a transformer, is the high-frequency section of the SST structure. These stages are common between all different SST configurations with DC busbars. Based on the different applications of the SST, the configuration is extended with single or three phase low-frequency DC/AC converters to provide proper connection points for the grid or AC components. The rectifier stages of the SST could be active switch based rectifier which potentially makes the SST a bi-directional converter or passive diode bridge rectifier which allows the power to transfer only in one direction.

SST offers several functionalities in a smart grid configuration including, protecting loads from power system disturbances, protecting power system from load disturbances, integrating energy storage systems (energy buffer), providing DC ports for distributed generation connection, and supporting voltage and power profiles [40]. Besides, SST can play an important role in realizing the DC/AC zonal power distribution system[11]. They will link the micro-grids to the

MV transmission system as well as low voltage AC and low voltage DC systems.

However, SST has some drawbacks in comparison to the regular transformers. First of all, the high-frequency switching in the SST converters increases the switching loss which affects negatively on the efficiency of the converter. Second, due to the higher number of components, the reliability of the converter reduces and also the converter control, especially for the grid application, would be very complicated.

One solution to tackle the issue of high switching loss in the SST is using the resonant circuits to achieve ZVS [56] and ZCS. Having resonant circuit in the topology of the converter enables soft switching which ultimately improves the efficiency of the converter. Figure 2-2 shows a DC-DC SST with series load resonant (SLR) circuit included. The experimental tests on this configuration show the efficiency improvement from %92 to %96.5.

Several articles have been published on the different resonant circuit configuration for soft switching in HF converters. Jung et al. (2013) described a CLLC topology for a bidirectional SST for DG interface [15]. A complex dead-band control at the sub-resonant frequency is used, and the switching frequency is limited to the resonant frequency. Agamy and Jain (2008) explained a three-level resonant single-stage PFC converter which is suitable for high power applications [16]. Variable frequency phase shifted modulation (VFPSM) is used in [16], and switching frequency is limited above resonant frequency to achieve ZVS, whereas ZCS operation is not targeted in this work.

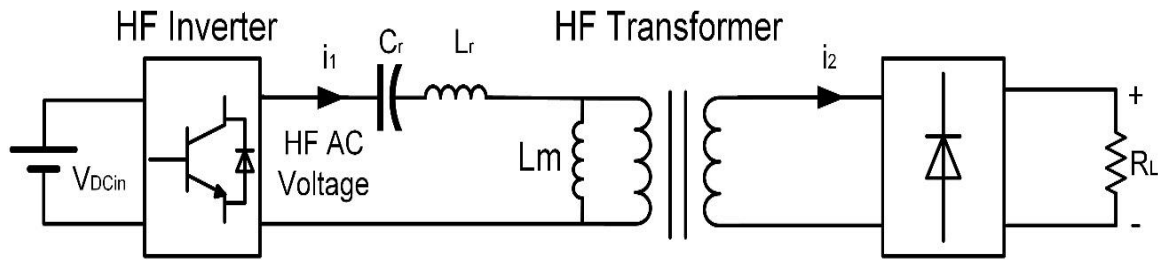


Figure 2-2. Series resonant SST configuration [13]

## 2.2 Analytical study of Multiport Solid State Transformer

Multi-port solid state transformer combines the needed converters, minimizes the number of components and increases the power density in the system. Also, application of MPSST enables modular expandable installation of DER and ESS in the distribution grid since the different flexible and isolated ports are provided using one adjustable converter.

Providing galvanic isolation through HF transformer, the optimal size and weight of transformer are achieved. Besides the component level size reduction of HF transformer design, the MPSST application in the power system reduces the total size of the system since it reduces the needed components in the system.

Each port of the MPSST could be adjusted to connect to the different types of components. The MPSST configuration has a high-frequency section which includes the HF converters of the ports and a multi-winding transformer. The ports of this HF section of the topology of this study are DC ports, and it could be adjusted for the single or three phase AC components by adding low-frequency inverters.

Ideally, there is no limit for the number of the ports in the MPSST configuration, but the flux management and power exchange control in the transformer become very complicated by increasing the number of the connected ports.

In this study, a four-port MPSST configuration is suggested, studied and built to be used as an active converter for microgrid application and in the smart distribution system to isolate voltage zones in the power system while it is providing extra ports for utilizing DER and energy storage systems into the grid on the same converter.

Existing distribution networks are low voltage AC systems. In the conventional DS configuration, the small-scale DERs and microgrids which is defined as a controlled interconnection of ESS, DER and loads within defined boundaries (Figure 1-1) [17], are connected to the low voltage zones. As a result, feeding of the low voltage end-user loads inside the microgrid is easier and design and building of the switch based power electronic converters, which are indispensable components of the renewable based microgrids, are simpler and relatively cheaper for the lower voltage applications.

Chapter 3 illustrates the different distribution systems architecture. In this chapter, the conventional distribution system is compared with the possible active design of distribution system based on PE based converters like SST. One big difference between these grid architectures is the different methods of utilization of the DER components in the grid. In this study, a four-port SST configuration which uses a combination of active and passive converters is introduced as a converter which enables efficient microgrid utilization in the grid. The expected advantages of the grid-scale application of this converter are discussed in the next chapter.



Figure 2-3. General structure of a microgrid

Figure 2-4 shows the general configuration of the MPSST of this study. There are three active converters on three of the ports of the converter, and the last port has a single-phase diode bridge rectifier. The active switch-based converters are full-bridge single-phase converters and enable bi-directional power flow. This type of converter is needed for grid and energy storage ports.

On the other hand, feeding the load port does not need a bidirectional converter and the optimal converter for this port to convert from AC to DC is a single-phase diode bridge rectifier. It is also known that every conversion from DC to AC, which is the case for the generation ports



(higher zone of voltage) and DER ports must have a switch based active converter even for the cases that their power flows only in one direction. The parameters of the fourth part are controlled through the three other controllable converters.

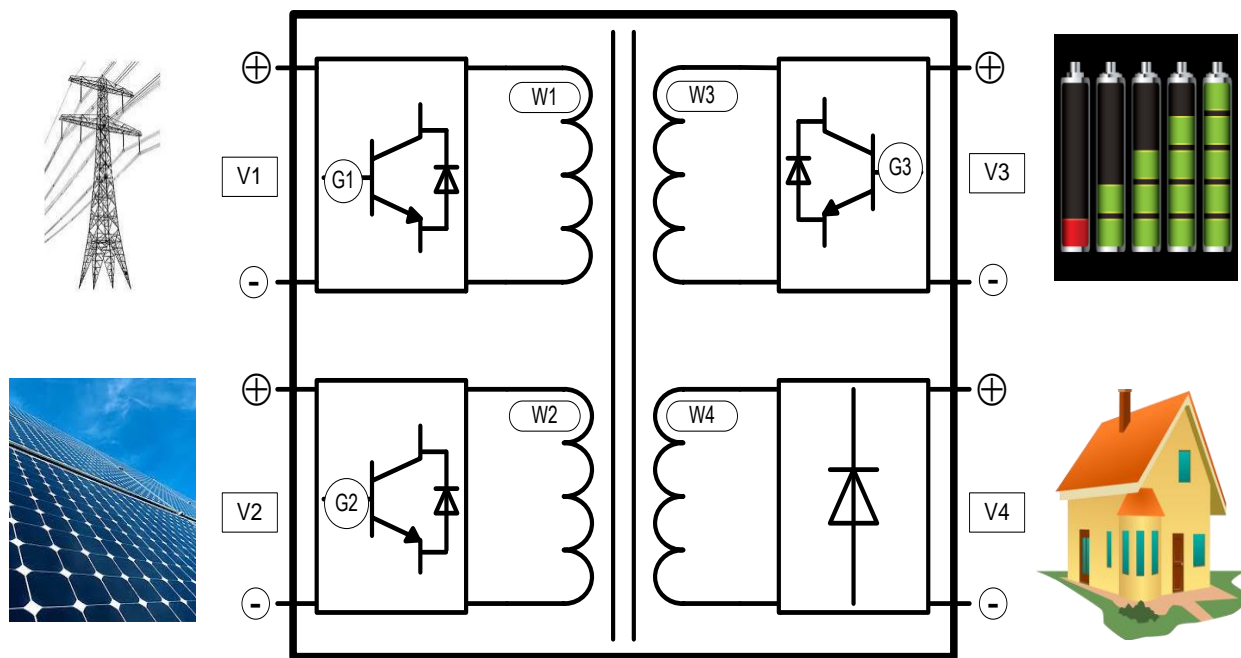


Figure 2-4. Configuration of the Four Port SST

### 2.2.1 Voltage polarity, Current direction and Power flow in MPSST

It is necessary to have an equal circuitry for the new configuration to be able to analyze the electrical characteristic of the converter. The circuitry should include voltage polarity for the DC components and the positive direction of the current flow to be followed in mathematical analysis and in calculating the system transfer functions for controller design. Figure 2-5 shows the voltage polarity and the current direction in the equal circuit of the four port SST which is proposed in this study. This circuit which is based on the designed configuration of the converter and final implementation of the prototype includes only the HF stages of the MPSST. The DC bus polarities

shown in the figure and the currents are assumed to flow from converters to the core of the transformer. The directions of the currents are chosen based on the positive power flow direction from the port converter to the transformer and arrow on the AC waveform indicates the positive direction for writing a differential equation using Kirchoff's voltage loop (KVL) and Kirchoff's current loop (KCL) for this converter.

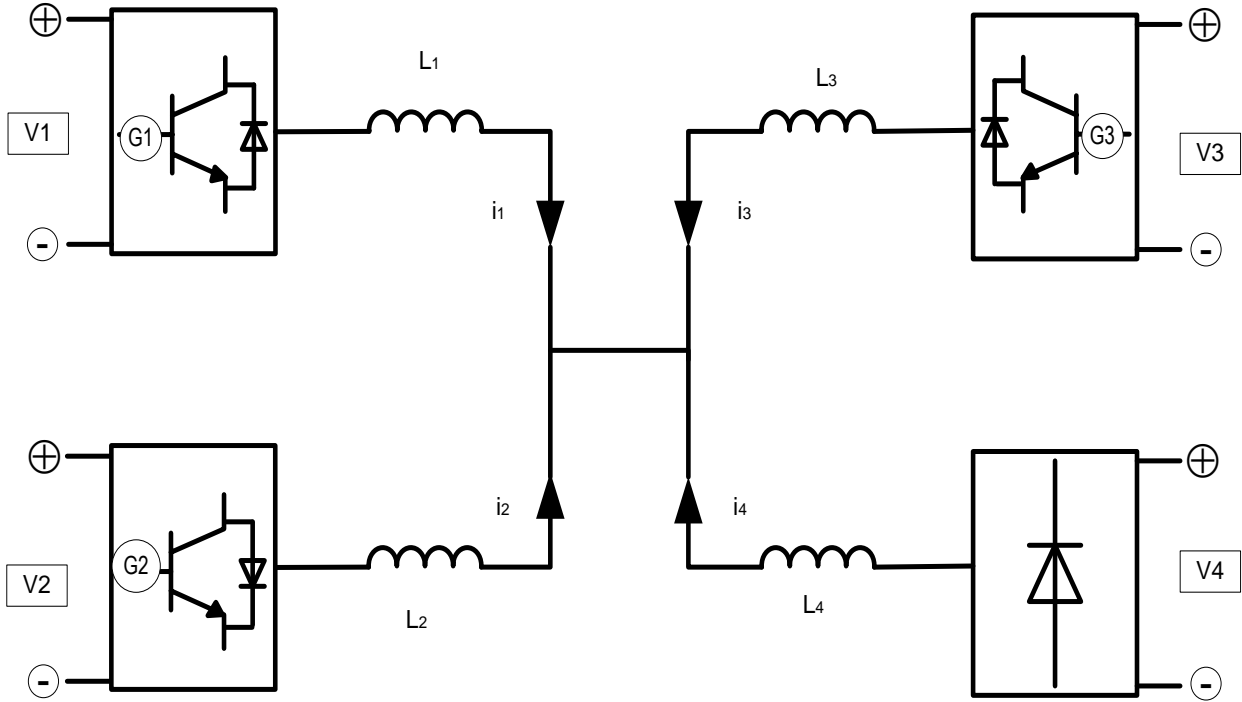


Figure 2-5 Standard Voltage polarity and current direction in the four port configuration

The study cases of this project assume that the converter is controlling the system parameters to feed the demanded power to the load on the fourth port with a regulated voltage. The power-sharing logic in chapter IV discusses the controller strategy in details. This port is unidirectional and defined to be connected to the load or the lower voltage zone, and it does not send any power back to the higher zone.

The inductance of each port of the figure is the equal impedance of the leakage inductance on the port plus any possible resonant component and magnetizing impedance.

### **2.3 Advantages of MPSST in Comparison to the Regular SST**

The power distribution system configuration includes several galvanically isolated voltage zones. The components inside each zone of voltage are sharing same voltage level, or they use an extra converter to match to the standard voltage level of the voltage zone. These converters could be PE converters or in some cases AC transformers for changing the voltage levels. With the increasing penetration of the RER, ESS, and DC and smart loads in the distribution system, the number of these extra converters in the different voltage zones increases which decreases the efficiency and reliability of the system by adding components and conversion stages to the system. Having MPSST in the power system helps to minimize the number of converter and components by providing several isolated ports for different components using one compact converter. This modular optimized sized converter simplifies the installation and maintenance process of the future distribution system. Also, it enables direct utilization of DC components in the different voltage zones of the power system which increases the efficiency.

Figure 2-6 shows the difference between a system which uses a two-port SST and a system which uses MPSST for feeding several components. In Figure 2-6 (a) all of the components are sharing a busbar. Then based on the type each component, separate converters are used to match their voltage type with the busbar voltage. The configuration of Figure 2-6 (b) uses MPSST and combines the needed components in one converter. The shared point in this configuration is the multi-winding transformer in the core of MPSST. This configuration benefits the system by

minimizing the number of the component which decreases the size and increases the efficiency and reliability of the whole system. It also enables connecting components with different voltage levels (MV/LV) by adjusting the turn ratio between different windings.

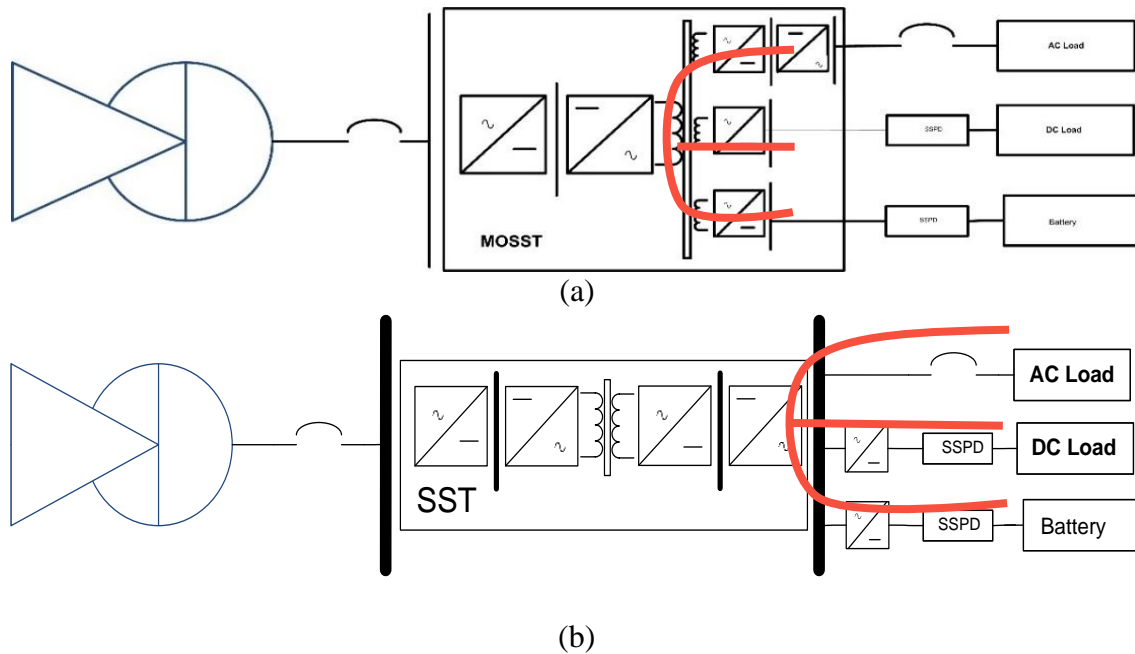


Figure 2-6. Feeding multiple loads with (a) SST based system and (b) MPSST bases system

On the other hand, the power flow between every two ports and total exchanged power from the ports are controlled actively by one controller. Using one controller for multiple components simplifies the system control strategy which is a very important factor in the grid application of MPSST. The MPSST controller is discussed in detail in chapter IV.

Replacing passive LFT with MPSST helps the distribution system by offering active and reactive power flow control for the different connected branches. Figure 2-7 shows the difference between power flow control in a system with two port SST (or regular transformer) and a system with MPSST. In the first configuration, the system is passive, and Kirchhoff's law specifies the share of power of different components, or the extra power converters are needed to control the

power flow of the branches. In a system with MPSST (Figure 2-7. (b)), the converters of the ports of MPSST control the flow of power from each port.

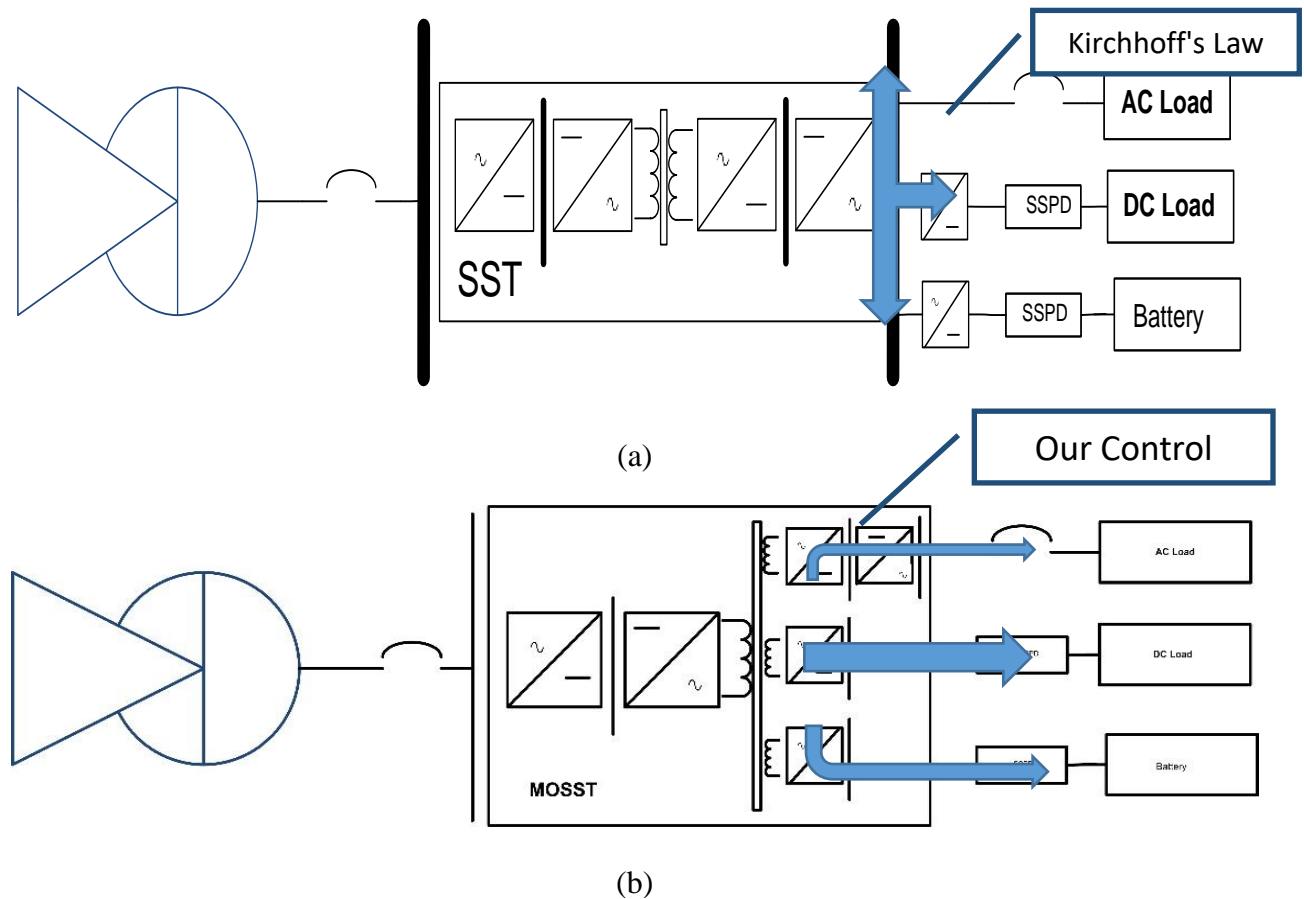


Figure 2-7 Power flow control in a system with multiple loads components (a) SST based system and (b) MPSST bases system

### 2.3.1 DC Bus Fault Analysis in a System Including MPSST

Different types of faults could happen in a system including isolated power electronic converter with DC ports. The faults could happen in the transformer or the power electronic components. Also, the faults could happen as the result of the failure of one or several components, or it could be an external fault which affects the functionality of the converter.

These faults include internal faults, lightning surge, switching transient, non-ideal load and the short circuit on the DC busbar [50]. The DC bus fault has been discussed in multiple articles for the different DC converters and topologies [41][43]. It is the main subject of this section since it is the most common type of system level fault in the grid application of PE converters.

Since the fault is an external fault and the converter is expected to continue feeding the branches with no fault, it is necessary to minimize the fault damage by analyzing this fault and defining possible response scenarios for treating this type of fault.

The DC bus faults could be categorized into two major groups. Line-to-line fault (Figure 2-8) which usually is characterized as low impedance fault and line-to-ground fault (Figure 2-9) which has both high and low fault impedance and it is the most common fault in the distribution system[44][46][48].

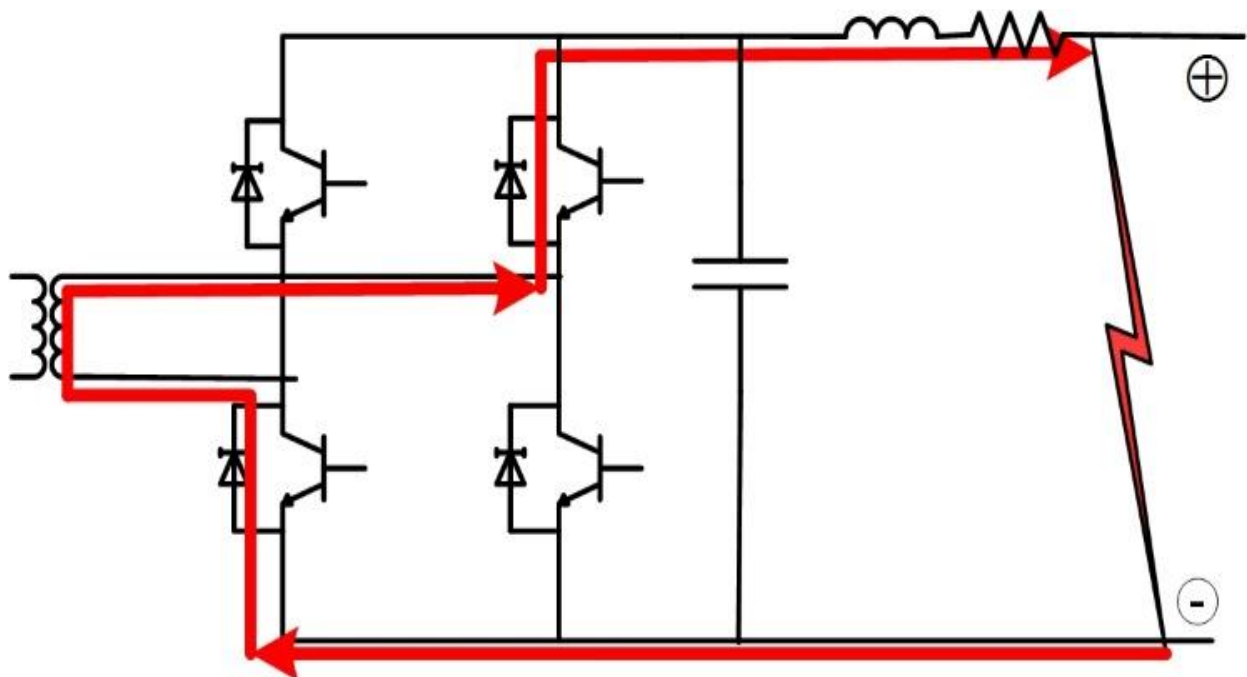


Figure 2-8 Line to Line fault on DC bus [51]

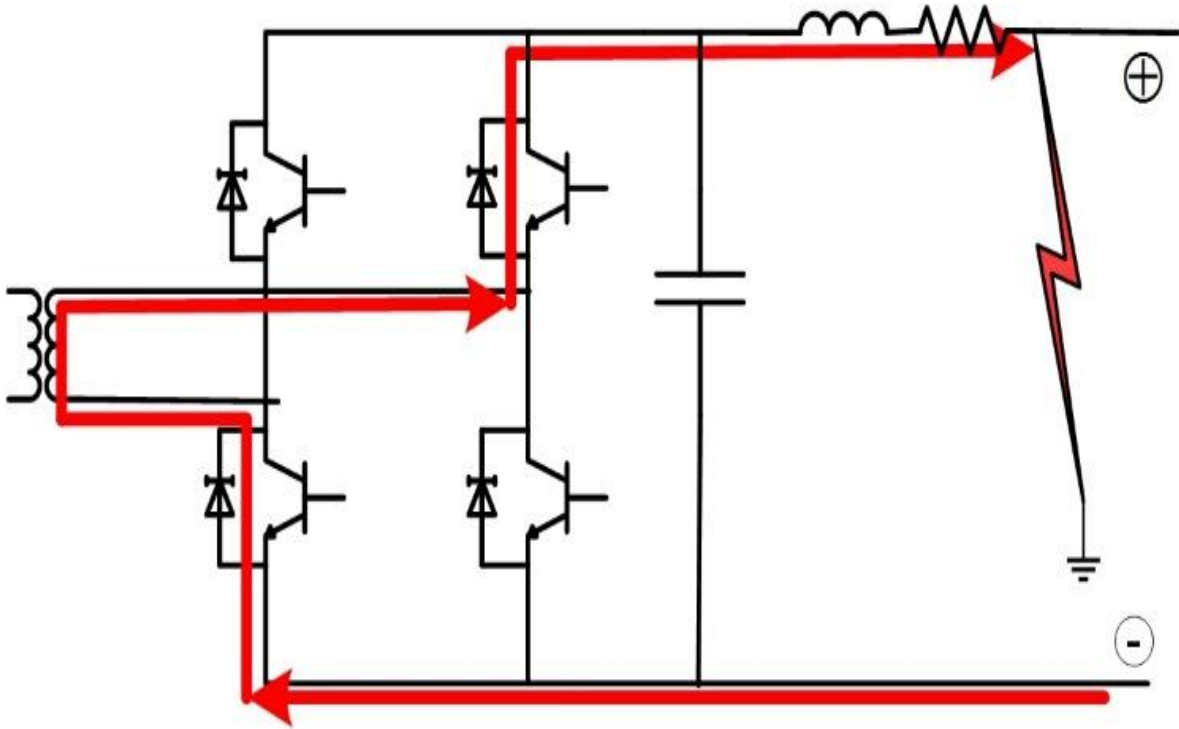


Figure 2-9 Line to Ground fault on DC bus

Single H-Bridge configurations are used as the port converters in the design of four port SST of this project. One major problem with the H-Bridge configuration is that if a DC side fault occurs in this system, the IGBTs (or MOSFETs) lose control on the current and the freewheeling diodes become a path for the current in the form of a full bridge rectifier, and the converter continues feeding the fault [47]. The DC fault results in short-circuit and the current rapidly increases within few milliseconds which is sourced from the converter. The large short-circuit current may overheat the conductors and devices and causes malfunctioning of the system.

*A. Available DC Fault protection in AC\DC converter based systems*

DC power distribution has some advantages and disadvantages over the AC systems [52]. In the DC system, the synchronization and reactive power control are no longer problematic.

However, dealing with the fault situation is a big concern. Unlike the AC protective equipment's there is still no commercial reliable, cost-effective DC protective device which could detect and break DC faults [49].

The basic idea of circuit protection in the fault condition is to isolate the fault from the main feeder.

Traditionally, the link between AC and DC opens when a fault in DC system is detected. The mechanism of the conventional AC circuit breaker relies on the natural zero crossing of the AC waveform to open the circuit and since it is not a valid solution for the DC circuits the ACCB should be placed at the AC side of the converter[42], [44].

Another solution to protect the system from DC side fault is to use protective devices like fuses and DC CBs directly on DC side and isolate the fault from the rest of the grid[44].

The main problem with the fuses is they can trip the faulted circuit, but energizing the same circuit after clearing the fault needs replacement of the fuse by an operator. DC Circuit Breakers do not have the problems of the fuses and could reset with the control signal but their design for reliable operation to limit the current in the case of fault to disconnect the circuit is very complicated and expensive.

In the case happening a fault, one of the first steps is to limit fault current [45]of the faulted line. The main methods current limiting in the DC system are:

- **Superconductors:** Superconducting materials have no resistance and cause little conduction loss during the normal operation situation.
- **DC limiting reactor:** When a short-circuit fault occurs, the dc limiting reactor can limit the increasing speed of the fault current.



➤ Solid state circuit breakers.

In the MPSST configuration of this study, the DC fault could occur on the secondary of the port with diode bridge converter (Figure 2-11) or on the DC side of the active H-Bridge converters (Figure 2-10).

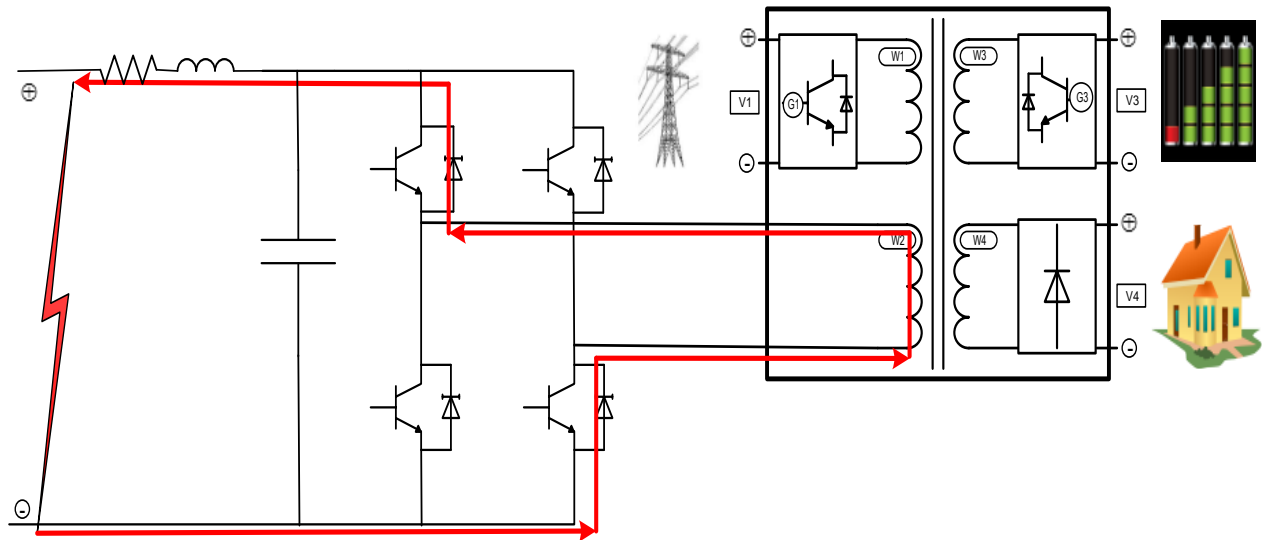


Figure 2-10. DC side fault on a port with active H-Bridge

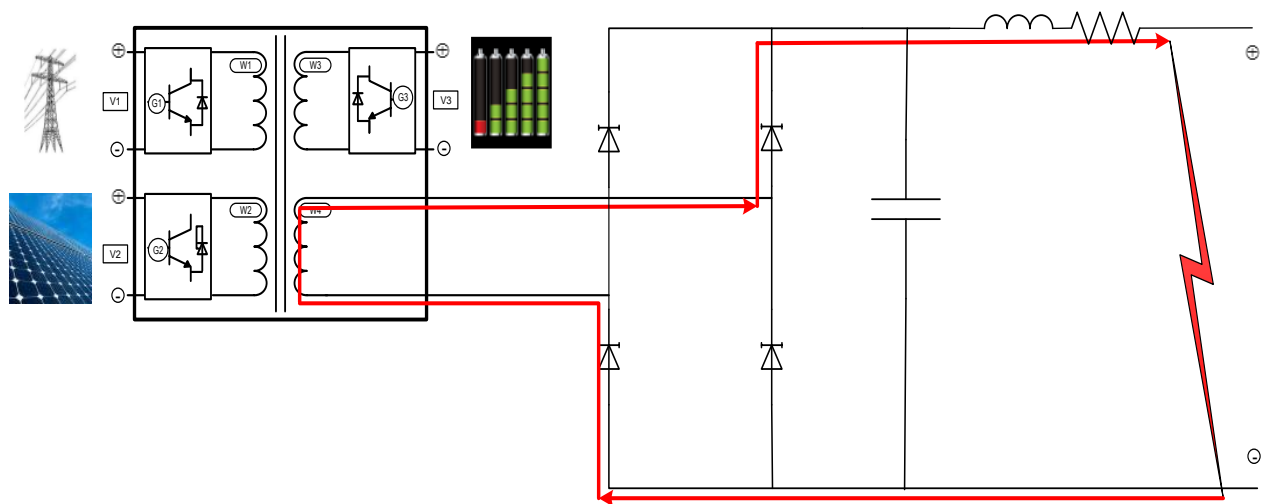


Figure 2-11. DC side fault on a port with full bridge diode rectifier

The fault protection equipment discussion is not in the scope of this research, but for any solution to successfully protect the system and effectively disconnect the faulted branch from the system, it is necessary to limit the current by limiting the sources which feed the faulted branch. It is also very important to keep the maximum number of branches energized after a fault. A post-fault action strategy is designed for the system level application of MPSST based on the topology of this study to be used in the fault and protection studies.

Based on the designed fault protection strategy, if the fault happens on the load leg, the reference current for all of the legs change to zero [46] (turn off all of the switches). Then the AC side circuit breaker opens. Finally, the converters start charging the battery and grid leg after fault cleared until the faulted leg is energized again.

In the other case, if the fault happens on one of the generation legs, the reference current for all of the legs change to zero (turn off all of the switches). Then the switches of the faulted leg converter turn off and finally after faulted leg decoupled the other generation legs continue feeding the load and the winding of the faulted leg is going to operate in open circuit mode.

## CHAPTER 3

# Future Configuration of Active Efficient Power

## Distribution System

Current distribution systems are typically low voltage systems. The main advantage of low voltage distribution is enabling direct connection of low-voltage end-user loads with minimum voltage conversion. It is also much simpler for the renewable based microgrids or single DERs to get connected to the power system since the output voltages of DERs are relatively low. Furthermore, design and building of low voltage switch based power electronic converters which are essential components for the DER applications, are relatively cheaper and simpler than MV PE converters.

### 3.1 Conventional Power Distribution

Figure 3-1 shows the general architecture of the conventional power distribution system (DS). This configuration uses AC voltage with one standard frequency. In the current distribution systems, the DC components are connected to the system using separate AC/DC converters.

Current power systems include several voltage zones which are defined based on the optimal voltage levels of the potential elements in each zone. These voltage zones are galvanically isolated from each other using low-frequency passive transformers. Due to the magnetic design constraints, the low-frequency transformers are relatively larger and heavier than the other components in the same zone of voltage. On the other hand, keeping the voltage relatively low for

transferring power leads to higher current and transmission loss in comparison to a system with the same power rating and higher voltage, but because of the relatively larger size and weight of the MV transformers, they are not applicable components in the distribution systems.

In the configurations of the current grid (Figure 3-1), power is mainly generated in the big scale power plants and flows through the whole path to the end user load. Introducing the concept of microgrids which is mainly based on the small-scale DER, especially renewable energy resources (RER) and energy storage systems as the source of power in the last years, has added another element to the last zone of the distribution network. The DER elements could also be utilized into the system as a single power generator for supporting small loads with an alternative source of power.

Utilizing DERs in the grid as a part of a microgrid is simpler than connecting a single small-scale DER to the system directly since the microgrid has its internal controllers and all of the needed voltage conversion are done inside the microgrid, and there is only one point of connection to the grid. On the other hand, the small-scale DER utilization in the grid as a single separate generator needs a separate converter for each DER to control their output voltage, synchronization, and flow of power.

Also, since the whole conventional power network is 50/60 Hz AC system, providing power for the DC loads or adding storages to the grid as an alternative source of power for the important loads needs proper PE converter. Moreover, the passive LFTs between the voltage zones of the conventional distribution system do not have any role in the fault detection and voltage and current regulation of their connected components.

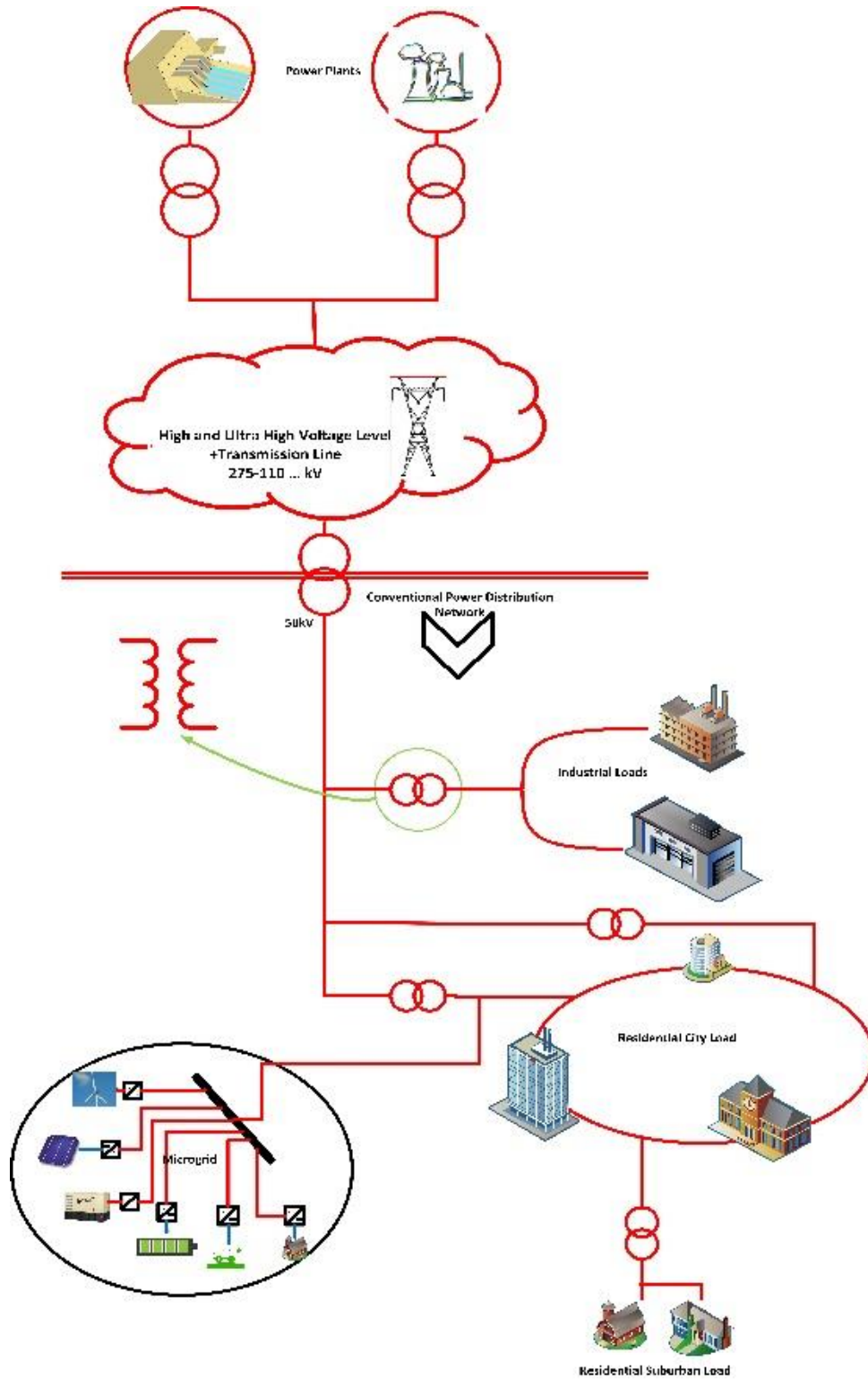


Figure 3-1. Conventional distribution system

### **3.2 SST Based Zonal Distribution System**

The growing penetration of the DC load and DER components in the power grid has affected the grid architecture and control strategy since these components use the PE converters to get connected to the electricity grid. On the other hand, the technology development has made these type of applications cost-effective for wide installation in the electricity grid and move from the conventional electricity grid with only passive LF transformers as the main converter to the new generation of distribution systems based on the isolated PE converters. An isolated PE converter provides galvanic isolation which is a basic requirement for the power system with different voltage zones and helps to change the voltage level using transformer turn ratio to match the voltages at the different zones. Also, the PE converters enable better online monitoring and active local control on the parameters of the system.

Moreover, using components like SST the direct utilization of the DER in the power system is possible. This enables bringing alternative sources of power in different zones of voltage and combining the concept of microgrid and voltage zones to form an efficient zonal controllable distribution system.

The concept of zonal DER based distribution system has a lot of advantages in comparison to the conventional DS. First and foremost, it includes DERs dispersed in all of the zones of the system. Having alternative sources of power in the voltage zones improves system sustainability. Also, this transmission power loss decreases since at least a portion of the demanded power is locally generated.

On the other hand, power electronic stages in the SST enable feeding the transformer with high-frequency AC voltage which has a huge impact on the size and weight of the converter. Using HF in the design of SST resolves the issue of size and weight of the conventional transformers and enables medium voltage distribution system which reduces the distribution loss and increases the efficiency of the system.

Furthermore, the PE based transformers with online sensing and control capability provide a proper infrastructure for enabling the concept of smart grid.

A schematic of the potential architecture of the future controllable distribution system is shown in Figure 3-2. In this design, the regular transformers between zones of the distribution system are replaced with two-port solid state transformers[4].

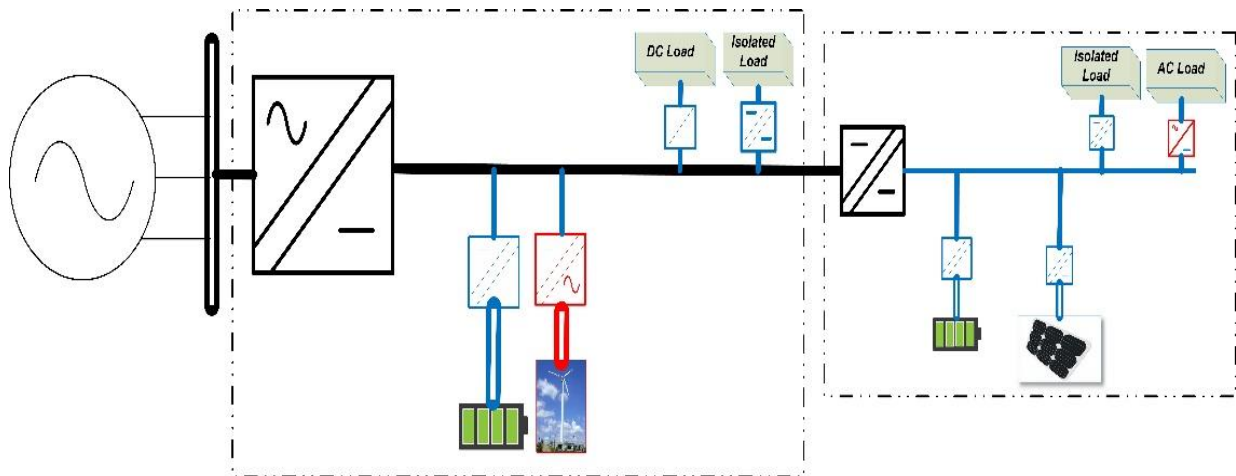


Figure 3-2. Zonal AC-DC DG based distribution structure based on two port SST application

A DC&AC zonal distribution system configuration is shown in Figure 3-3 which provides proper AC and DC port for the different types of components like RER and ESS or loads to be utilized in the grid directly with minimum conversion steps. The configuration of Figure 3-3 is simulated in MATLAB/Simulink environment. The different levels and types of voltage are

regulated in this configuration. Figure 3-4 shows the simulation results. The blue lines and components are DC components and the components with red color using AC voltage.

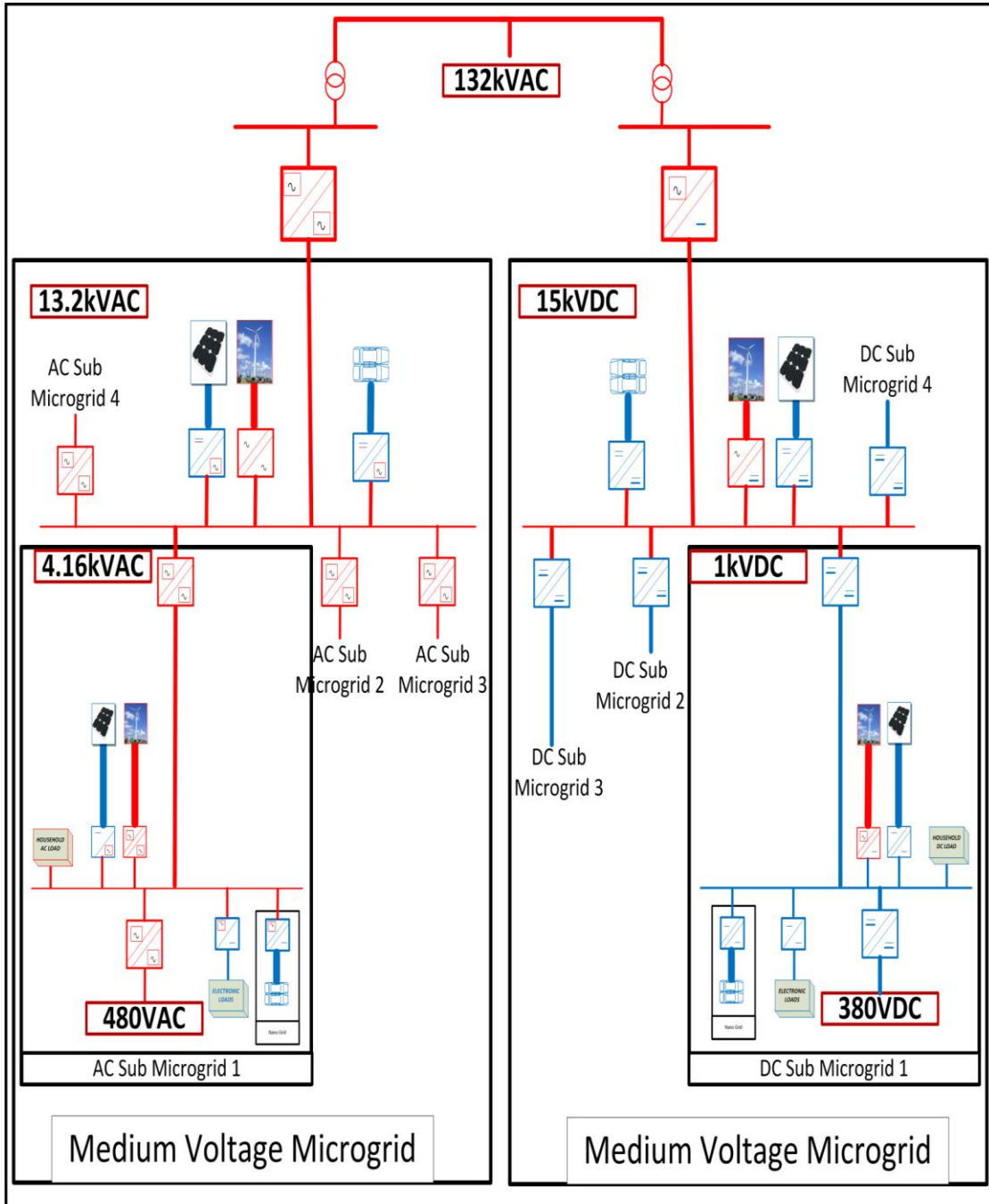
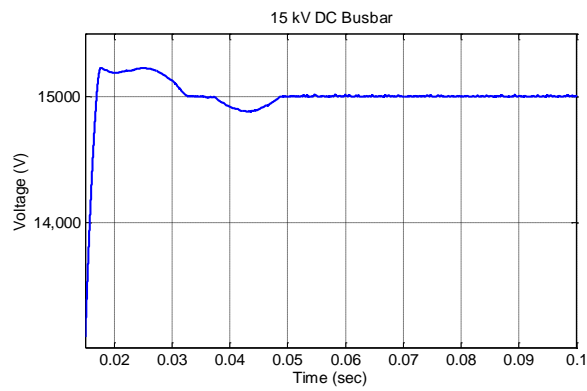
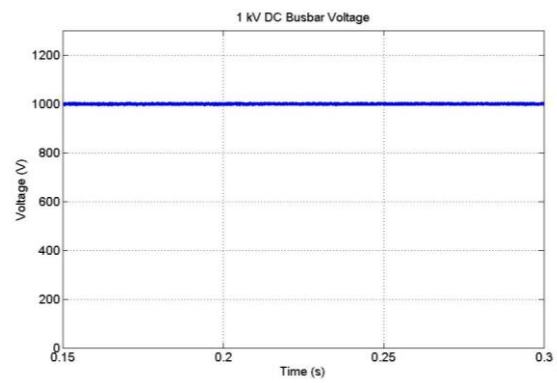


Figure 3-3.AC DC zonal distribution system based on SST [2]

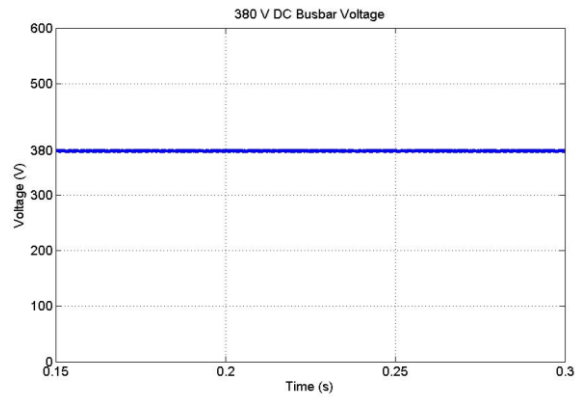




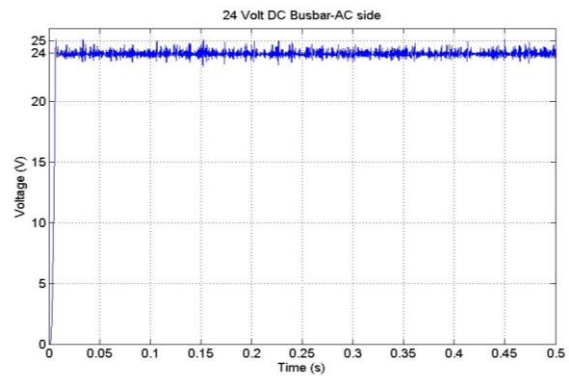
(a)



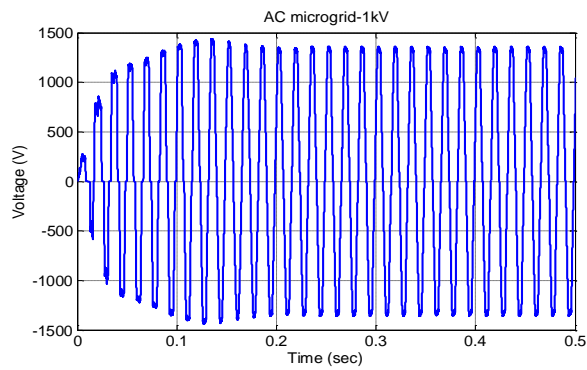
(b)



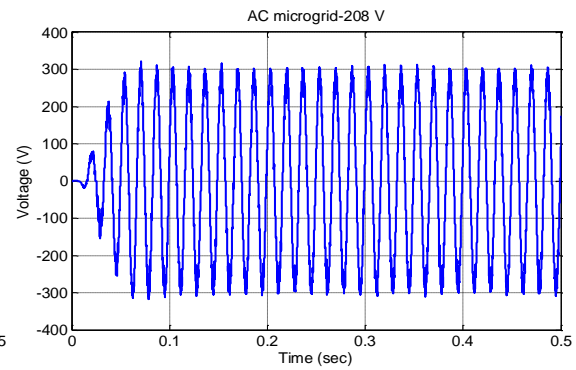
(c)



(d)



(e)



(f)

Figure 3-4. Different levels of regulated DC voltage in an AC DC zonal distribution system based on SST, (a) 15kVDC, (b) 1kVDC, (c) 380VDC (d) 24VDC (e) 1kVrms (f) 208Vrms

### **3.3 MPSST Based Zonal Distribution System**

Dispersing small scale DERs in the different voltage zones of the power system has the advantage of decreasing the transmission loss and improving the reliability and survivability of the system since some of the power demand is generated locally in the power zones and the distance between demand and generation is minimized. It also provides a local alternative source of power to support the grid by providing active and reactive power for frequency and voltage regulation. However, there is a tradeoff between making the system more efficient and controllable with isolated PE components like SST (Figure 3-3) and increasing the complexity and cost of the system. The system control in Figure 3-3 is complicated due to the number of converters which are used to connect all of the components. Also, adding a new component like RER or ESS to the system needs a separate SST which makes the configuration a difficult choice for the large-scale grid applications.

MPSST offers a solution to tackle the problems above by combining several needed converters and forming a multiport converter with several isolated ports. Figure 3-5 shows a proposed distribution configuration using MPSST. MPSST reduces the number of converters and simplifies the control of the whole system dramatically. Besides, it is capable of voltage regulation on different ports. Also, connecting different types of components with various voltages inside a voltage zone is enabled with minimum hardware and/or software adjustment in the converter. Furthermore, modular expansion of DER with minimum cost and hardware modifications is possible in the system configuration which uses MPSST. In the grid architecture of Figure 3-5, the common busbar of each zone in the regular distribution architecture is replaced with the HF

transformer inside the MPSST, which leads to a huge reduction of the conversion loss and total size of the system.

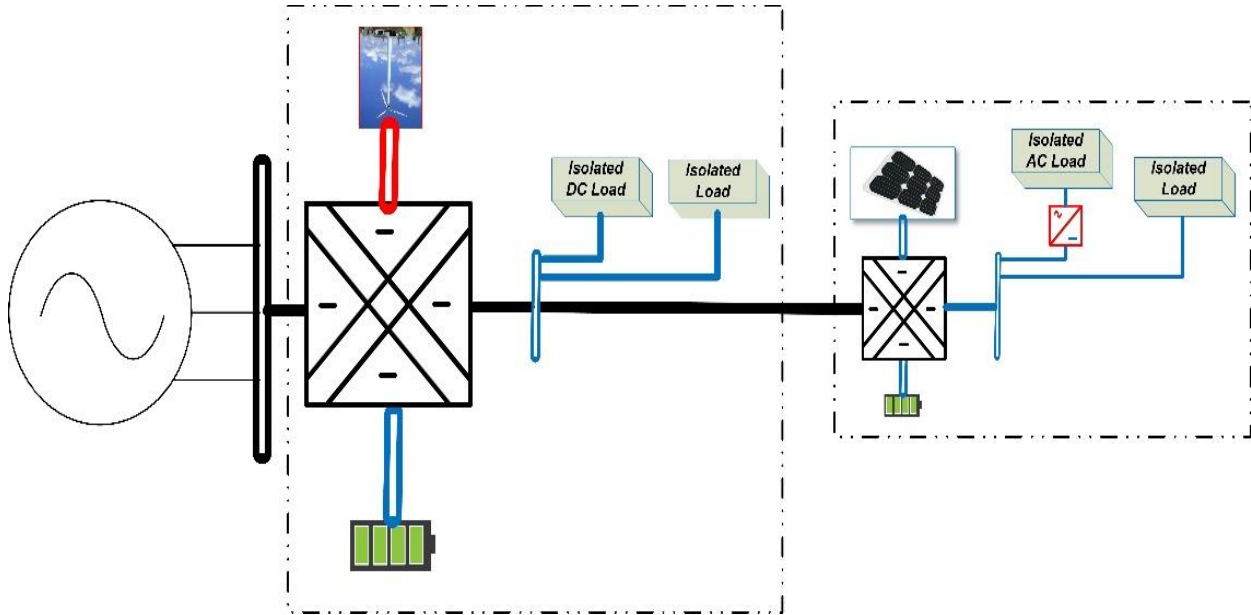


Figure 3-5 Zonal AC-DC DG based distribution structure based on four-port SST application

The four-port SST in Figure 3-5 is used to utilize hybrid RER/ESS in the different zones of voltage. Also, MPSST as a modular and compact component provides a cost-effective and fast solution for electrification of the loads which do not have access to a reliable grid.

### 3.4 MPSST Application for Grid Support

Controllable power electronic based converters which are inevitable components of the new generation of power systems enable the fast and efficient solution to support the grid by providing local active and reactive power in response to the variations of the power demands or occurrence of any fault to regulate the voltage and frequency of the voltage zones [18][19].

### **3.4.1 Active Power Management in a Power Network Which includes MPSST**

The ports of four port SST could be connected to different components, including various types of DG, ESS, and different AC or DC loads. The controller of the converter is modified based on the type of components and their defined application in the system to adjust the power-sharing between the different ports of the converter and between each port and the grid properly.

The power-sharing control method which is used for the MPSST is called pool of power method (PPM). PPM is the first block of the higher layer of the MPSST control strategy. The current control and voltage regulation blocks of the MPSST which generate gate signals are analyzed mathematically in chapter IV as the lower layer of the control strategy.

The priority chart of PPM is the decision-making process to determine the demanded share of power for each port to be sent or absorbed. The pool of power method includes several logic loops to specify the exchanged share of power for the next layer of the controller.

The PPM chart controls the exchanged power between each port and the isolation transformer of the MPSST. The results of this chart are used as the inputs to the second layer of the controller to control the flow of power from/to each port.

Ultimately, the load demand is equal to the total provided power from the other ports of the multiport converter. Seven modes of operations are defined for the power sharing of the MPSST topology which is used as case study in this project. This four-port SST provides connecting ports for load, upper grid, RER, and ESS. Table 3-1 shows that the energy storage port absorbs power to charge the ESS in some modes of operation which is reflected in the system equations as the negative value for the share of power of this port.

Two main constraints of the PPM chart are feeding the demanded power to the load port

and absorbing the whole generated power from RER port in the system.

$$[P_1, P_3] = fcn(soc, P_2, P_4) \quad (3-1)$$

Table 3-1.PPM Modes of Operation

	Constraints	Power Sharing
1	$ P_2  \geq  P_4 $ $soc \geq 0.95$	$ P_1  =  P_2  -  P_4 $ $ P_3  = 0$
2	$ P_4  <  P_2  \leq  P_4  + (0.95 - soc) * Bcap$ $soc < 0.95$	$ P_1  = 0$ $ P_3  =  P_2  -  P_4 $
3	$ P_4  + (0.95 - SOC) * Bcap \leq  P_2 $ $soc \leq 0.95$	$ P_3  = (0.95 - soc) * Bcap$ $ P_1  =  P_2  -  P_4  -  P_3 $
4	$ P_4  =  P_2 $	$ P_1  = 0$ $ P_3  = 0$
5	$ P_2  <  P_4  \leq  P_2  + (soc - 0.2) * Bcap$ $soc > 0.2$	$ P_1  = 0$ $ P_3  =  P_4  -  P_2 $
6	$ P_2  + (soc - 0.2) * Bcap <  P_4 $ $soc > 0.2$	$ P_3  = (soc - 0.2) * Bcap$ $ P_1  =  P_4  -  P_2  -  P_3 $
7	$ P_2  <  P_4 $ $soc \leq 0.2$	$ P_3  = 0$ $ P_1  =  P_4  -  P_2 $

The inputs of the decision-making chart are the state of charge of the battery (SoC), power generation capacity of the RER at the moment, the power demand of the load and the mode of

connectivity to the grid as an infinite source of power. Assuming the system is planned to feed all of the power demand and absorb all of the generated power of the RER, the outputs of the PPM chart are the exchanged (positive or negative) power of the grid and energy storage ports. The results of the PPM are used as an input parameter for the next block of the controller which calculates the phase shift between AC sides of the converters of the ports to control the current flow from/to each port. This chart is continuously running during the operation of the system since the RER capacity and SoC of energy storage changes during operation.

Table 3-1 shows the different modes of operation and the related equation for each mode to specify the shares of power from the ports.

In Table 3-1,  $P_1$  indicates the share of power of the grid port. This parameter is equal to zero in mode 2, 4 and 5 because the system generates enough power for its internal demand. In these modes, the combination of RER and ESS provide enough power to cover the load demand, and if the RER generates more power than the demand, the energy storage has enough capacity to absorb the extra power. In modes 1 and 3, power flow of the port 1 is negative, and that means the generated power of RER port is more than the sum of the load demand and ESS free capacity. Also,  $P_1$  is positive in modes 6 and 7 since the demand is larger than the sum of RER output and ESS charge of power. Parameter  $P_2$  shows the power of RER port, and because of the nature of the renewable energy resources,  $P_2$  is either zero or the generated power at the time. This port is not able to absorb or store any power.  $P_3$ ,  $B_{cap}$ , and SoC are the share of power of energy storage port, the energy storage capacity and the state of charge of the storage system. This port is capable of participating in the power generation, storing power or being connected to the system without exchanging any power with the other ports. Based on the state of charge of the ESS an upper limit

and a lower limit of the SoC is considered as the constraints in the chart to prevent deep discharge or overcharge of the battery. The last parameter is  $P_4$  which is the load demand. This value is the main priority in the power-sharing logic of the system. The port is always unidirectional, and  $P_4$  could be zero or negative. The converter on this port is a full bridge diode rectifier, and the commanded parameters for this port is regulated using a proper control on the converters of the other ports of the MPSST.

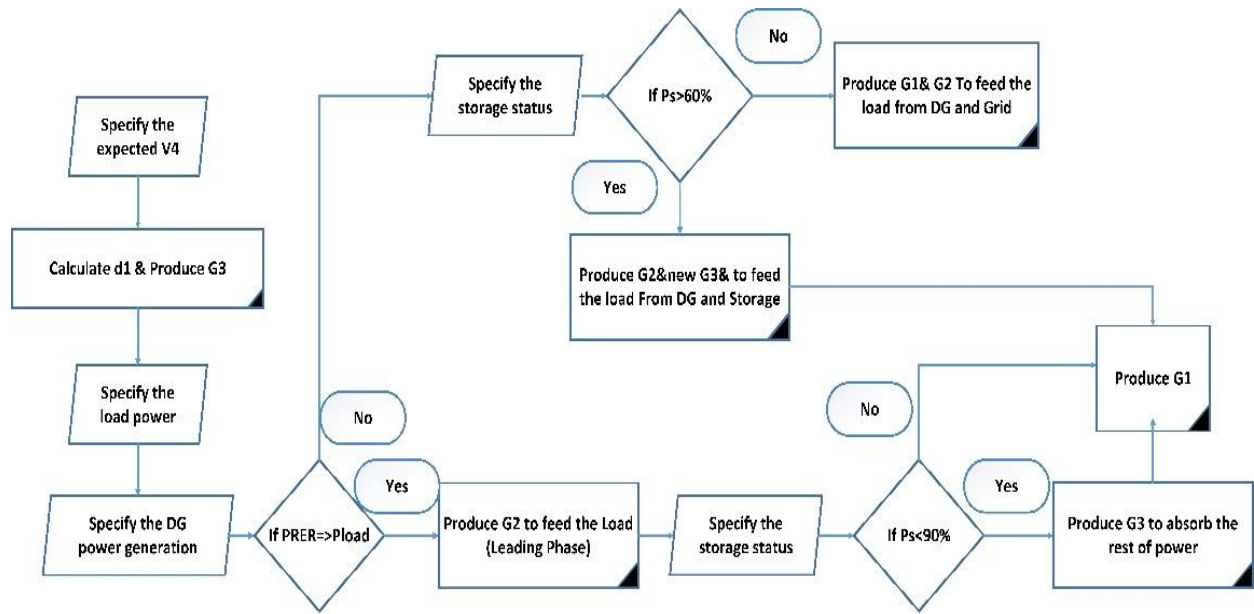


Figure 3-6. Simplified block diagram of the controller based on PPM for power-sharing

The transferred power between each pair of converters depends on their AC side voltage magnitudes, impedances of the line and the phase angle difference between the two waveforms [20][21]. Equation (3-2) shows the relation between these parameters and the exchanged power between two AC busbars for the sinusoidal and square shape AC waveforms.

$$\begin{cases} P_{sine} = \frac{V_{rms1}V_{rms2}}{2\pi f_s L} \sin \varphi \\ P_{square} = \frac{nV_1V_2}{2\pi^2 f_s L} \varphi(\pi - \varphi) \end{cases} \quad (3-2)$$

In this converter the phase shift control (PSC) method is modified for the four port converter, to achieve the power-sharing modes of operation of Table 3-1. The mathematical analysis and the equations of the control method are illustrated in chapter IV.

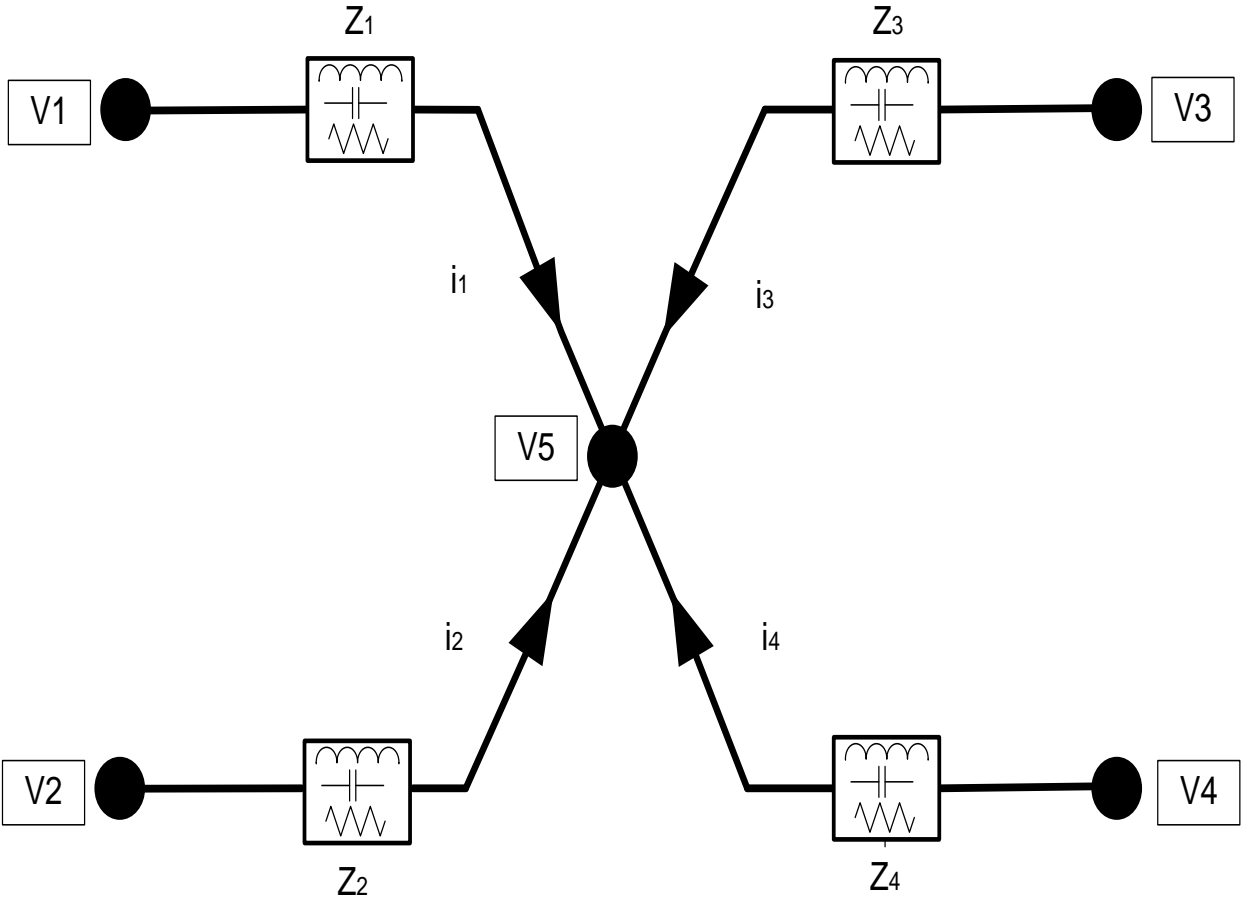


Figure 3-7. Equivalent circuit of MPSST for power-sharing analysis

The current flow toward load port in Figure 3-7 follows a nonlinear multivariable function. Assuming  $V_1, V_2, V_3, V_4$  are the square shape AC voltages which are resulted from transferring DC bus voltages to the AC side of their converter using a transfer coefficient which includes the angle of the AC voltage and its modulation index, the current of the fourth port is calculated from (3-3).



$$I_4 = -\left(\frac{K_4 K_1}{K_5}\right) v_1 - \left(\frac{K_4 K_2}{K_5}\right) v_2 - \left(\frac{K_4 K_3}{K_5}\right) v_3 + \left(K_4 - \frac{K_4^2}{K_5}\right) v_4 \quad (3-3)$$

$$\left\{ \begin{array}{l} K_1 = \frac{1}{j\omega L_1} = \frac{1}{sL_1} \\ K_2 = \frac{1}{j\omega L_2} = \frac{1}{sL_2} \\ K_3 = \frac{1}{j\omega L_3} = \frac{1}{sL_3} \\ K_4 = \frac{1}{j\omega L_4} = \frac{1}{sL_4} \\ K_5 = \frac{L_1 L_2 L_3 + L_1 L_2 L_4 + L_1 L_3 L_4 + L_2 L_3 L_4 + s^2 L_1 L_2 L_3 L_4 C}{sL_1 L_2 L_3 L_4} \end{array} \right. \quad (3-4)$$

$$v_{ac} = v_{dc} * v_C \quad (3-5)$$

$$v_C = m \sin(\omega_s t - \varphi) \quad (3-6)$$

Figure 3-8 shows a schematic of the applied method of control on the phase angles of the square wave AC output of the converters to regulate the power flow. The fourth black waveform is the fundamental frequency waveform of the transformer voltage. The simulation results are shown in Figure 3-9.

The simulation results of Figure 3-9, show the exchanged power of different ports. In the case study of this simulation, a step load happens at 0.1 seconds, and the controller responds to that by increasing the share of power from the other ports. However, since the power generation capacity of the RER is limited and all of the generated power of this port is expected to be extracted at each time, the extra needed power is provided from the two other ports. This is the mode 6 of the PPM chart.

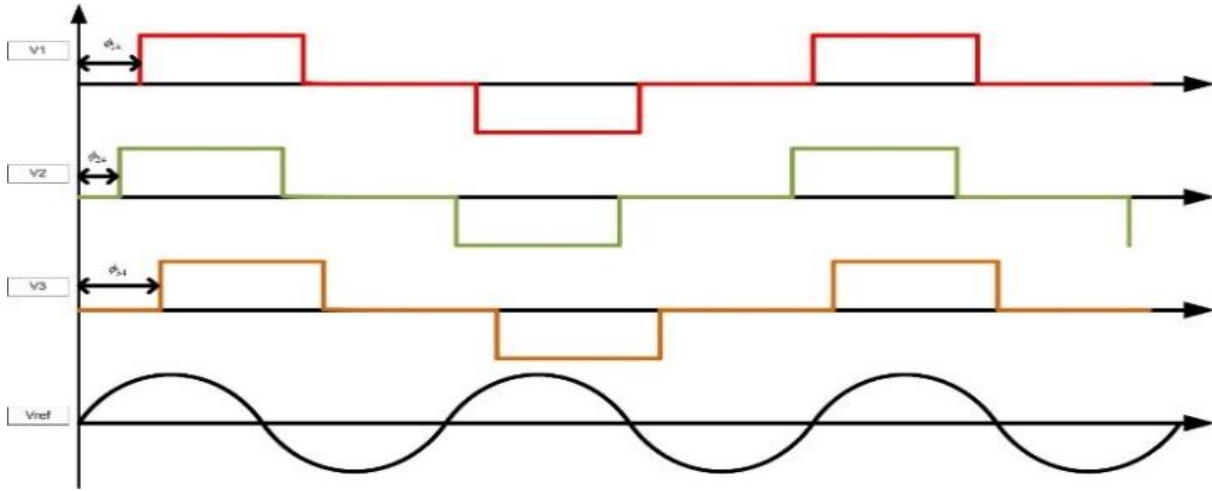


Figure 3-8 Phase shift between the output voltages of three active converters and transformer voltage for very light load

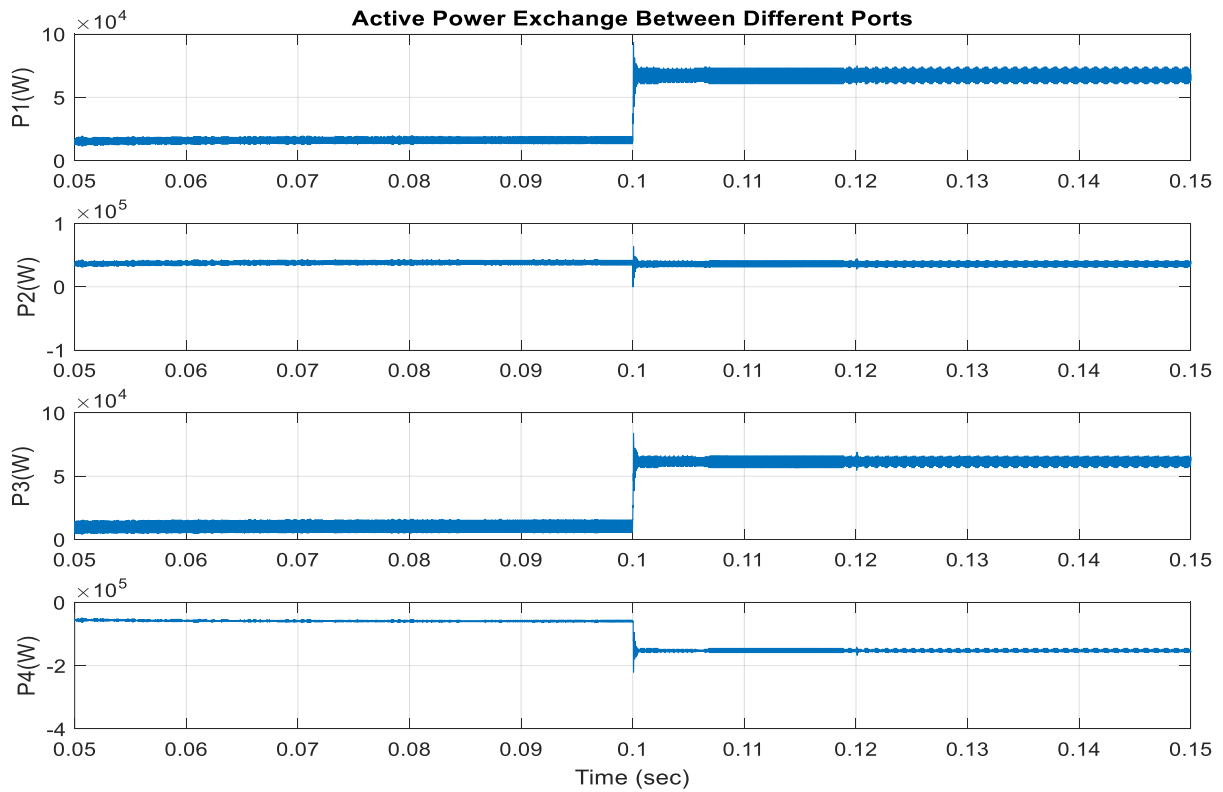


Figure 3-9 Phase shift effect on the power-sharing between different ports and the response of the controller in load power change

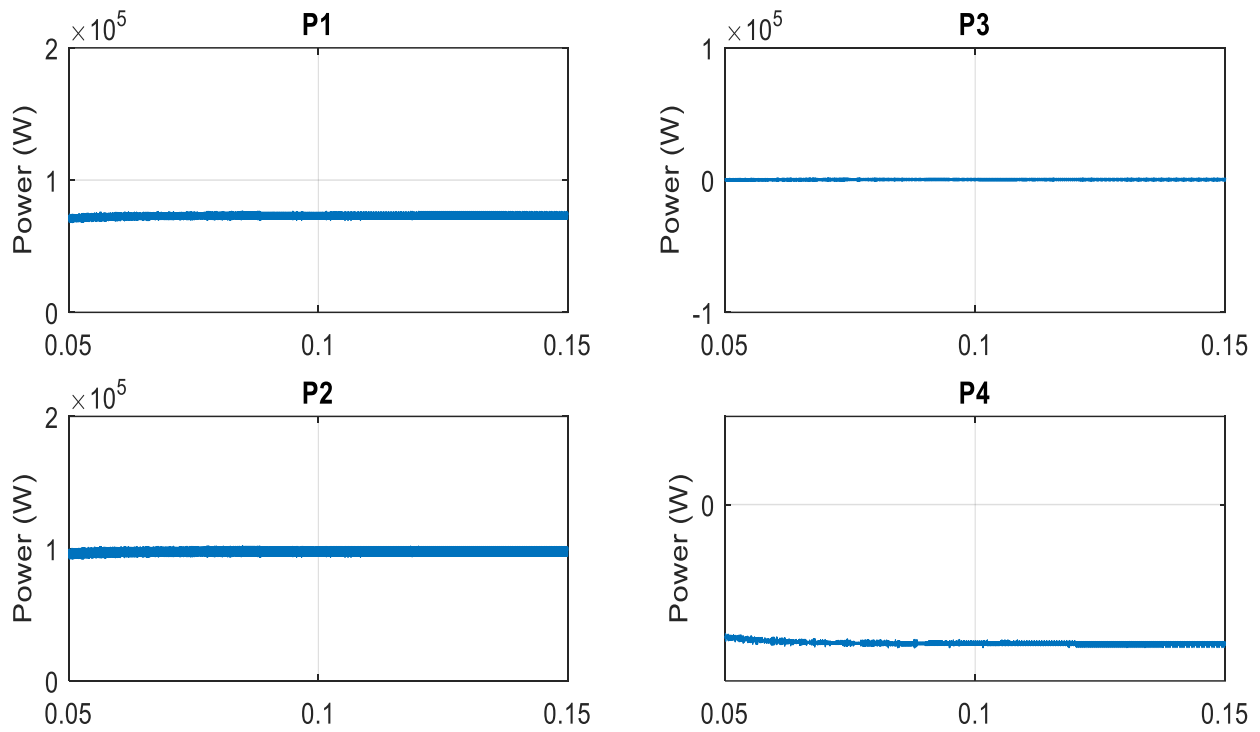


Figure 3-10 Power sharing control of the converters using Phase Shift Control for mode 7

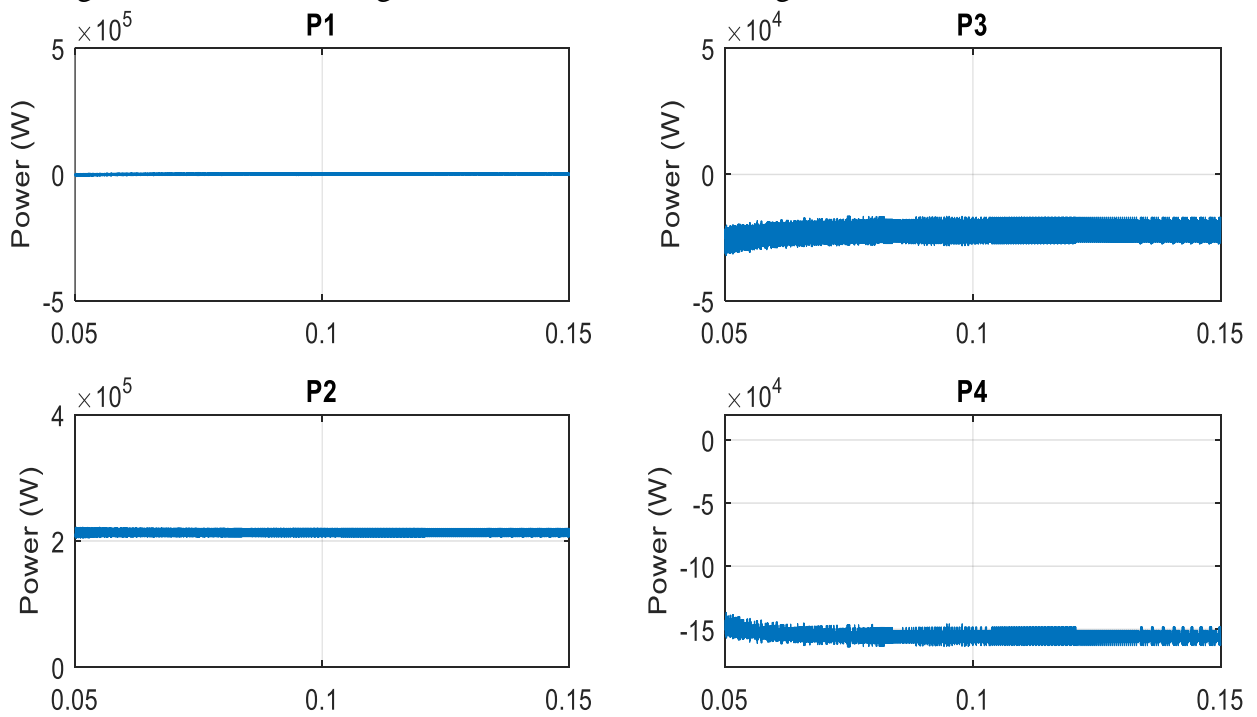


Figure 3-11 Power sharing control of the converters using Phase Shift Control for mode 2

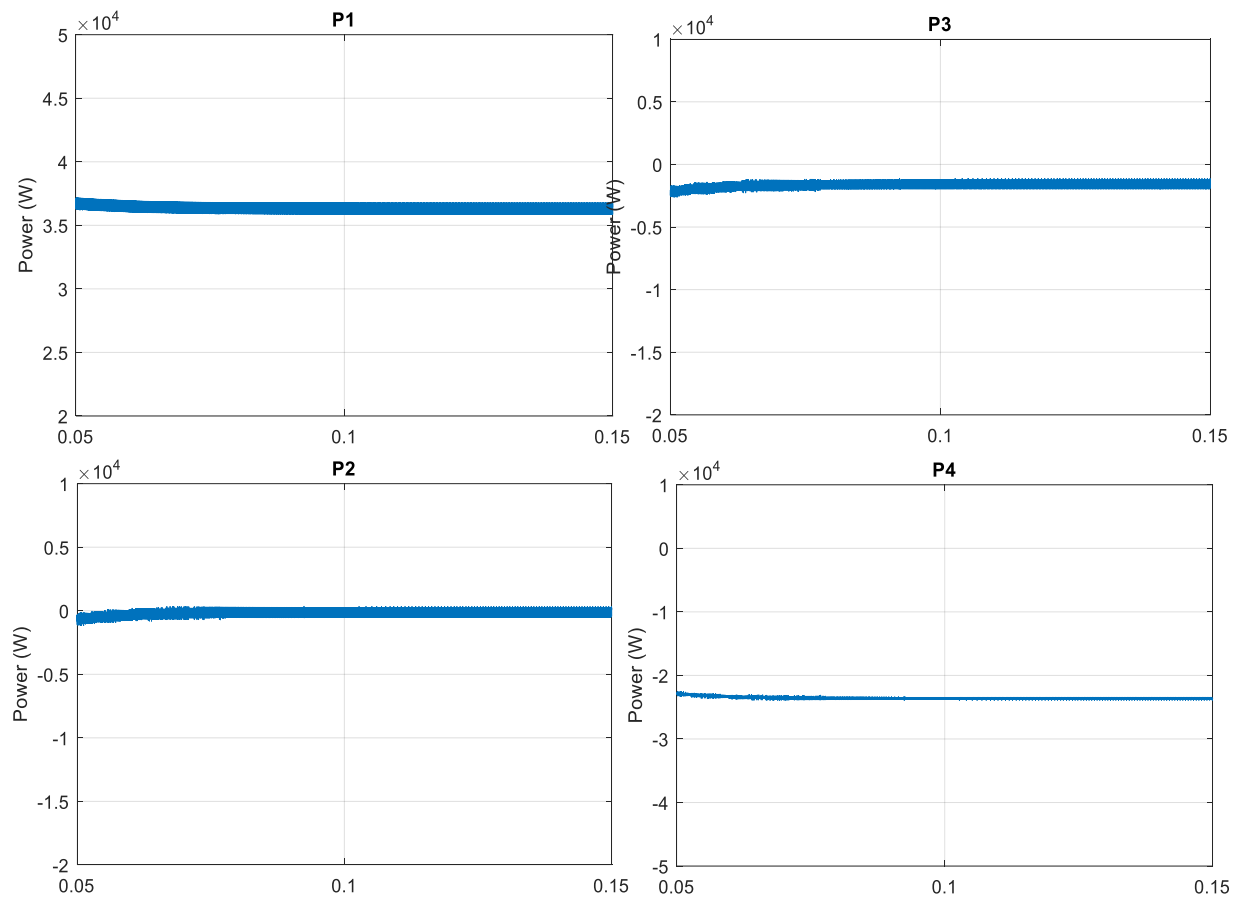


Figure 3-12. Power sharing control of the converters using Phase Shift Control when the RER port does not generate power

Figure 3-10 shows the simulation results of mode 7 of the power-sharing chart. In this mode, the SoC of the energy storage is below lower level, and the generated power of the RER is not enough to feed the load. The whole power of the RER is fed to the load, and the remained demand is provided from the grid while the energy storage port stays connected to the system, but it does not exchange any power.

Figure 3-11 shows the simulation results of another mode of operation which is categorized under mode 2 in the chart. In this case, the grid does not feed the system. The ESS port in this mode stores the extra power from the RER port since the generation capacity of the RER is bigger

than power demand of the load and the energy storage has enough free capacity to store the extra power. This study is performed for the modes of operation which the converter is always connected to the grid as an infinite source of power. The chart could be extended for the islanded modes when the converter is not connected to the grid. Two important differences between islanded mode and connected mode are the modes which include load shedding and the modes which include forcing the RER to generate less power than its full capacity.

### 3.4.2 Volt-VAR Control for Frequency Support in Electricity Grid including MPSST

The MPSST in the new design of power system Figure 3-5 replaces the conventional transformers to connect MV and LV voltage zones. Also, in this application, the converter is capable of supporting grid by measuring the system parameters and working as an active local component to inject reactive power locally from the alternative sources of power which are connected directly to the converter for Volt-VAR control. The four-port DC MPSST in Figure 1-1 could be extended with inverter stages to be integrated into an AC power system. The active and reactive power generation for the AC grid system support are controlled by controlling the low-frequency transformer at the last stage. However, this power should be provided from one (or more than one) of the generation ports.

The bidirectional active and reactive power at each leg is calculated from (3-7) and (3-8) respectively.

$$P_i = \frac{1}{2} (v_{di}i_{di} + v_{qi}i_{qi}) \quad (3-7)$$

$$Q_i = \frac{1}{2} (v_{di}i_{qi} - v_{qi}i_{di}) \quad (3-8)$$

Where P and Q are the active and reactive power at the three-phase inverter on port “i” which transfers power between the converter and the connected component.  $v_{di}$ ,  $v_{qi}$  and  $i_{di}$ ,  $i_{qi}$  are the d-q transformation of voltage and current at leg i. calculated from (3-9) and (3-10) [13].

$$v_i = v_{di}\sin(\omega t) + v_{qi}\cos(\omega t) \quad (3-9)$$

$$i_i = i_{di}\sin(\omega t + \varphi) + i_{qi}\cos(\omega t + \varphi) \quad (3-10)$$

### B. Control Strategy

Figure 3-13 shows the control strategy which is used for Volt-VAR control in a system which includes MPSST. The main goal is to keep the voltages of the system busbars within the standard limits. The system voltages are monitored online, and the data from different busbars of the system are sent to the controller to make sure that the voltage is kept in the standard expected voltage range. If the controller detects any change in the bus voltage as the result of fault or load change, the needed reactive power is calculated based on the lowest detected voltage in the system and the command is generated to the MPPST converter to inject the calculated  $Q^*$  based on the control strategy in a gradually manner in order to compensate for the voltage limit violation. This infinite loop ensures that the voltage is always in the expected range. Some minor voltage spikes may occur during the transition period [54].

In this control strategy, the converter detects the voltage sag in the system locally and provides the needed reactive power from the alternative power sources which are utilized in the system on the ports of the MPSST to regulate the voltage in the standard voltage range.

To verify the capabilities of the applied control strategy in a system with MPSST, IEEE 14-Bus test system is simulated using Matlab/Simulink tool. The scenario is intended to test the control strategy shown in Figure 3-13, where the voltage levels at all nodes are being monitored continuously. At a certain time, a high load demand occurs on one of the buses. The local MPSST with the control strategy injects ramp reactive power values until the voltage is retrieved within

limits. At 0.2s, an overload occurs on bus 4 which affects the rest of the system buses, and the lowest voltage level happens at node 10. The control strategy responds to this change by calculating the needed reactive power and injecting it in a ramped manner to retrieve the voltages to their acceptable levels.

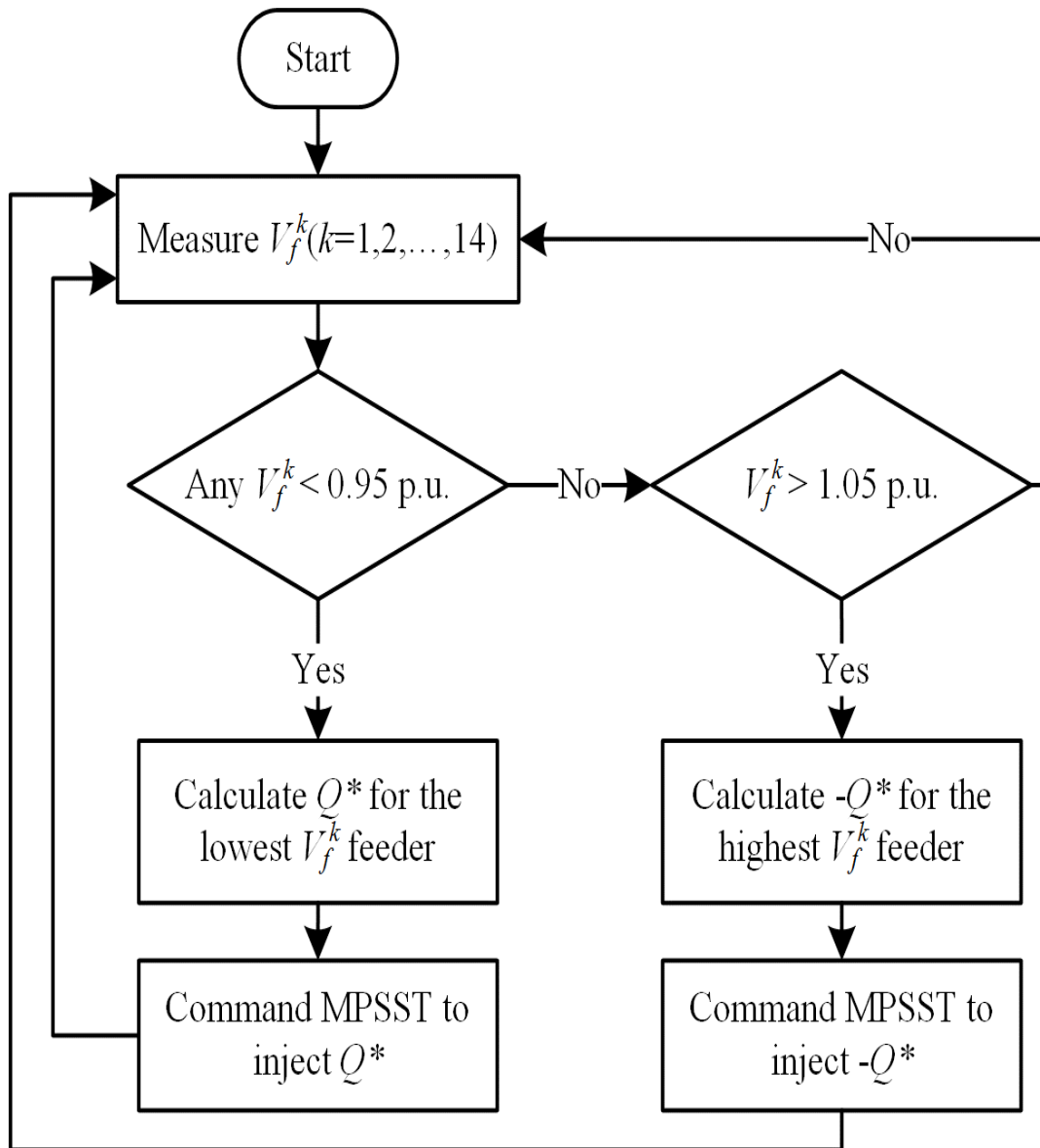


Figure 3-13. Volt-VAR control Strategy [54]

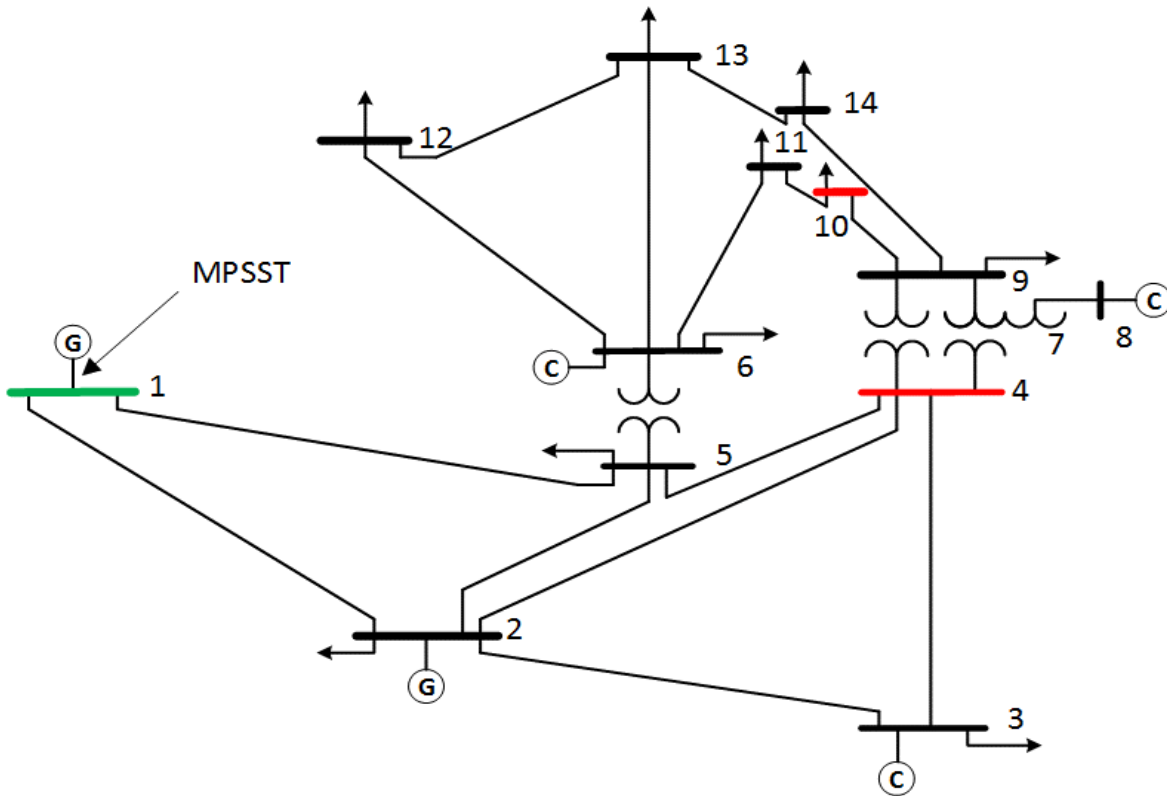


Figure 3-14. IEEE 14 Bust Test System.

Table 3-2. Bus voltages during the transition period.

Node	Normal load V(p.u.)	High load V(p.u.)	After Q* command
Vf 1	1.011	0.9695	1.008
Vf 2	1.004	0.961	1.003
Vf 3	0.9779	0.9371	0.9642
Vf 4	0.9901	0.9266	0.9584
Vf 5	0.995	0.9396	0.9732
Vf 6	0.9972	0.9621	0.9786
Vf 7	0.9934	0.9482	0.9685
Vf 8	0.9836	0.9555	0.9657
Vf 9	0.9811	0.9358	0.9564
Vf 10	0.9778	0.9345	0.9542
Vf 11	0.9781	0.9392	0.9571
Vf 12	0.9813	0.9461	0.9626
Vf 13	0.9752	0.9394	0.9561
Vf 14	0.9859	0.9444	0.9634



As Table 3-2 shows, at normal load conditions, all of the voltages are within  $\pm 5\%$  of the nominal voltage. Then, increasing the power demand causes voltage violation, and the control strategy tries to retrieve voltages to acceptable levels by feeding reactive power to the system. MPSST at node 1 feeds a calculated amount of reactive power to the system. The reactive power is fed gradually while the system voltages are continuously monitored to avoid overvoltage at any other node.

Figure 3-15, Figure 3-16 and Figure 3-17 show the 3-phase RMS voltage at the bus nodes 1, 4, and 10 respectively. At 0.2s, an overload occurs on bus 4 which affects the rest of the system buses, and the lowest voltage level happens at node 10. MPSST and the control strategy applied to respond to this change by calculating the reactive power to be injected in a ramped manner to retrieve the voltages to their acceptable levels, the MPSST response begins at 0.3s (within 0.1s of the overload).

MPSST at node 1 feeds the system with the calculated amount and ramp of reactive power while monitoring the system voltages to avoid overvoltage at any other node. Figure 3-18 shows the reactive power curves of the three feeders under testing during the transition period. Reactive power injected by the MPSST at node 1 increases and reaches a steady state at 0.6 p.u., while node 4 absorbs approximately 0.4 p.u. of the reactive power, 0.2 p.u. is absorbed by the rest of the nodes as their voltage where affected by the overload at node 4 (Table 3-2).

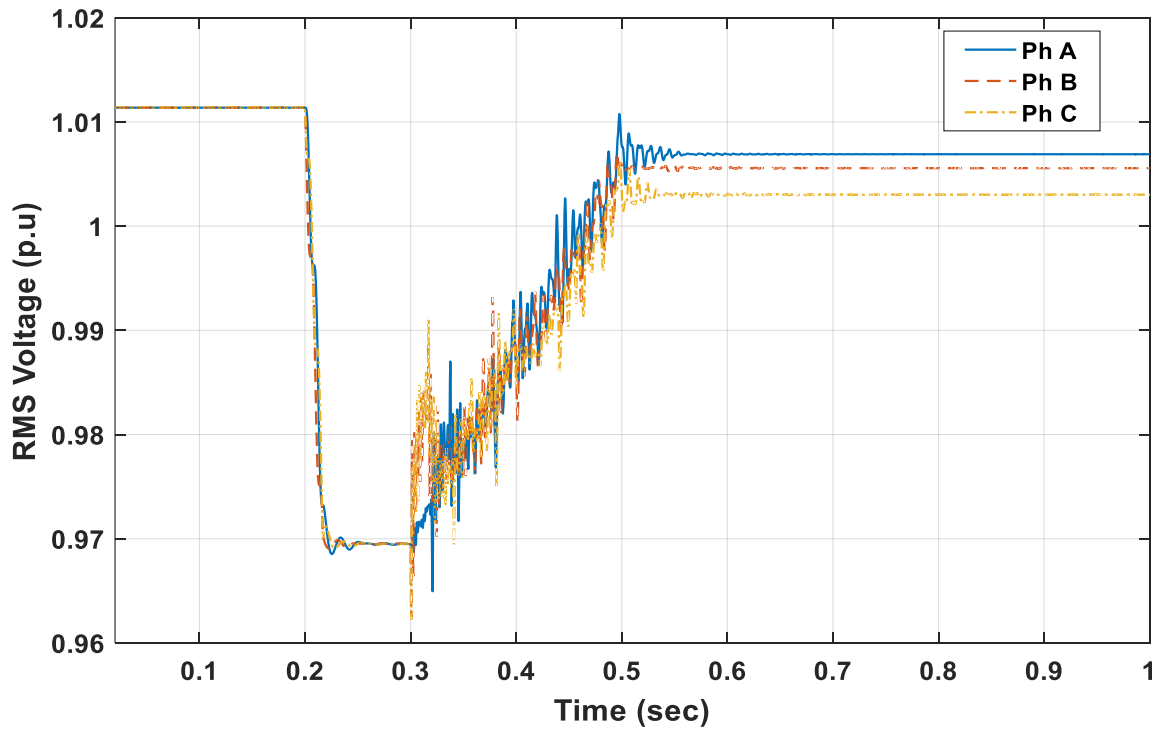


Figure 3-15. Three-phase RMS voltage at bus #1

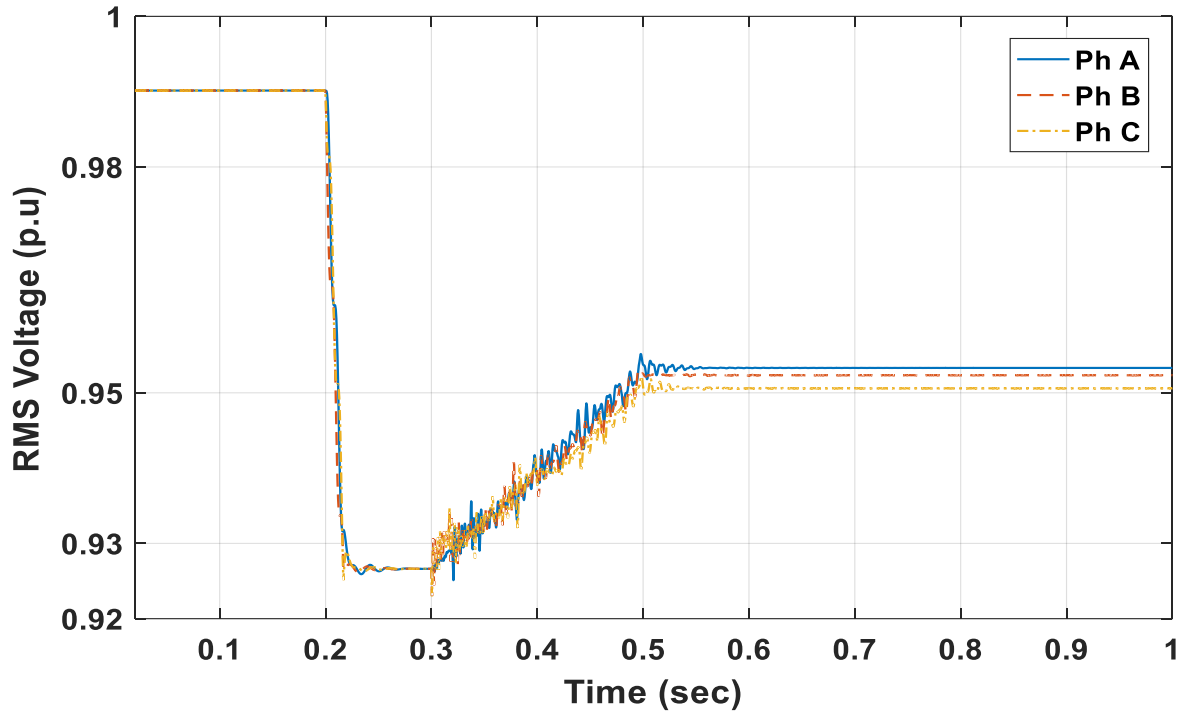


Figure 3-16. Three-phase RMS voltage at bus #4

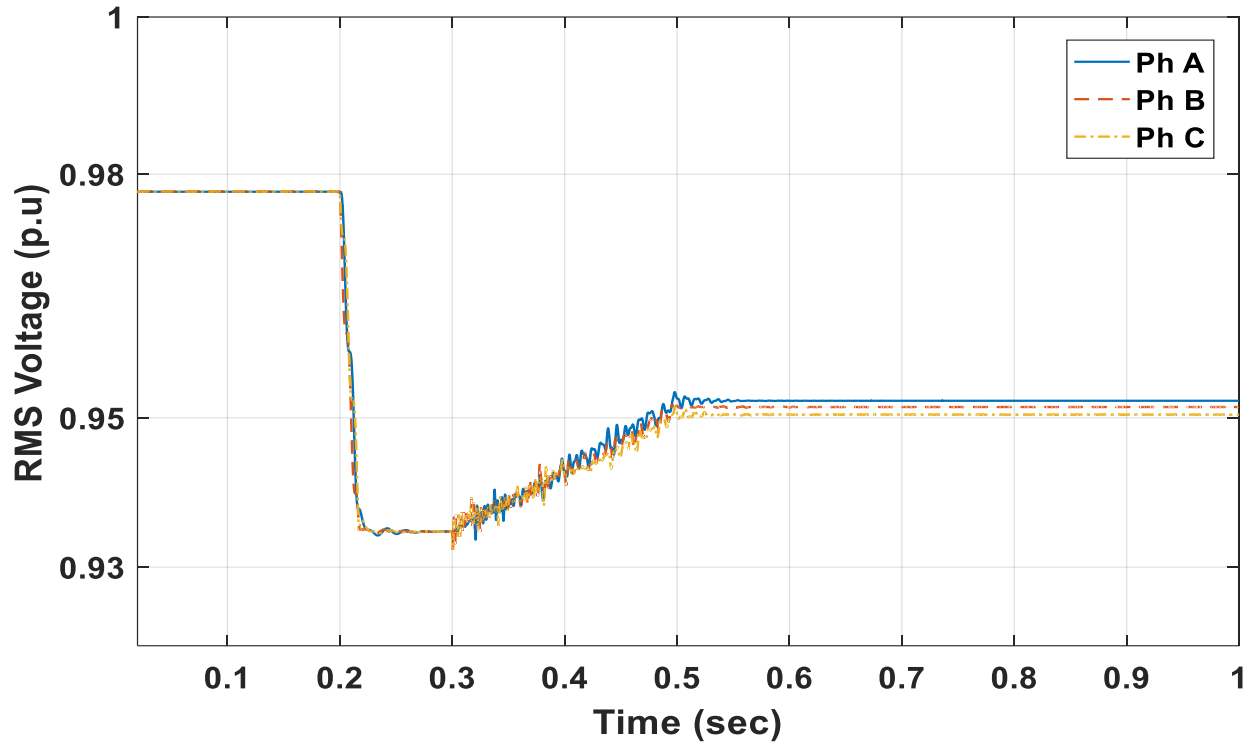


Figure 3-17. Three-phase RMS voltage at bus #4

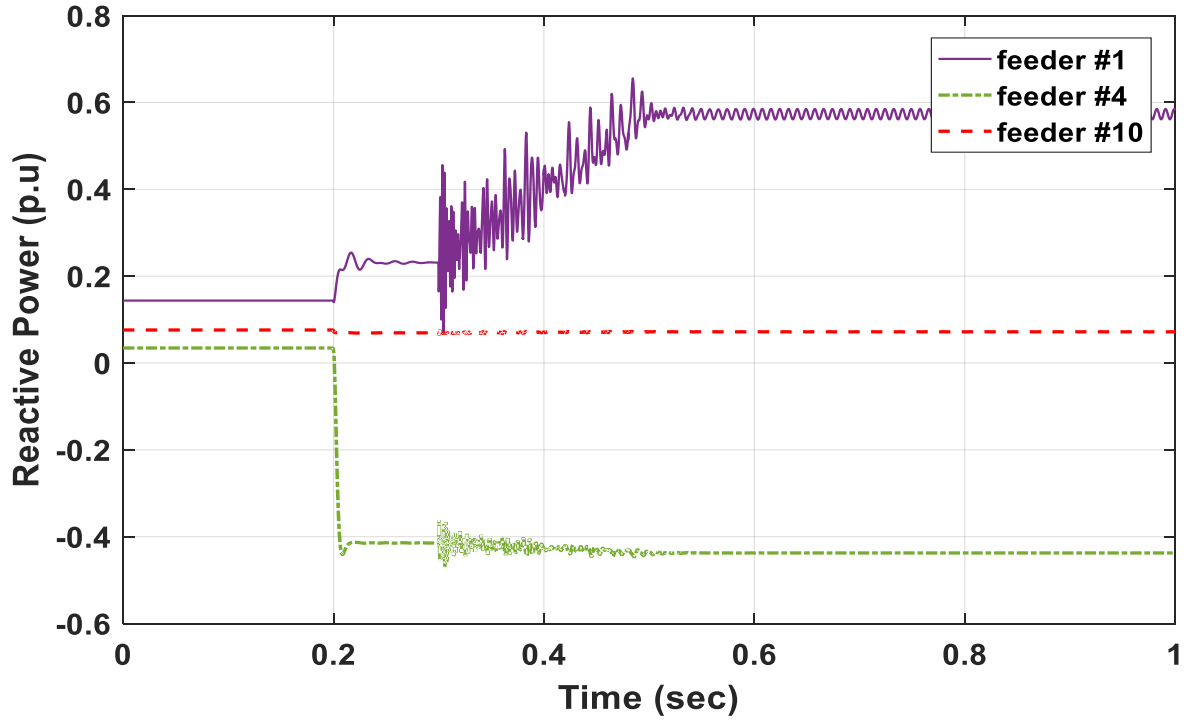


Figure 3-18. Reactive power curves of the three feeders during transition

# CHAPTER 4

## Mathematical Modeling and Control of MPSST

### 4.1 Power Sharing Control Logic

It is necessary to properly model the system parameters and their relation to design a controller for controlling the power flow and voltage of different ports in the MPSST. The system in this study has multiple inputs, and multiple outputs and each of the parameters is dependent on several other variables.

In the control strategy of the four-port topology with the discussed application, the voltages and currents of the DC and AC sides of the converters of the ports are used to provide full control

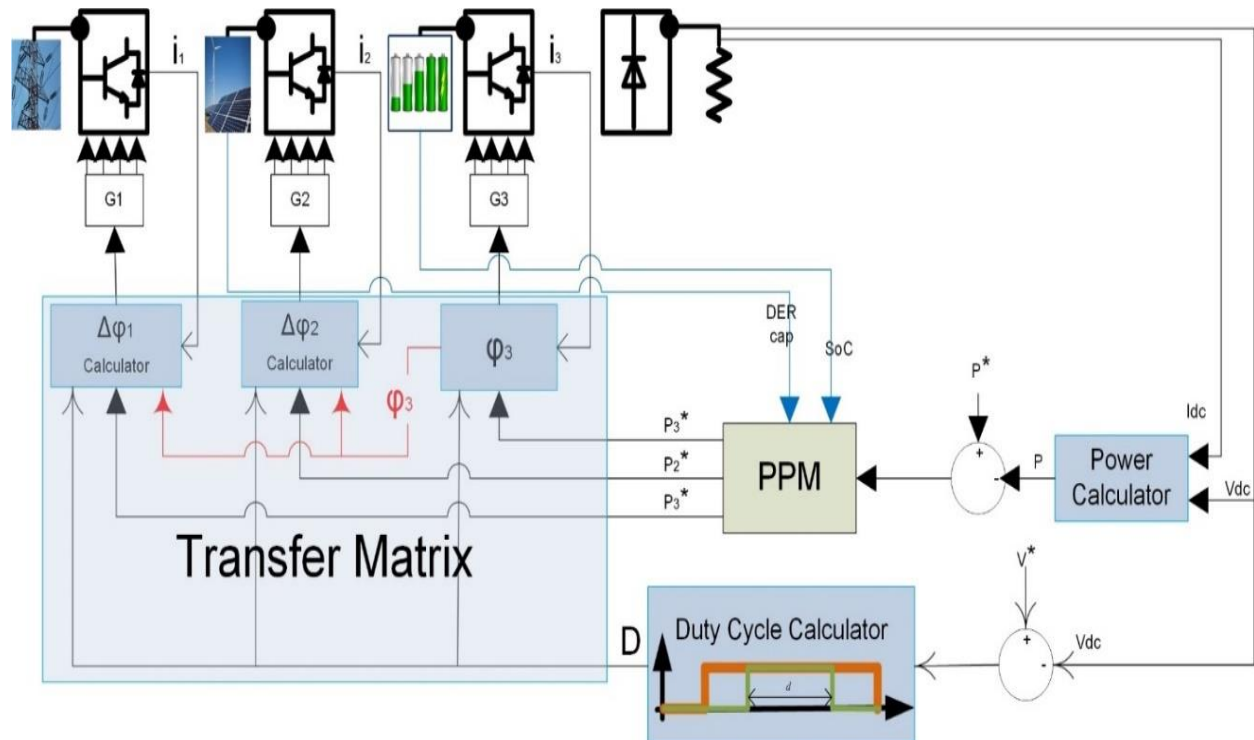


Figure 4-1 General architecture of MPSST control strategy

on the system parameters. The current and voltage of this four-port converter are controlled using proper gate signal for the three H-Bridge converters on the active legs.

Even though the converter of the fourth port is a full bridge diode rectifier, the parameters of this port are also controlled through a properly designed control of the three other controllable converters.

## **4.2 Multilayer Control for Voltage and Power Regulation in MPSST**

A two-layer control method is introduced and used in this project to regulate voltage and control power flow for the different ports. The output DC voltage is controlled using duty cycle control, which regulates the harmonic content of the square shape output voltage at the AC side of the converters. Then controlling the AC side of the converter, the output is regulated. The storage port converter is the reference converter for the voltage regulation since it is assumed to be the last remained source of power in the system. The result of primary control is sent to the second layer of the controller to control the current flow (and power exchange) of the different ports. The second layer of control uses a modified phase shift control (PSC) to adjust the power flow from the ports of converter based on the calculated values in the PPM chart.

### **4.2.1 Primary control**

Each active port in the MPSST has a high-frequency full bridge single phase inverter (Figure 4-2 (a)). In each H-bridge, the switch pairs  $S_1$ & $S_4$  and  $S_2$ & $S_3$  turn on and off alternately to form the square shape AC output voltage. Figure 4-2 shows an H-Bridge structure and a set of four gate signals which are used to generate a square shape ac voltage at the output. The second pair of the gate signals has the same D and frequency as the first set with  $180^\circ$  phase shift to generate a

symmetric output waveform. One switch from each pair ( $S_1$  &  $S_2$  in this case) is turned on for %50 of the time (minus the dead time in practical application), and by controlling the duty cycle of their paired switch, the harmonic content of the output voltage is controlled. Keeping one switch of each pair turned on for the cases of  $D < 50\%$  until just before turning on the parallel pair switches, creates zero potential between A and B for the off period and enables having zero states in the output waveform. If both of the switches are turned off before  $T/2$ , the current flows through the antiparallel diodes which creates a voltage at the load port and prevents having zero states. The peak value of the square shape output waveform of the converter is always equal to the DC bus voltage. However, controlling the duty cycle ( $D$ ) of the AC voltage, the average rectified DC voltage at the output of the diode bridge rectifier is controlled. Assuming the DC input voltages are regulated to be the same, all of the three H-Bridge converters receive the same duty cycle to have the same shape of AC voltage at the output.

In section 4-2-2 a transfer function between DC bus voltage and the AC side harmonic content is defined based on Fourier transform of the output AC voltage. The duty cycle control

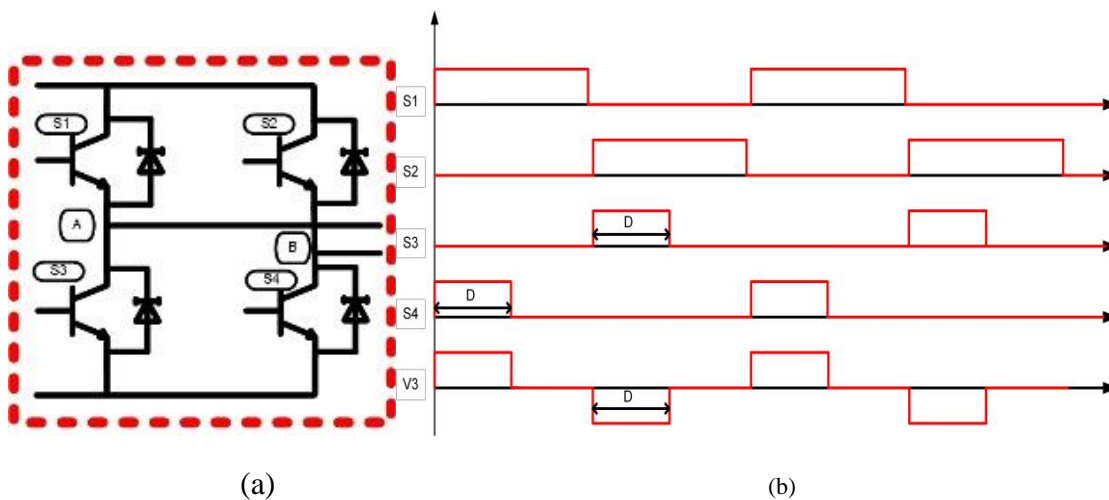


Figure 4-2 a) The configuration of an H-Bridge converter b) Duty cycle control for a single phase H-Bridge

also helps the controller to regulate the DC voltage fluctuation of the connected DC components with variable DC voltages like the ESS and RER.

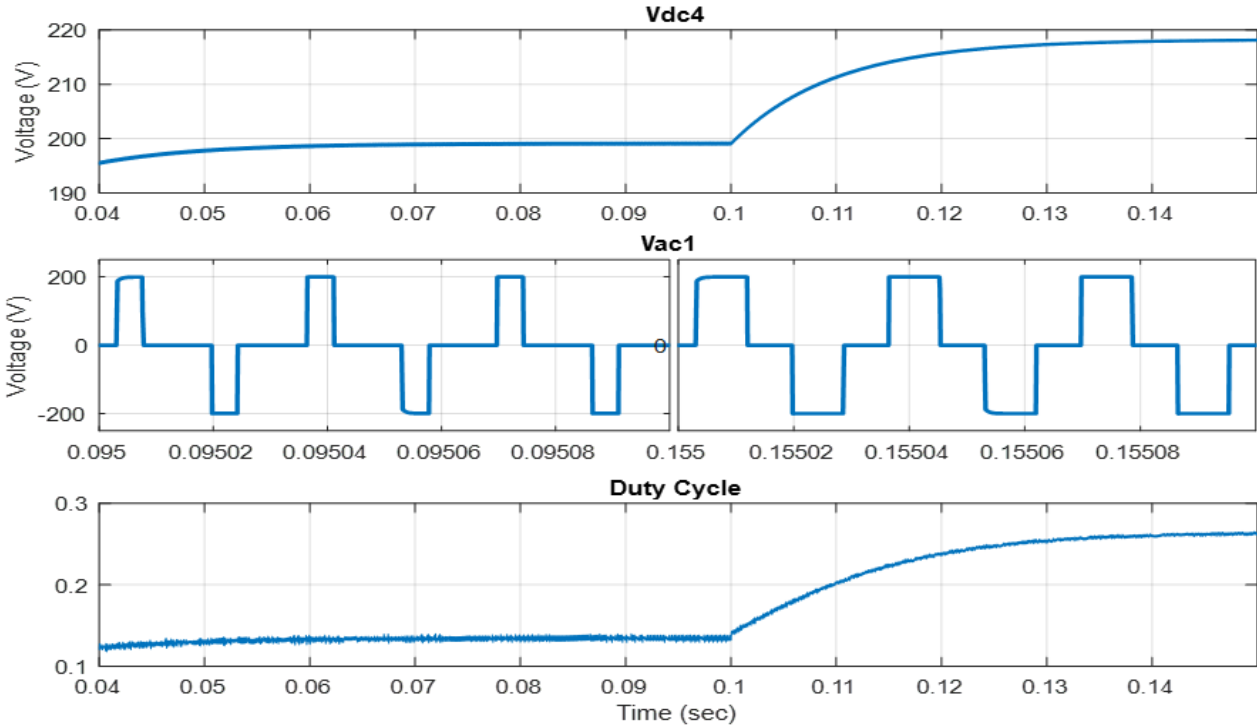


Figure 4-3. Simulation results of applying duty cycle control to regulate DC voltage

#### 4.2.2 Secondary control

The second layer of the controller controls the flow of power from different ports. Ultimately the summation of the exchanged power plus losses is zero.

$$P_1 + P_2 + P_3 + P_4 + P_{loss} = 0 \quad (4-1)$$

In the designed control strategy of MPSST, the pool of power method is the highest control block which specifies the share of power from each port to be absorbed or fed to the system. The results of PPM chart is one of the inputs to the component level controller to regulate the specified power from the ports. The current flow between the AC sides of each pair converters depends on

the magnitude and frequency of the voltages and the phase difference between two waveforms (4-5). The power flows between two sources if there is a voltage magnitude difference and/or phase shift between the two connected electrical buses [14][16], [19]. Assuming the AC output of the converters are regulated to have the same RMS value using duty cycle control, the current and power flow between each pair of converters is affected by their phase difference. The second layer of the component level controller uses a modified PSC method which controls the phase shift of the converter outputs to control the current and power the ports. Equation (4-5) shows that the power is proportional to  $\sin \varphi$  on the AC side of the converter. The calculated value of the equation for each port could be positive or negative which indicates feeding or absorbing power.

The transferred power between two AC voltages is calculated in (4-5). Each of the AC voltages is shown as a vector in Figure 4-4.

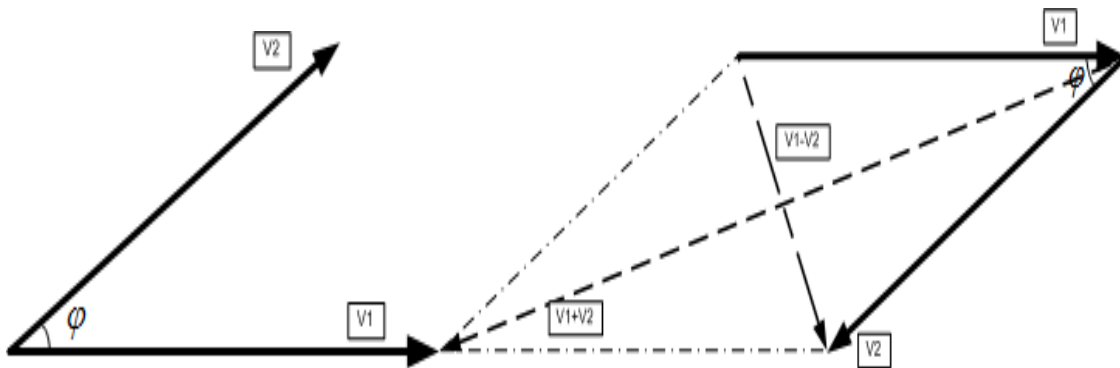


Figure 4-4. Two AC voltage vectors with phase shift

$$V_1 < 0 - V_2 < \varphi = \sqrt{(V_1 \cos 0 - V_2 \cos \varphi)^2 + (V_1 \sin 0 - V_2 \sin \varphi)^2} =$$

$$\sqrt{V_1^2 + V_2^2 \cos^2 \varphi - 2V_1 V_2 \cos \varphi + V_2^2 \sin^2 \varphi} \quad (4-2)$$

Assuming  $|V_1|=|V_2|$ :



$$V\sqrt{2(1 - \cos \varphi)} = V\sqrt{2(1 - 1 + 2 \sin^2 \frac{\varphi}{2})} = 2V \sin \frac{\varphi}{2} \quad (4-3)$$

$$I = \frac{V_1 < 0 - V_2 < \varphi}{Z} = \frac{V < 0 - V < \varphi}{Z} = \frac{2V \sin \frac{\varphi}{2}}{Z} \quad (4-4)$$

$$P = V * I = V < 0 * \frac{2V \sin \frac{\varphi}{2}}{Z} = V < \varphi * \frac{2V \sin \frac{\varphi}{2}}{\omega L - \frac{1}{\omega C}} < -\frac{\pi}{2} \approx V < \frac{\varphi}{2} * \frac{2V \sin \frac{\varphi}{2}}{\omega L - \frac{1}{\omega C}} = V \left( \cos \frac{\varphi}{2} + \right.$$

$$\left. \sin \frac{\varphi}{2} \right) * \frac{2V \sin \frac{\varphi}{2}}{\omega L - \frac{1}{\omega C}} = \frac{2V^2 \sin \frac{\varphi}{2} \cos \frac{\varphi}{2}}{\omega L - \frac{1}{\omega C}} = \frac{V^2 \sin \varphi}{\omega L - \frac{1}{\omega C}} \quad (4-5)$$

In the MPSST converter, the power flow of each port is affected by multiple parameters, but the total power exchange of each port is equal to the summation of the power flows between that port and each of the other ports. A modified phase shift control (PSC) is used to control the exchanged power from different ports.

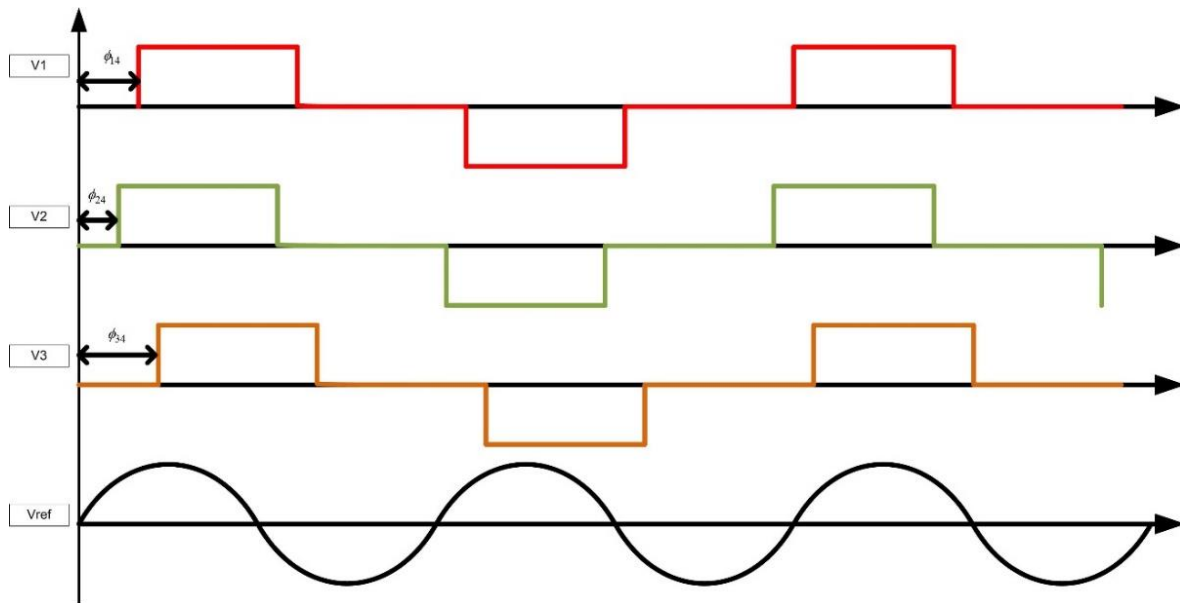


Figure 4-5. Phase shift control

### 4.2.3 4-Port black-box method for calculation of MPSST transfer matrix

In the four port SST of Figure 1-1, the output voltage of the load port and the current of the three other ports are dependent parameters which are calculated from PPM block or the demanded load or the lower voltage zone in the distribution application. Also, the load port current and voltages of the rest of the ports are independent parameters. A multi-input multi-output transfer matrix is calculated in (4-7) to show the effect of dependent parameters on each of the independent parameters.

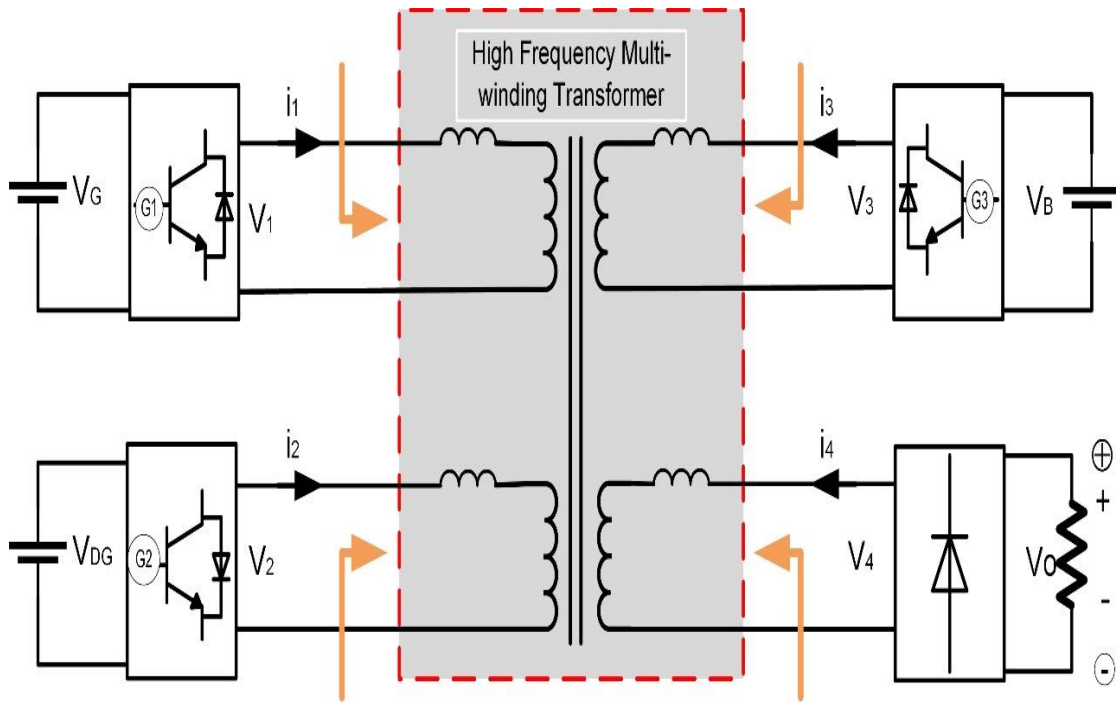


Figure 4-6. The general components of a four-port SST to calculate the transfer matrix of MPSST

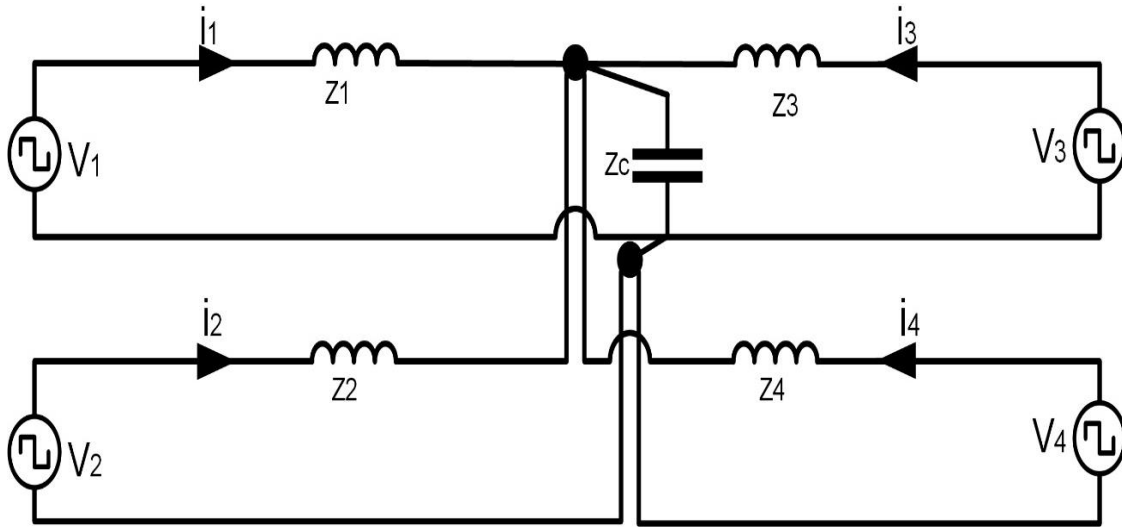


Figure 4-7. Equivalent circuit of the internal elements of four-port SST for calculation of transfer matrix

In this analysis, the gray box of Figure 4-6 which includes leakage inductance, magnetizing inductance, resonant circuit if any and any measured capacitance are considered as a single body with eight inputs and outputs parameters. The characteristics of the whole circuitry inside this box are simplified with four voltages and four currents of the related ports. The matrix elements are calculated using short circuit and open circuit analysis on the circuit. The SC and OC are applied on the circuit four times for each of the voltage sources separately.

The matrix elements show the relationship between independent and dependent parameters of the converter. This matrix could be used to optimize the system efficiency by finding the best operation points for each case based on the different constraints.

The MIMO transfer matrix of MPSST is shown in (4-6).

$$\begin{bmatrix} i_1 \\ i_2 \\ i_3 \\ v_4 \end{bmatrix} = \begin{bmatrix} A_{11} & A_{12} & A_{13} & A_{14} \\ A_{21} & A_{22} & A_{23} & A_{24} \\ A_{31} & A_{32} & A_{33} & A_{34} \\ A_{41} & A_{42} & A_{43} & A_{44} \end{bmatrix} \begin{bmatrix} v_1 \\ v_2 \\ v_3 \\ i_4 \end{bmatrix} \quad (4-6)$$

The MPSST topology of this study is a four-port converter with four DC voltages as the inputs. The phase shift control on the transferred power of the ports is applied on the AC voltages, and it is necessary to define an accurate transfer coefficient between DC and AC side of each H-Bridges which considers the control parameters like duty cycle and phase of each AC waveform.

The AC output of each port is a square shaped voltage. Figure 4-8 shows the generated output on the AC side of a single phase H-Bridge. The conversion coefficient “d” is a sinusoidal waveform with the frequency of  $f_s$ , scaled by modulation index and shifted with a controlled angle of  $\varphi$ .

$$v_i = v_G * d \tag{4-7}$$

The AC side waveform of each converter is a repeating square shape AC voltage (Figure 4-8). This waveform could be formulated like equation (4-8).

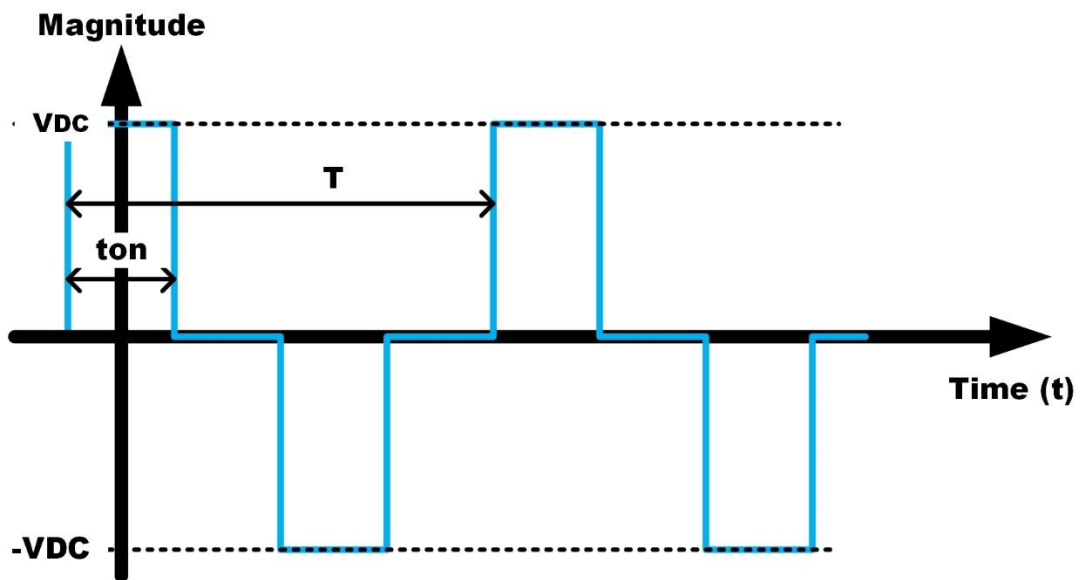


Figure 4-8. Square shape AC output of each active H-Bridge

$$V_i = \begin{cases} 1 & -\frac{T_{on}}{2} \leq t < \frac{T_{on}}{2} \\ 0 & \frac{T_{on}}{2} \leq t < \frac{T}{2} + \frac{T_{on}}{2} \\ -1 & \frac{T}{2} + \frac{T_{on}}{2} \leq t < \frac{T}{2} + \frac{3T_{on}}{2} \\ 0 & \frac{T}{2} + \frac{3T_{on}}{2} \leq t < T - \frac{T_{on}}{2} \end{cases} \quad (4-8)$$

The Fourier Transform of  $V_i$  shows that the repeating square waveform of Figure 4-8 contains a spectrum of different harmonics of the voltage including fundamental frequency. Equation (4-10) shows that the magnitude of the AC side voltage could be adjusted by controlling the duty cycle ( $\frac{t_{on}}{T}$ ). The general Fourier Transfer formula of this waveform which includes the phase shift is shown in (4-11).

$$f(t) = 0 + \sum_{n=1}^{\infty} (a_n \cos(n\omega_0 t) + 0) \quad (4-9)$$

$$a_n = 2 * \frac{2V_{DC}}{n\pi} \sin\left(n\pi \frac{t_{on}}{T}\right) \quad (4-10)$$

$$f(t - \varphi) = 0 + \sum_{n=1}^{\infty} (a_n \cos(n\omega_0 t - \varphi) + 0) \quad (4-11)$$

The same formula could be used for the diode bridge rectifier. In the case of diode bridge rectifier,  $t_{on}$  in Equation (4-11) is always equal to  $\frac{T}{2}$  and the equation is simplified to:

$$a_n = 2 * \frac{2V_{DC}}{n\pi} \sin\left(n \frac{\pi}{2}\right) \quad (4-12)$$

### 4.3 State Space Modeling of MPSST

The general form of the state space model of a system is shown in (4-13)

$$\begin{cases} \dot{X} = AX + BU \\ Y = CX + DU \end{cases} \quad (4-13)$$

In (4-13),  $U$  is the matrix of inputs,  $X$  represents the independent state vectors of the system and  $Y$  is the matrix of defined outputs of the system. Also  $A$ ,  $B$ ,  $C$  and  $D$  are the constant matrices of state, input, output and direct transition.

The first step in deriving the state space representation of a system is defining the independent state vectors of the system. It is necessary to analyze the equivalent circuit of the converter and simplify it to choose the independent state vectors properly to have an accurate state space model of the system.

Figure 4-9 shows the most general structure of a four-port SST. It includes possible inductors and capacitors of the filters, resonant circuits, snubber circuits, wire impedances, and transformer impedances.

Considering this general circuitry for the MPSST, the results of this analysis apply to any four-port configuration with similar topology like this converter.

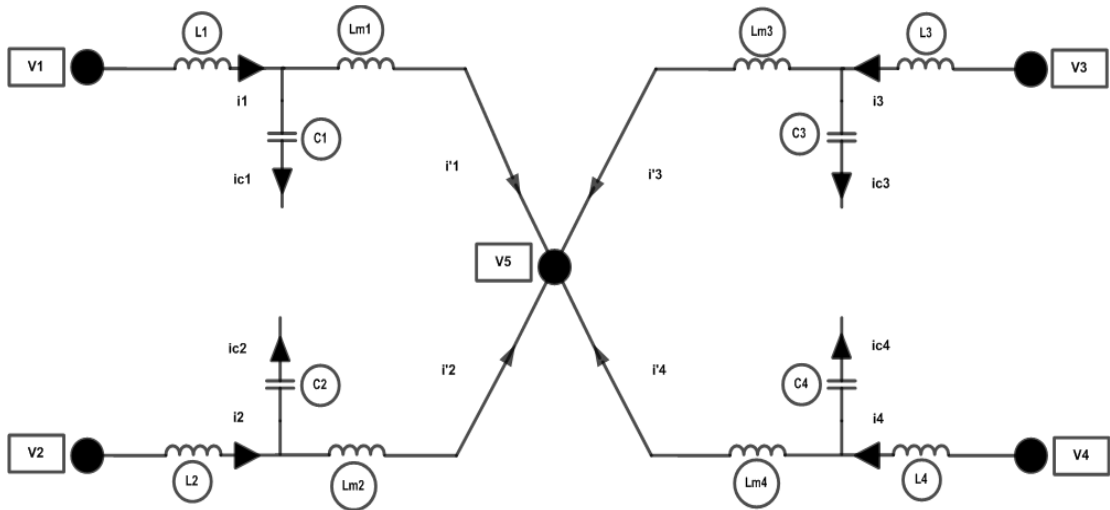


Figure 4-9. The equivalent circuit of general configuration of a four-port SST

The circuit in Figure 4-9 could be simplified by transferring the inductors to one side of the capacitor using an equivalent inductor (Figure 4-10 (a)). Then in the next step, the parallel capacitors on the four legs are replaced with an equivalent capacitor value (Figure 4-10 (b)).

$$L' = \frac{LL_m C \omega^2 - L - L_m}{LL_m C^2 \omega^3 - L_m C \omega^2 - 1} \quad (4-14)$$

$$C_z = C_1 + C_2 + C_3 + C_4 \quad (4-15)$$

The circuit in Figure 4-10 (C) is the final simplified form of the MPSST equivalent circuit. The idea is to select the independent state vectors which could represent any possible state of the system. In the state space analysis of the electrical circuits, the current of the inductors and the voltages of the capacitors are considered as system states vectors. Based on the chosen states and selected input and output parameters the differential equations of the system are derived to calculate the elements of the coefficient matrices (A, B, C, and D).

The matrix of inputs for the state space model of this topology includes the voltages of the grid port ( $v_{grid}$ ), RER port ( $v_{RER}$ ) and ESS port ( $v_{ESS}$ ) (4-16).

$$U = [v_G, v_{DG}, v_B] \quad (4-16)$$

Considering the circuit in Figure 4-10 (c) as the final simplified circuit, the currents of the inductors and the capacitor voltage are considered as the states in this analysis and the matrix of the state vectors is shown in (4-17).

$$X = [i_1, i_2, i_3, i_4, v_5] \quad (4-17)$$

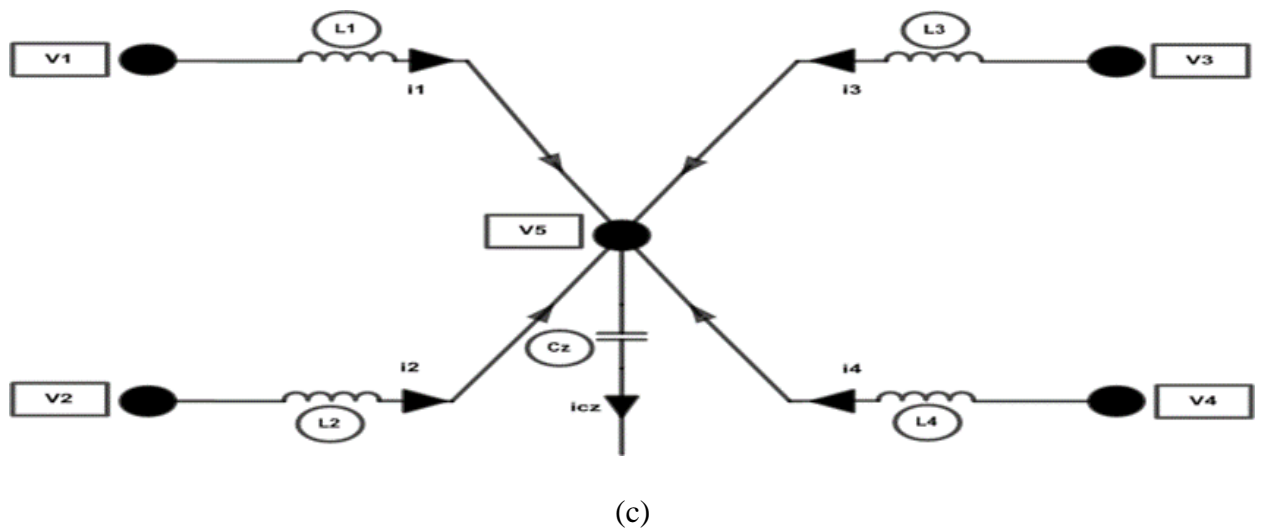
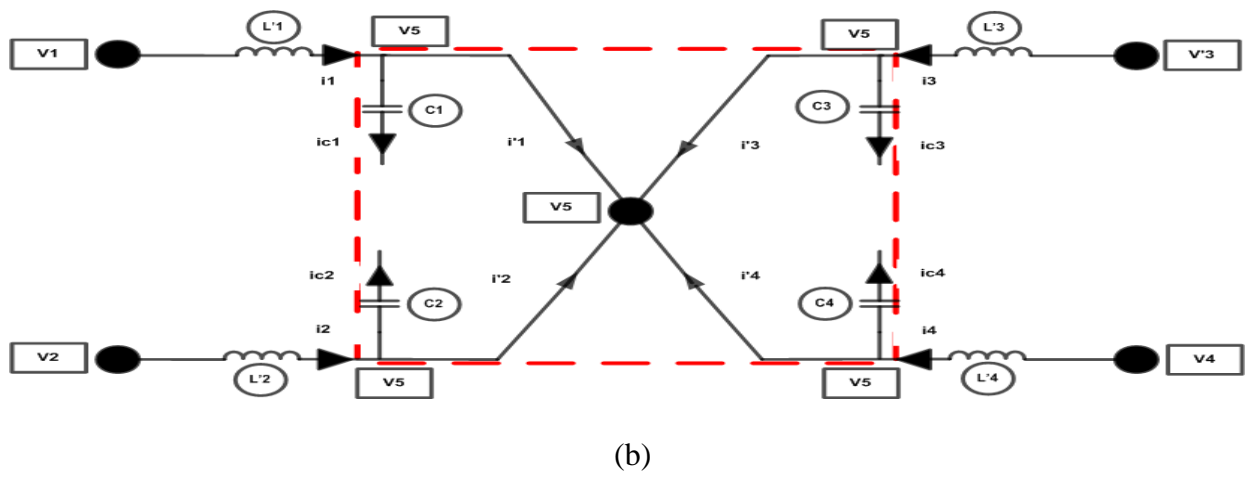
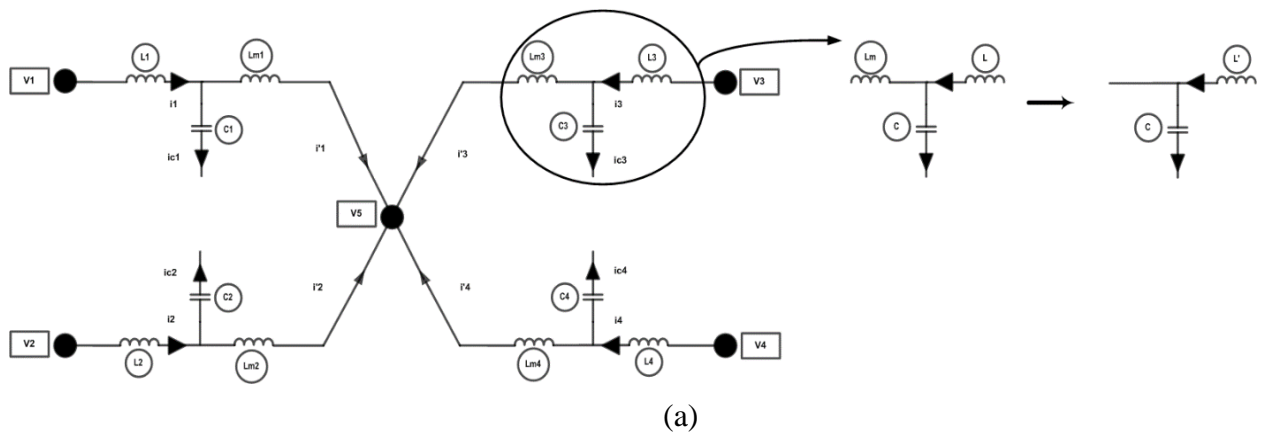


Figure 4-10. Circuit simplifications to optimize the number of states



And the Y matrix which includes the desired output parameters of the system is shown in (4-18).

$$Y=[i_1, i_2, i_3, v_4] \quad (4-18)$$

Then based on the defined matrices of inputs, states and outputs, the differential equations of the system are derived.

The differential equations of the system in (4-19) to (4-27) are used to form the state space matrices of the converter. In each equation, the derivative of that specified state is calculated in the form of a linear function of the inputs and the states. In the matrix representation form of these equations, all of the inputs and states are included, while some of the coefficients are zero.

$$i_1 = i^*_1 + i_{c1} \quad (4-19)$$

$$i_{c1} = C_1 \frac{dv_5}{dt} \quad (4-20)$$

$$v_1 - v_5 = L_1 \frac{di_1}{dt} = L_1 i^*_1 \quad (4-21)$$

$$i^*_1 = \frac{v_1 - v_5}{L_1} \quad (4-22)$$

$$i^*_2 = \frac{v_2 - v_5}{L_2} \quad (4-23)$$

$$i^*_3 = \frac{v_3 - v_5}{L_3} \quad (4-24)$$

$$i^*_4 = \frac{-Ri_4 - v_5}{L_4} = -\frac{R}{L_4} i_4 - \frac{1}{L_4} v_5 \quad (4-25)$$

$$C_z v^*_5 = i_{Cz} = i_1 + i_2 + i_2 + i_4 \quad (4-26)$$

$$v^*_5 = \frac{i_1 + i_2 + i_2 + i_4}{C_z} \quad (4-27)$$

Considering (4-28) as the AC side representation of the DC inputs, the matrixes of state space model of the MPSST are shown in equations (4-29) to (4-32).

$$\begin{cases} v_1 = d_1 V_G \\ v_2 = d_2 V_{RER} \\ v_3 = d_3 V_{ESS} \end{cases} \quad (4-28)$$

$$A = \begin{bmatrix} 0 & 0 & 0 & 0 & -\frac{1}{L1} \\ 0 & 0 & 0 & 0 & -\frac{1}{L2} \\ 0 & 0 & 0 & 0 & -\frac{1}{L3} \\ 0 & 0 & 0 & -\frac{R}{L4} & -\frac{1}{L4} \\ \frac{1}{Cz} & \frac{1}{Cz} & \frac{1}{Cz} & \frac{1}{Cz} & 0 \end{bmatrix} \quad (4-29)$$

$$B = \begin{bmatrix} \frac{d1}{L1} & 0 & 0 \\ 0 & \frac{d2}{L2} & 0 \\ 0 & 0 & \frac{d3}{L3} \\ 0 & 0 & 0 \\ 0 & 0 & 0 \end{bmatrix} \quad (4-30)$$

$$C = \begin{bmatrix} 1 & 0 & 0 & 0 & 0 \\ 0 & 1 & 0 & 0 & 0 \\ 0 & 0 & 1 & 0 & 0 \\ 0 & 0 & 0 & -R & 0 \end{bmatrix} \quad (4-31)$$

$$D = \begin{bmatrix} 0 & 0 & 0 \\ 0 & 0 & 0 \\ 0 & 0 & 0 \\ 0 & 0 & 0 \end{bmatrix} \quad (4-32)$$

The step response of the system with replacing the R, L and C with the actual measured values are shown in Figure 4-11, Figure 4-12 and Figure 4-13. In these figures, the snubber capacitor values are changed to change the overshoot of the step response.

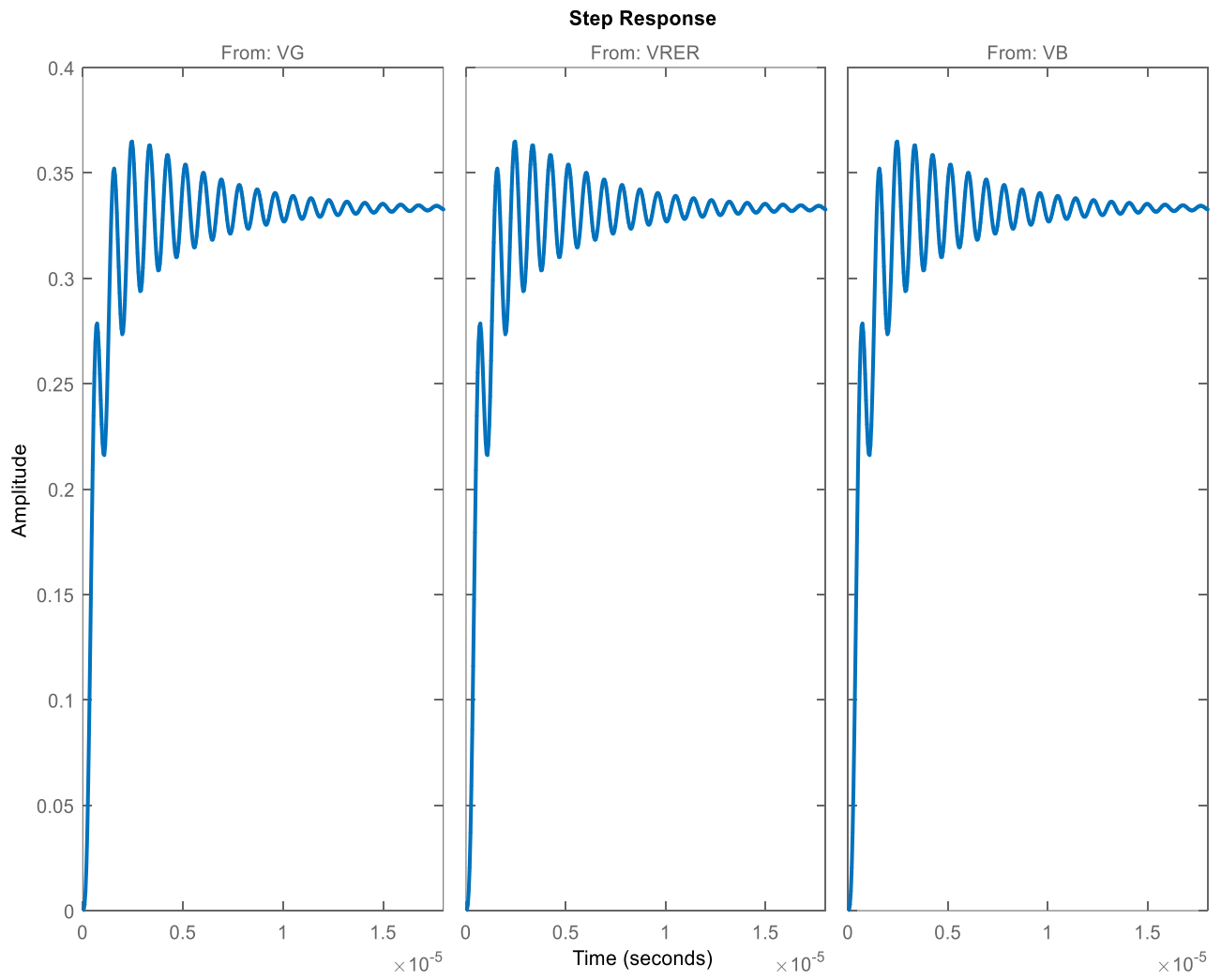


Figure 4-11. System step response considering V4 as the output and  $C=40\text{nF}$

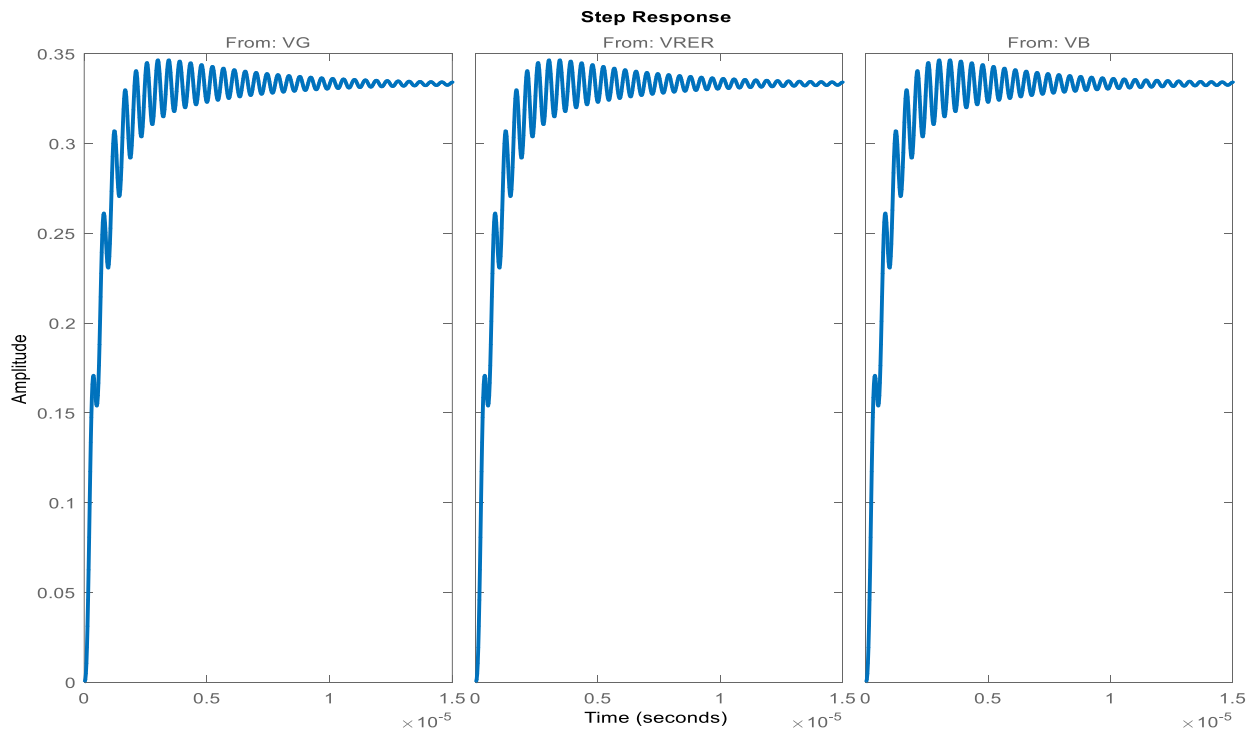


Figure 4-12. System step response considering V4 as the output and C=10nF

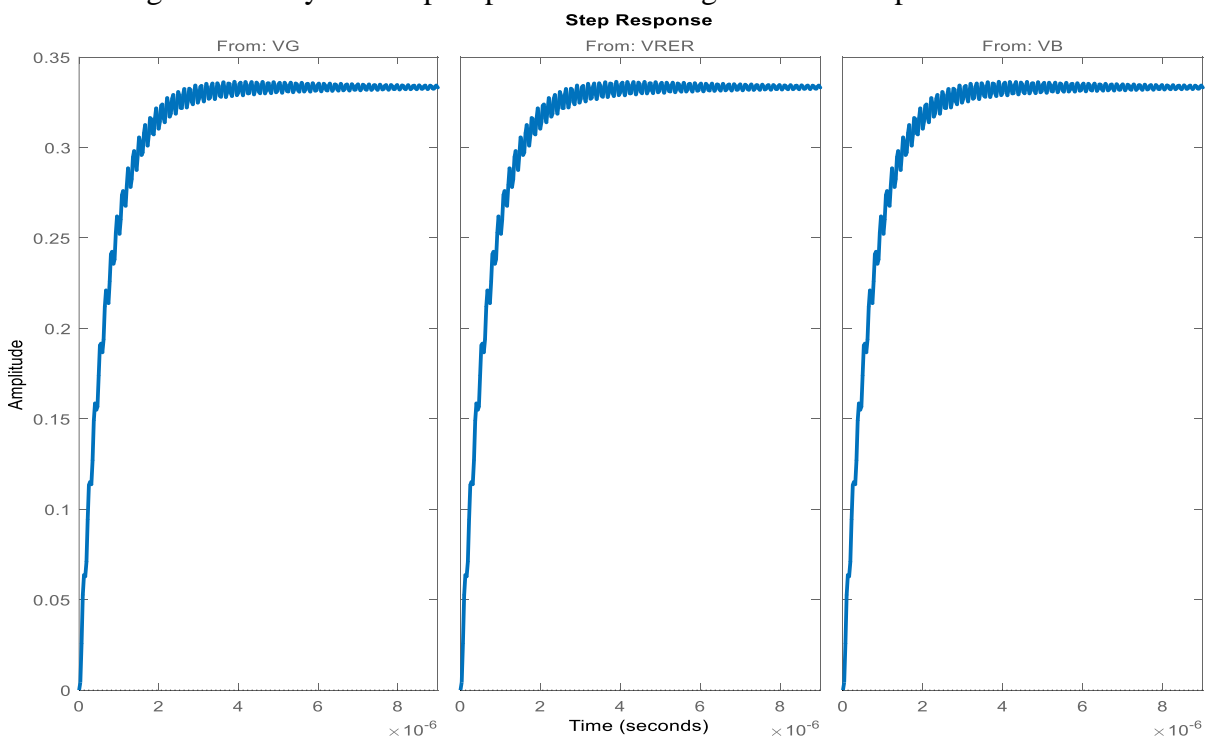


Figure 4-13. System step response considering V4 as the output and C=10nF

### 4.3.1 Modeling in dq reference frame

Transferring the system model to the dq reference frame, simplifies the control of the transferred power in the converter. The equation for calculating the exchanged power is shown in (4-33).

$$P = \frac{1}{2}(v_d i_d + v_q i_q) \quad (4-33)$$

For transferring the model to dq frame, all of the AC voltage and currents of the differential equations are transferred to dq frame using the general forms which are shown in (4-34) and (4-35).

$$i = i_d \sin(\omega_s t) + i_q \cos(\omega_s t) \quad (4-34)$$

$$V = v_d \sin(\omega_s t) + v_q \cos(\omega_s t) \quad (4-35)$$

$$i_1 = i_{1d} \sin(\omega_s t) + i_{1q} \cos(\omega_s t) \quad (4-36)$$

$$i_2 = i_{2d} \sin(\omega_s t) + i_{2q} \cos(\omega_s t) \quad (4-37)$$

$$i_3 = i_{3d} \sin(\omega_s t) + i_{3q} \cos(\omega_s t) \quad (4-38)$$

$$i_4 = i_{4d} \sin(\omega_s t) + i_{4q} \cos(\omega_s t) \quad (4-39)$$

$$v_1 = v_{1d} \sin(\omega_s t) + v_{1q} \cos(\omega_s t) \quad (4-40)$$

$$v_2 = v_{2d} \sin(\omega_s t) + v_{2q} \cos(\omega_s t) \quad (4-41)$$

$$v_3 = v_{3d} \sin(\omega_s t) + v_{3q} \cos(\omega_s t) \quad (4-42)$$

$$v_4 = v_{4d} \sin(\omega_s t) + v_{4q} \cos(\omega_s t) \quad (4-43)$$

$$v_5 = v_{5d} \sin(\omega_s t) + v_{5q} \cos(\omega_s t) \quad (4-44)$$

Then the matrices of the inputs, state vectors, and outputs are formed by transferring parameters to dq frame and considering the d and q component of each parameter separately.

$$U = \begin{bmatrix} V_{Gd} \\ V_{Gq} \\ V_{DGd} \\ V_{DGq} \\ V_{Bd} \\ V_{Bq} \\ -i_{4d} \\ -i_{4q} \end{bmatrix} \quad (4-45)$$

$$X = \begin{bmatrix} i_{1d} \\ i_{1q} \\ i_{2d} \\ i_{2q} \\ i_{3d} \\ i_{3q} \\ v_{5d} \\ v_{5q} \end{bmatrix} \quad (4-46)$$

$$Y = \begin{bmatrix} i_{1d} \\ i_{1q} \\ i_{2d} \\ i_{2q} \\ i_{3d} \\ i_{3q} \\ v_{4d} \\ v_{4q} \end{bmatrix} \quad (4-47)$$

Finally, replacing the parameters of the equations in the ABC frame with the new parameters, the equations are transferred to the dq frame. Then using the new set of the equations, the A, B, C, and D matrices of the state space model of the MPSST are formed in dq frame which simplifies the control of the exchanged power.

$$i_{1d}^* \sin(\omega_s t) + \omega_s i_{1d} \cos(\omega_s t) + i_{1q}^* \cos(\omega_s t) + \omega_s i_{1q} \sin(\omega_s t) = \frac{1}{L_1} (v_{1d} \sin(\omega_s t) + v_{1q} \cos(\omega_s t) - v_{5d} \sin(\omega_s t) - v_{5q} \cos(\omega_s t)) \quad (4-48)$$

$$i_{1d}^* = \omega_s i_{1q} + \frac{1}{L_1} (m_{1d} v_G - v_{5d}); \quad (4-49)$$

$$i_{1q}^* = -\omega_s i_{1d} + \frac{1}{L_1} (m_{1q} v_G - v_{5q}) \quad (4-50)$$

$$i'_{2d} = \omega_s i_{2q} + \frac{1}{L_2} (m_{2d} v_{DG} - v_{5d}); \quad (4-51)$$

$$i'_{2q} = -\omega_s i_{2d} + \frac{1}{L_2} (m_{2q} v_{DG} - v_{5q}) \quad (4-52)$$

$$i'_{3d} = \omega_s i_{3q} + \frac{1}{L_3} (m_{3d} v_B - v_{5d}); \quad (4-53)$$

$$i'_{3q} = -\omega_s i_{3d} + \frac{1}{L_3} (m_{3q} v_B - v_{5q}) \quad (4-54)$$

$$\begin{aligned} v'_{5d} \sin(\omega_s t) + \omega_s v_{5d} \cos(\omega_s t) + v'_{5q} \cos(\omega_s t) - \omega_s v_{5q} \sin(\omega_s t) = \frac{1}{C_z} (i_{1d} \sin(\omega_s t) + \\ i_{1q} \cos(\omega_s t) + i_{2d} \sin(\omega_s t) + i_{2q} \cos(\omega_s t) + i_{3d} \sin(\omega_s t) + i_{3q} \cos(\omega_s t) + i_{4d} \sin(\omega_s t) + \\ i_{4q} \cos(\omega_s t)) \end{aligned} \quad (4-55)$$

$$v'_{5d} = \omega_s v_{5q} + \frac{1}{C_z} (i_{1d} + i_{2d} + i_{3d} + i_{4d}) \quad (4-56)$$

$$v'_{5q} = -\omega_s v_{5d} + \frac{1}{C_z} (i_{1q} + i_{2q} + i_{3q} + i_{4q}) \quad (4-57)$$

$$A = \begin{bmatrix} 0 & \omega_s & 0 & 0 & 0 & 0 & 0 & 0 & -\frac{1}{L_1} & 0 \\ -\omega_s & 0 & 0 & 0 & 0 & 0 & 0 & 0 & 0 & -\frac{1}{L_1} \\ 0 & 0 & 0 & \omega_s & 0 & 0 & 0 & 0 & -\frac{1}{L_2} & 0 \\ 0 & 0 & -\omega_s & 0 & 0 & 0 & 0 & 0 & 0 & -\frac{1}{L_2} \\ 0 & 0 & 0 & 0 & 0 & \omega_s & 0 & 0 & -\frac{1}{L_3} & 0 \\ 0 & 0 & 0 & 0 & -\omega_s & 0 & 0 & 0 & 0 & -\frac{1}{L_3} \\ 0 & 0 & 0 & 0 & 0 & 0 & -\frac{R}{L_4} & \omega_s & 0 & 0 \\ 0 & 0 & 0 & 0 & 0 & 0 & -\omega_s & -\frac{R}{L_4} & 0 & 0 \\ \frac{1}{C_z} & 0 & \frac{1}{C_z} & 0 & \frac{1}{C_z} & 0 & \frac{1}{C_z} & 0 & 0 & 0 \\ 0 & \frac{1}{C_z} & 0 & \frac{1}{C_z} & 0 & \frac{1}{C_z} & 0 & \frac{1}{C_z} & 0 & 0 \end{bmatrix} \quad (4-58)$$

$$B = \begin{bmatrix} \frac{1}{L_1} & 0 & 0 & 0 & 0 & 0 \\ 0 & \frac{1}{L_1} & 0 & 0 & 0 & 0 \\ 0 & 0 & \frac{1}{L_2} & 0 & 0 & 0 \\ 0 & 0 & 0 & \frac{1}{L_2} & 0 & 0 \\ 0 & 0 & 0 & 0 & \frac{1}{L_3} & 0 \\ 0 & 0 & 0 & 0 & 0 & \frac{1}{L_3} \\ 0 & 0 & 0 & 0 & 0 & 0 \\ 0 & 0 & 0 & 0 & 0 & 0 \\ 0 & 0 & 0 & 0 & 0 & 0 \\ 0 & 0 & 0 & 0 & 0 & 0 \end{bmatrix} \quad (4-59)$$

$$C = \begin{bmatrix} 1 & 0 & 0 & 0 & 0 & 0 & 0 & 0 & 0 & 0 \\ 0 & 1 & 0 & 0 & 0 & 0 & 0 & 0 & 0 & 0 \\ 0 & 0 & 1 & 0 & 0 & 0 & 0 & 0 & 0 & 0 \\ 0 & 0 & 0 & 1 & 0 & 0 & 0 & 0 & 0 & 0 \\ 0 & 0 & 0 & 0 & 1 & 0 & 0 & 0 & 0 & 0 \\ 0 & 0 & 0 & 0 & 0 & 1 & 0 & 0 & 0 & 0 \\ 0 & 0 & 0 & 0 & 0 & 0 & -R & 0 & 0 & 0 \\ 0 & 0 & 0 & 0 & 0 & 0 & 0 & -R & 0 & 0 \end{bmatrix} \quad (4-60)$$

$$D = \begin{bmatrix} 0 & 0 & 0 & 0 & 0 & 0 \\ 0 & 0 & 0 & 0 & 0 & 0 \\ 0 & 0 & 0 & 0 & 0 & 0 \\ 0 & 0 & 0 & 0 & 0 & 0 \\ 0 & 0 & 0 & 0 & 0 & 0 \\ 0 & 0 & 0 & 0 & 0 & 0 \\ 0 & 0 & 0 & 0 & 0 & 0 \\ 0 & 0 & 0 & 0 & 0 & 0 \end{bmatrix} \quad (4-61)$$

In the last step, the conversion coefficients between DC and AC side of the full bridge converter on each port are transferred to dq frame.

The representation of the DC voltage transferred to the AC side of the H-Bridge inverter in dq frame is shown in (4-62).

$$v_i = m_i v_{DCi} \sin(\omega_s t + \varphi_i) = m_{id} v_{DCi} \sin(\omega_s t) + m_{iq} v_{DCi} \cos(\omega_s t) \quad (4-62)$$



## CHAPTER 5

### Implementation and Testing of MPSST

The design and implementation process of an isolated power electronic converter consists of six major phases. Figure 5-1 shows the major phases of the design process. Before starting the process, it is necessary to specify the nominal range of the inputs and the expected outputs. Then based on the defined applications of the converter, the configuration is selected and the design process starts.

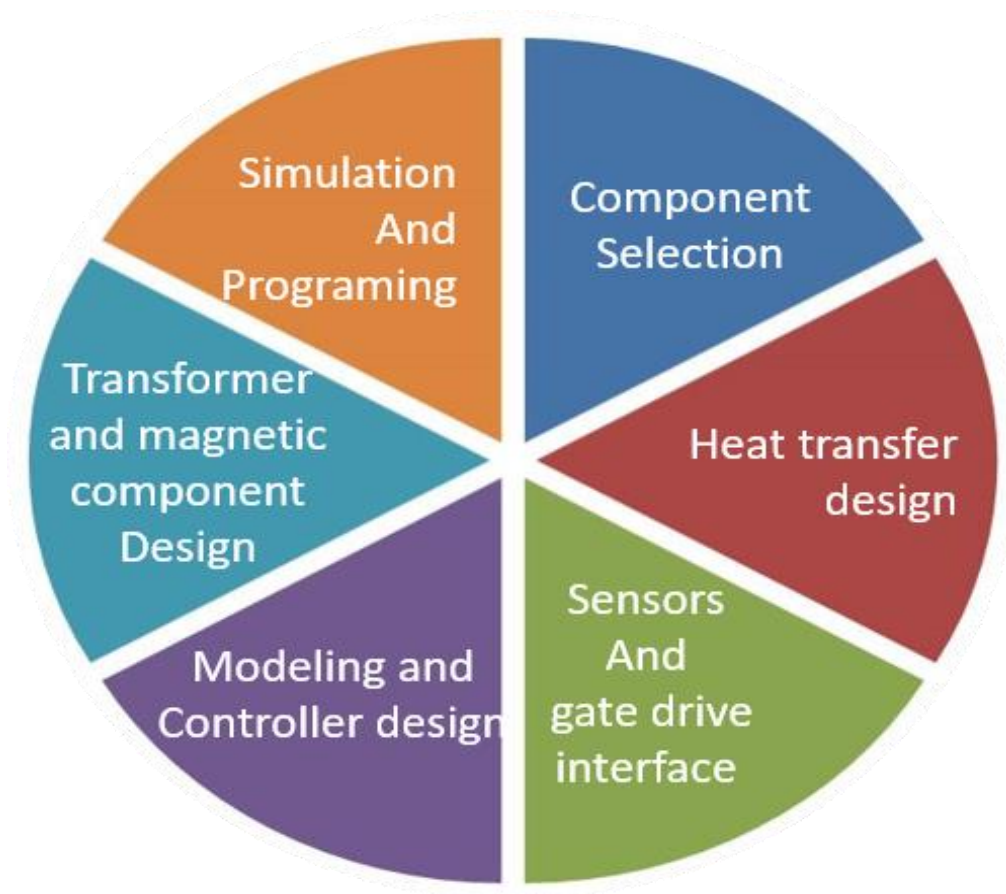


Figure 5-1. Design steps for building an isolated PE converter

The design target for this project is to achieve power density bigger than  $2.5\text{w}/\text{inch}^3$  for the first prototype of the four port solid state transformer in the operating voltage range of 200 V-450 V. The power target is 10 kW from each port. The 2-D drawing of the converter box and placement of the main components is shown in Figure 5-2. In this configuration, the transformer is in the middle of the box, and the heat sinks and converters are placed around it at the corners of the box. The ratios between the sizes of the components in this figure are same as the ratios of the sizes of the real components. The wirings and sensors are not shown in this figure. The positions of the components in Figure 5-2 are chosen to minimize the distances between capacitors and the DC side of the MOSFET modules, the length of wires between the transformer and the modules and the length of the ribbon cable between the controller and the gate drive boards.

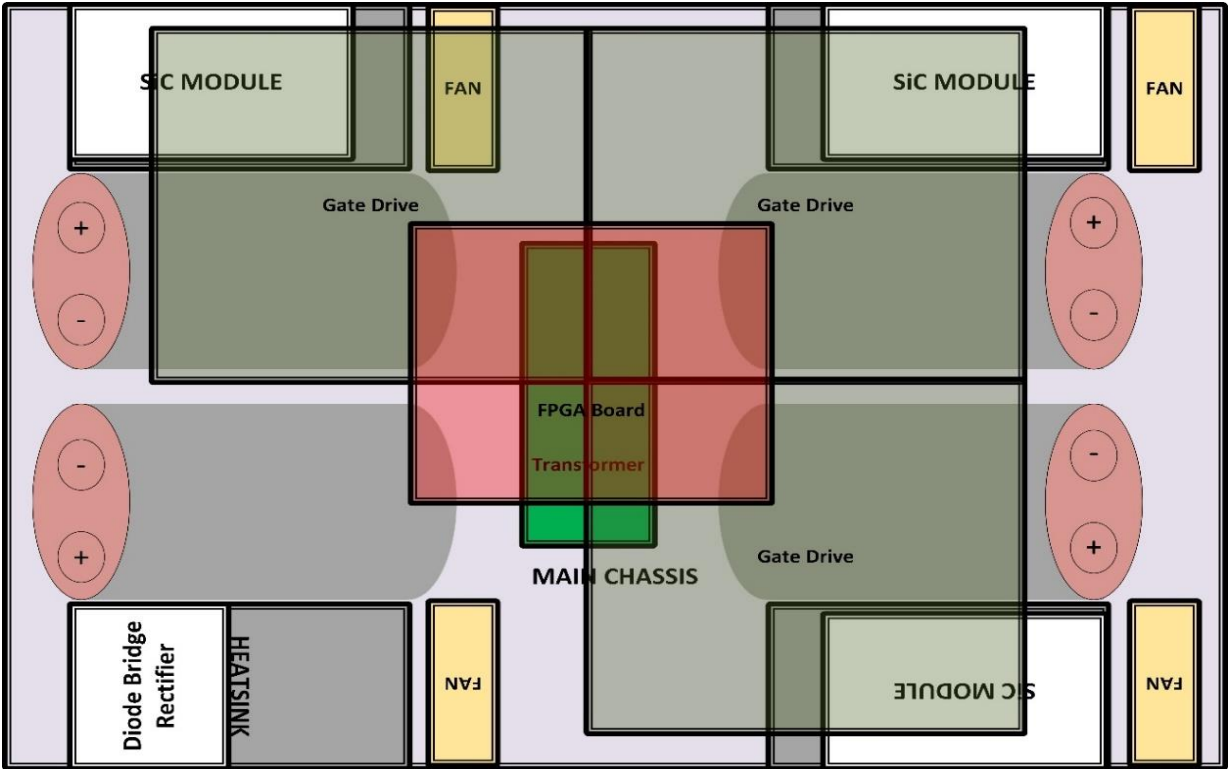


Figure 5-2. 2-D design of component placement in the converter box

The first step in the design process of the converter is simulating the converter using a software and running the system with the real parameters in the different modes of operation in a simulation environment. This simulation is used to prove the validity of the configuration and the designed controller. Then the mathematical model of the converter is developed and based on that a controller is designed to regulate the expected output parameters based on the given inputs. The designed controller should be verified in the simulation environment before application on the actual hardware. After this simulation analysis of the chosen configuration and the designed controller, the next steps are the design of the heat sink and cooling system, component selection, transformer design and snubber and filter circuit design.

## **5.1 Simulation and programming**

Three different simulation software are used in this project. The first software is ANSYS Maxwell 3D which, is used to analyze the design of transformer. Section 5-4 describes the transformer design process. Also, MATLAB/Simulink is used for simulating the MPSST converter and the SST based distribution system. Beside, PCB123 and Altium are used to develop the interface PCB for the converter.

In the converter level simulation, the four port SST is simulated in MATLAB/Simulink, and the suggested controller is implemented in the software. This simulation includes an embedded m-file code of the PPM block. This simulation is used to tune the controller gains. The ultimate goal of the simulation is to have a properly functioning simulation with a stable controller which follows the reference command values.

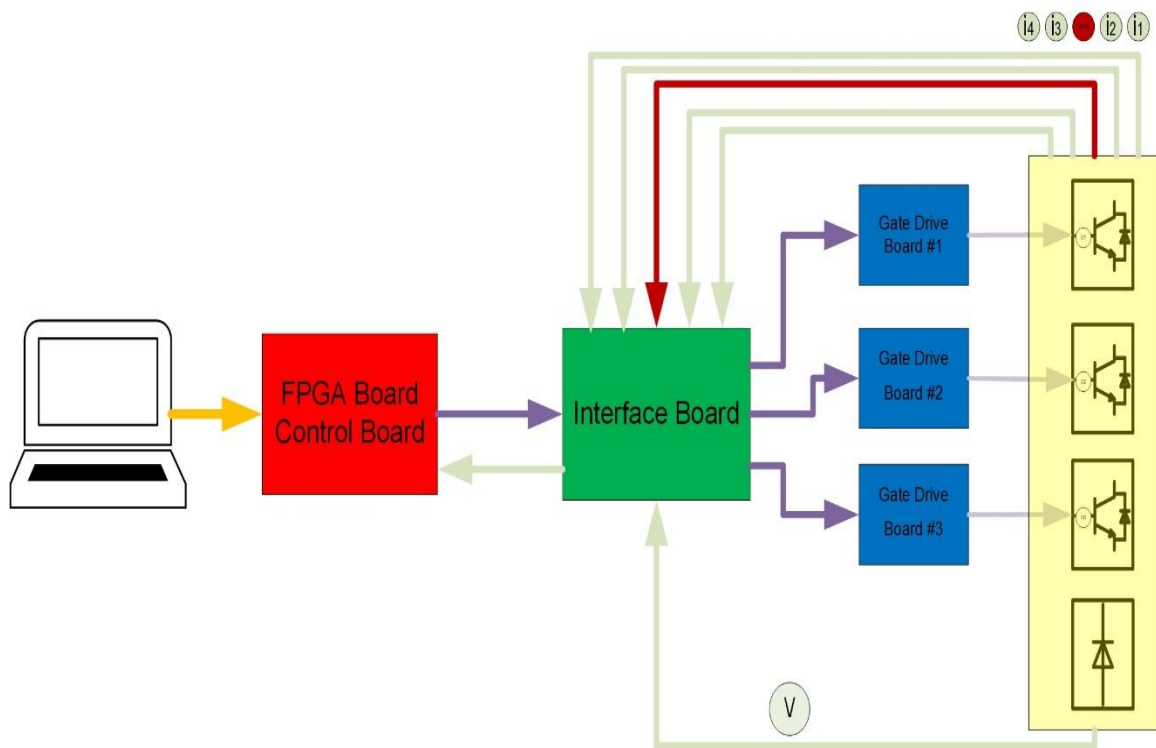


Figure 5-3. The control and sensing structure of the MPSST

After tuning the controller gains in the simulation, a VHDL code is developed based on the designed controller to program the hardware control board. The controller board is a customized FPGA board based on Altera MAXII IC. The code is used to generate three sets of gate signals for the MOSFET modules. It generates the duty cycle and the angle command of the AC outputs of the three H-Bridge converters.

Figure 5-3 shows the complete routes of the control signals and the measured parameter feedbacks. The output control signals of the control board are sent to the interface board. The interface PCB (Figure 5-4) is designed to distribute the generated gate signals from the control board to the gate drive boards and also to receive the voltage, current and temperature feedback signals and send them back to the controller. The design of the interface PCB is done using the PCB123 software.

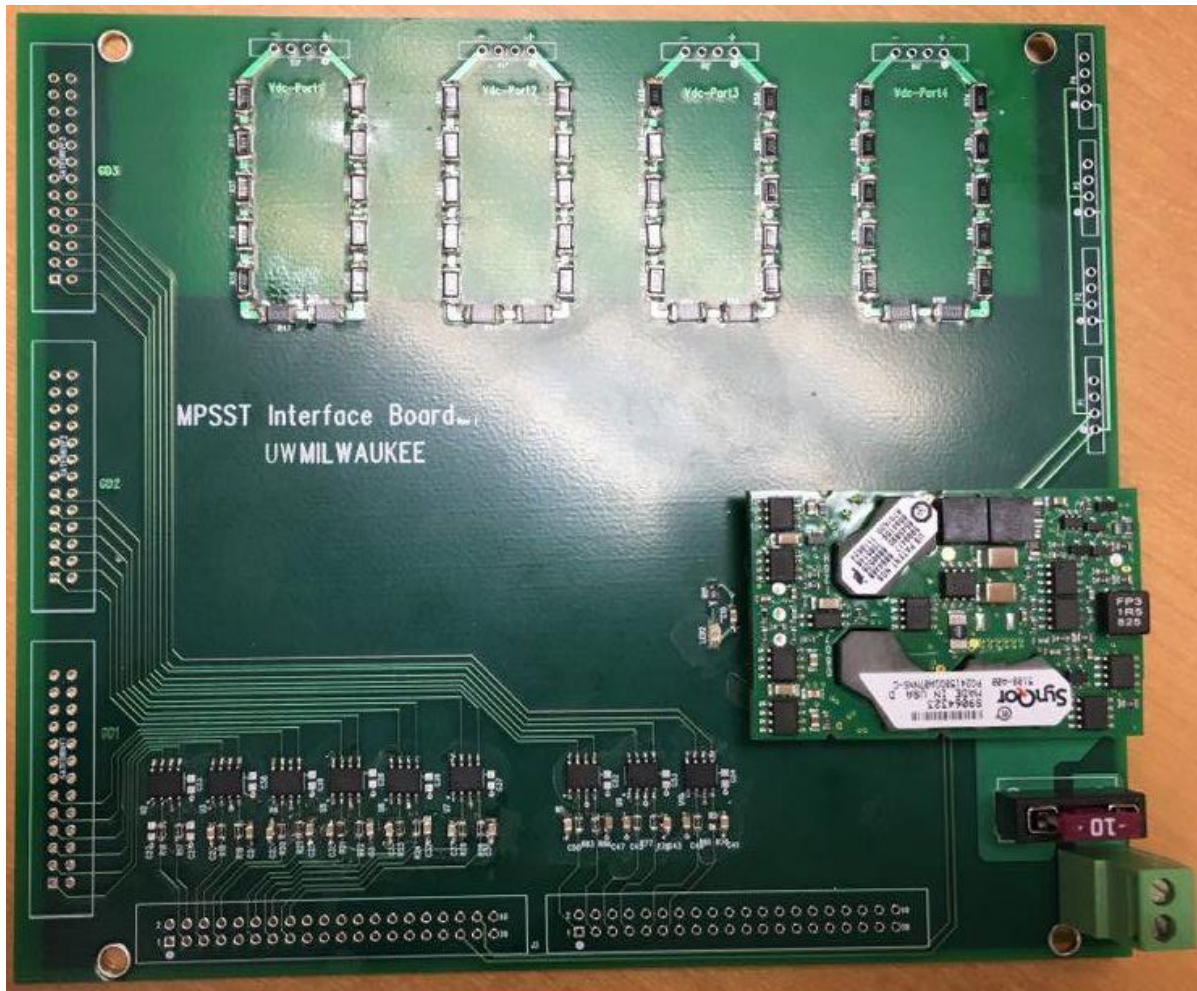


Figure 5-4 MPSST interface board

MATLAB/Simulink is used for simulating of a DC/AC zonal microgrid which is described in section 3.2 (Figure 3-3) which uses different types of SST to provide different zones of voltage for the load. The main idea of this architecture is to have a system which provides a combination of AC and DC connecting busbars for the connection of AC and DC components with minimum conversion steps. These simulations are used to study the benefits of having SST and MPSST in the power system as it is described in chapter 3.

An SST could have different input and outputs based on the design and number of the conversion stages. In the most general case, the voltages of the both sides of the converter are AC. An AC to AC solid state converter includes five stages of power conversion. The same conversion phases happen in a multi-port SST topology. A five-step AC/AC solid state transformer is shown in Figure 5-5. Figure 5-6 shows the simulation results of different waveform conversion in this converter.

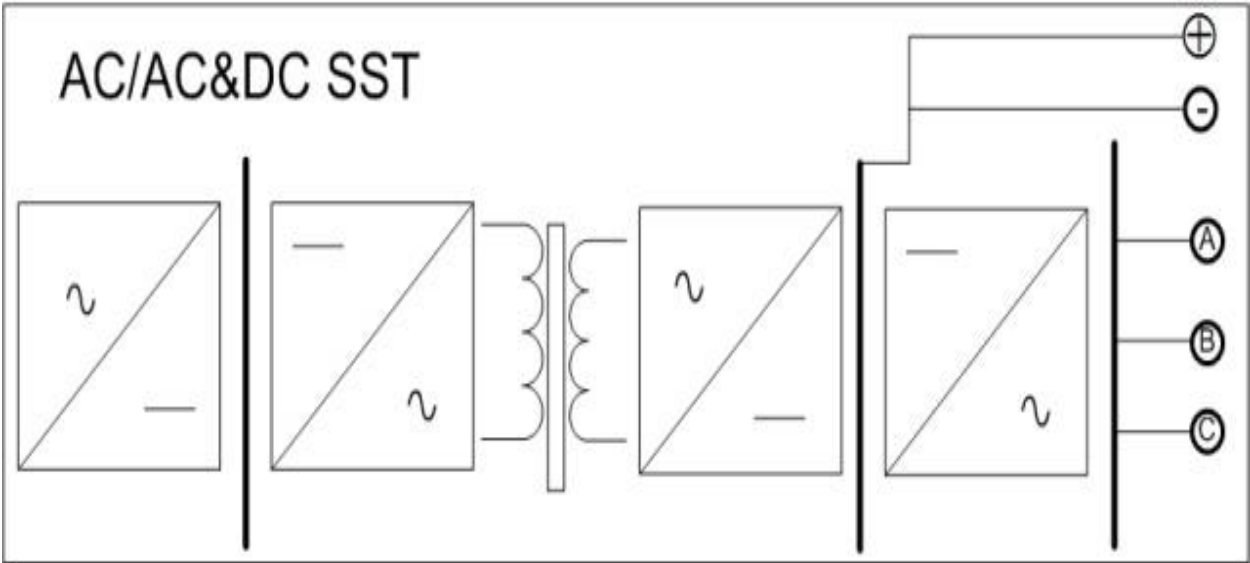


Figure 5-5. AC/AC solid state transformer

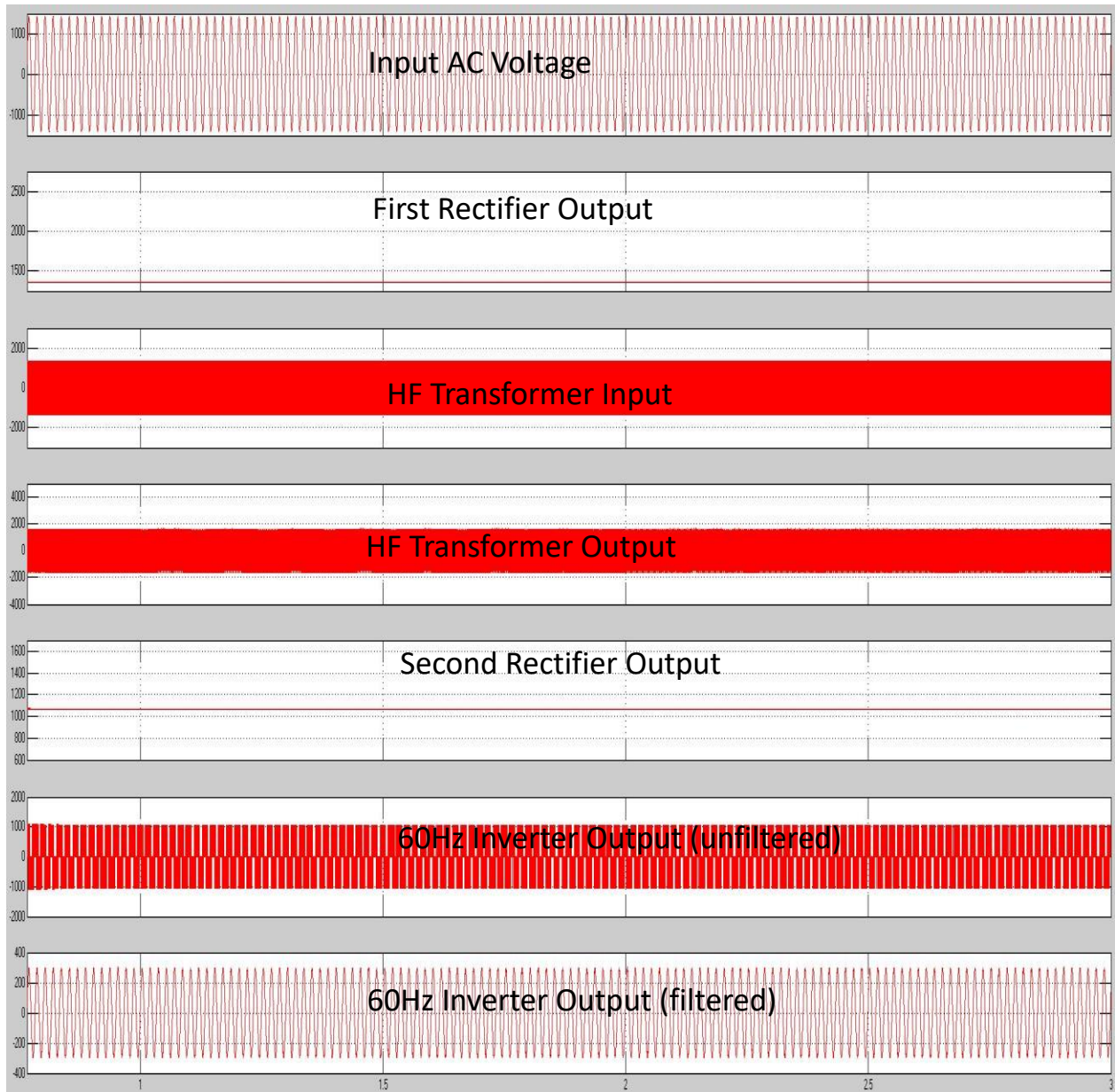


Figure 5-6. Simulation results of different conversion steps of a solid state transformer

## 5.2 Component Selection and Design Consideration

The component selection includes two major parts. The first part is main circuit components selection which includes selection of switches, diodes, capacitors and transformer material. The second part is selection of measurement components, and wires.

Due to the frequent target of up to 100 kHz, a large capacitor is needed for the DC bus. It is also important to have a connection link between the capacitor and the DC side of the converter with minimum possible inductance. The capacitors are connected to the switch modules using a copper bus to minimize the inductance values.

The frequency of the AC parts of the transformer is in the range of medium/high frequency to minimize the size of transformer. However, the high-frequency design dictates some constraints on the design of the transformer which are discussed in the next section.

Selecting a proper switch module is an important phase of high-frequency converter design since it affects the applicable frequency range and the module loss. Considering the available technologies in the market the silicon carbide (SiC) MOSFET modules are chosen for our application since it has very low on-resistance in compare to the Si-based switches and the MOSFET enables high-frequency switching. The lower loss improves the efficiency of the converter and decreases the size of cooling system

The final selected module is SiC MOSFET module-Wolfspeed-CCS050M12CM2. It has a voltage rating around 2.5 times of the defined voltage of the converter. The selected module is a three-phase switch module with three legs, but the topology of this project only uses two legs of the switches. However, the modules are capable of extending in the future for three-phase application and testing. The selected module is shown in Figure 5-7 (a), and the main characteristics of this module is summarized in Figure 5-1.





Figure 5-7. (a)The selected silicon carbide MOSFET module; (b) The selected fast recovery diode module

Table 5-1. Selected switch module characteristics

Blocking Voltage	1200 V
Current Rating	50 A
$R_{ds(On)}$ At 25°C	25 mΩ
Maximum Junction Temperature	150 °C

This switch module is used for three active H-Bridges on the three bi-directional ports. The fourth port uses a full bridge diode rectifier. Three characteristics which are considered in the selection of the diodes for this application are operation voltage range, operation current limit and the reverse recovery time since the input AC voltage to the diode bridge is a high-frequency waveform. The selected diode module is shown in Figure 5-7 (b). Each module includes two diodes, and a full bridge diode rectifier is formed with two modules. The nominal voltage of each diode is 1000 V, the nominal current is 60 A, and the reverse recovery is as small as 35 nanoseconds at max.

Table 5-2 shows the design parameters and the chosen components for MPSST application.

Table 5-2. The converter design parameter and components

Characteristic	Value
Input Voltage	All DC/200-400V
Passive Port Output Voltage	Load leg 300V
Nominal Power	Each port:10kW- 15kW max total at the same time
Transformer Turn Ratio	4:4:4:6
Target Frequency	<100kHz
Transformer Core Material	Ferrite B: 0.25 T
Transformer Winding Wire	Litz Wire, Eq 8AWG- 38AWG strand
Leakage and Magnetizing Inductance	$L_x(1-4)= 2e-6$ ; $L_m=75e-6$
Core Area	0.001 m <sup>2</sup>
Chosen Switch Modules	SiC MOSFET module-Wolfspeed-CCS050M12CM2
Fast recovery diode modules	IXYS DSEI 2x 61-10B X2
DC bus Cap	680 $\mu$ F
Snubber Cap	1nF
Control Board	Altera-FPGA max II chip

### **5.3 Transformer Design Consideration and Implementation**

The design of high-frequency transformer as the main component of the solid state transformer configuration is the most important part of the converter design process. In an MPSST converter, several windings feed the core of the transformer, and the coupling coefficients between windings are important parameters to be considered in an efficient converter design. Since the transformer is designed for high-frequency applications, the power loss in the wire and core of the transformer increases due to the higher skin effect and eddy current loss in the high frequency [53].

Three important parameters are studied for the optimal design of a multi-winding transformer for the MPSST converter. The first design parameter is core design including material selection for the HF application [10]. This parameter directly affects the core loss and the nominal frequency range of the converter [18]. Then the selection of the wire to minimize the skin effect and wire loss is studied. The third parameter is windings placement on the transformer core and distribution of wire turns. These factors are important in the design of any transformer, but they become critical for the MPSST converter, due to the application of high-frequency voltage to the transformer and having more than two windings on the transformer. The relation between transformer size, power rating, core flux density, and operation frequency is shown in (2-1).

#### **5.3.1 Core Material Selection and Design**

The first step of the transformer design is material selection for the core, as it affects transformer size, power density and power loss [13]. The efficient operation frequency range of the transformer is directly related to the selected core material. For a practical core material selection, four parameters including flux density, price and availability, frequency range, and core losses are studied in this research for the studied materials.

Four magnetic materials in the market which are suggested in the articles for the using in HF power transformer are studied here. These materials are Silicon Steel, Ferrite, Amorphous and Nanocrystalline. Silicon steel has relatively high saturation flux density [13] and permeability which supports high-frequency applications, but it has higher core losses for high frequency. Ferrite has relatively lower saturation flux density (0.4 T) which increases the size of transformer core [22], but it is available commercially in different shapes and lower cost. Also, ferrite cores could be used in very high frequency with a moderate power loss. Amorphous, has good saturation flux density (higher than 1.5T), while the cost factor remains relatively low, but the power loss is much higher than Ferrite for high power applications. Nanocrystalline has an acceptable saturation flux density in the high frequency (1.2T), and relatively low losses in the medium frequency, but for its core loss is higher than ferrite for the frequencies higher than 35 kHz. Moreover, this material is relatively expensive and is not available commercially in the different shapes [22]. The material study shows that for 100 kHz switching frequency which is the target in this design, ferrite material gives the best performance even though its saturation flux density is relatively lower than the three other studied materials. However, it is important to mention that some research projects have been performed on the new materials like advance silicon steels to improve their performance for high-frequency applications, but these materials are not commercially available in the market or their prices are still very high.

Table 5-3. Flux Density and Frequency Range of The Studied Materials [22], [23], [24], [61]

	Flux density (T)	Frequency Range (Hertz) With relatively low loss
Silicon steel	1.5-1.8	Audio frequency (20-20 kHz)
Ferrite	0.2-0.5	Audio frequencies up to hundred megahertz
Amorphous	0.5-1.6	<300kHz
Nanocrystalline	1-2	<30 kHz

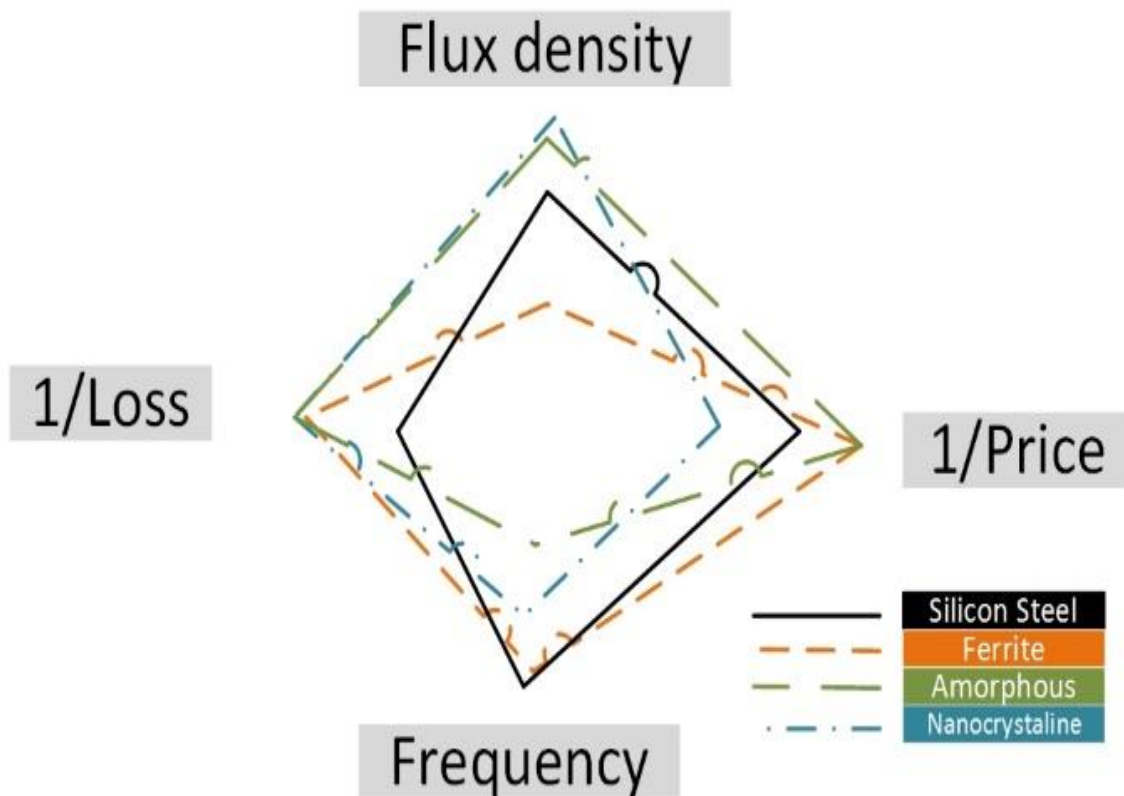


Figure 5-8. Core material comparison for HF design [61]

### **5.3.2 Cable Selection**

Another design parameter is cable selection. Transformer losses vary when the frequency increases, since the effective resistance increases as the result of higher skin effect in the higher frequency. AC current distributes in a metal conductor in a way that the current density of the outer layer (skin) of the conductor is much higher than the core of the conductor. This is called the skin effect in the conductors. One solution to decrease the influence of skin effect on effective resistance is using Litz wire [25][26]. Litz wire decreases this resistance by subdividing the conductor to very smaller insulated conductor strands with proper shields [4]. Each of very tiny strands in the wire is insulated from the other strands around it. Several hundreds of the strands form a thicker wire with the thickness equal to the wire size which is calculated in volt power calculations for transferring nominal current. The thinner wire strands give better high-frequency characteristics. The Litz wire strands are available in the market from 26 AWG to 52 AWG. To achieve an acceptable resistance performance from the windings in 100 kHz for transferring up to 10 kVA in the voltage range up to 600V, 36 gage strands are used to form an equal size to 8 AWG wire for this application.

### **5.3.3 Winding Placement**

The winding placement on the core is also important since it influences the mutual inductances and the coupling coefficients of the windings which directly affect the power loss and system efficiency. Winding placement is investigated in this paper for four possible configurations of placement of four windings on the core. The fourth (yellow) wire is the load port winding, and the design process in this study focuses on getting the best performance for power exchange with this port. The green wire is the third windings where energy storage is connected. The two other

windings are defined as generation port windings. The winding placement configurations are shown in Figure 5-9. The number of turns is tried to be minimized since increasing the number of turns, and the length of the winding wire increases the wire impedance and cause more loss even if the ratio is kept constant.

In case A, each of the windings is placed on one leg of the core. In the winding configuration of case B, all of the windings are wound around all of the legs of the core. In the configuration C, load winding is distributed between all of the other windings, and in case of D, load and storage windings are distributed between the two other windings.

The cores with different winding configurations are simulated in ANSYS Maxwell 3D software (Figure 5-9) with real dimensions and magnetic material data of ferrite material and Litz wire gage 8. The transformer size is optimized based on the nominal voltage and power of the MPSST which is built in the lab. The leakage inductance calculation of the simulation for the defined wire and other conditions is around 2  $\mu\text{H}$ . Also, the MAXWELL3D simulations calculate the coupling factors for the different winding positions which are shown in Table 5-4.

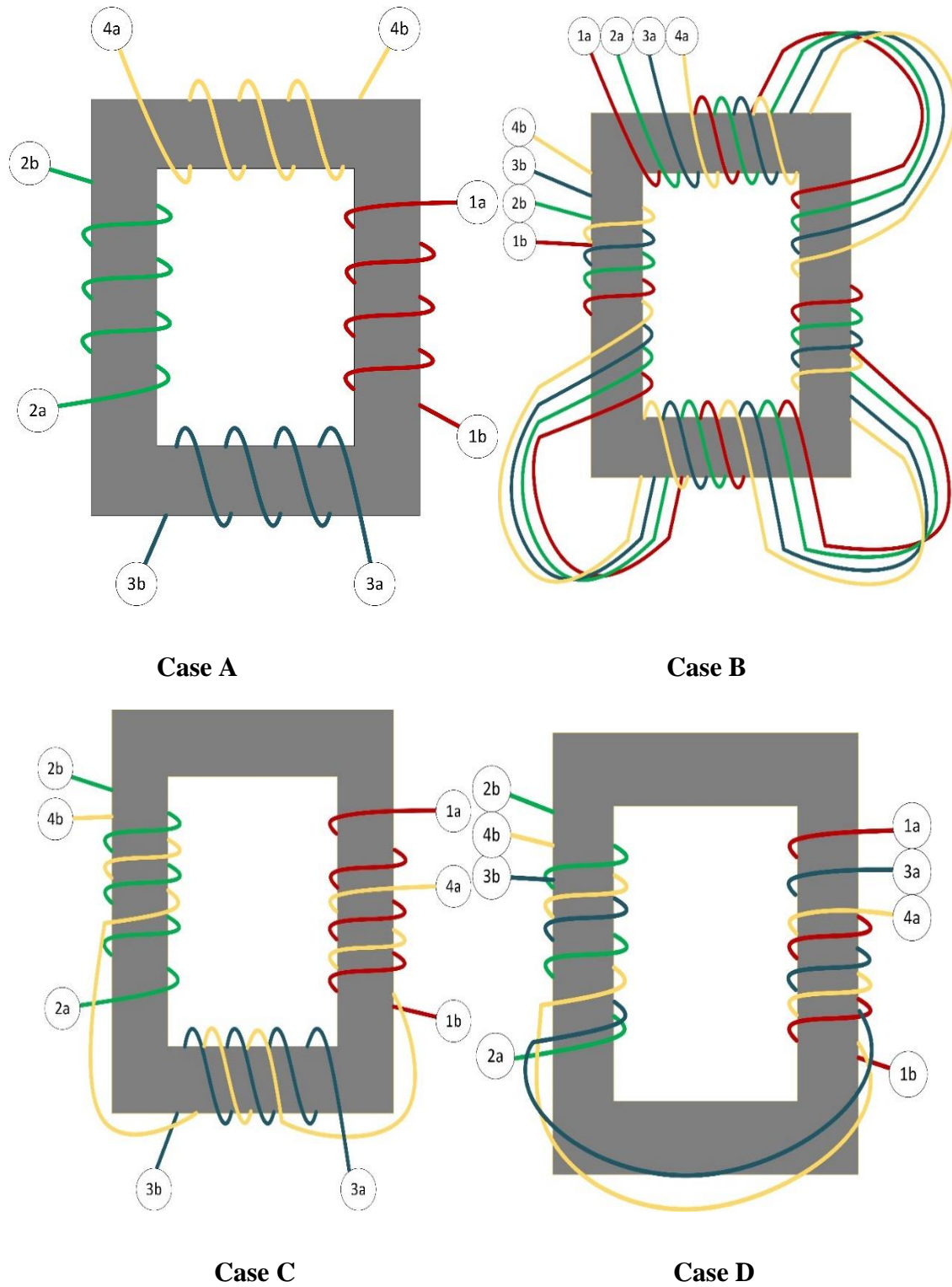


Figure 5-9. Test cases of MPSST windings placement: (1) Grid (red). (2) DG (blue). (3) ES (green). (4) Load (yellow).



The simulation is also done for the magnetic characteristics of the chosen material to verify the capability of the transformer to operate in the defined operating range without saturation.

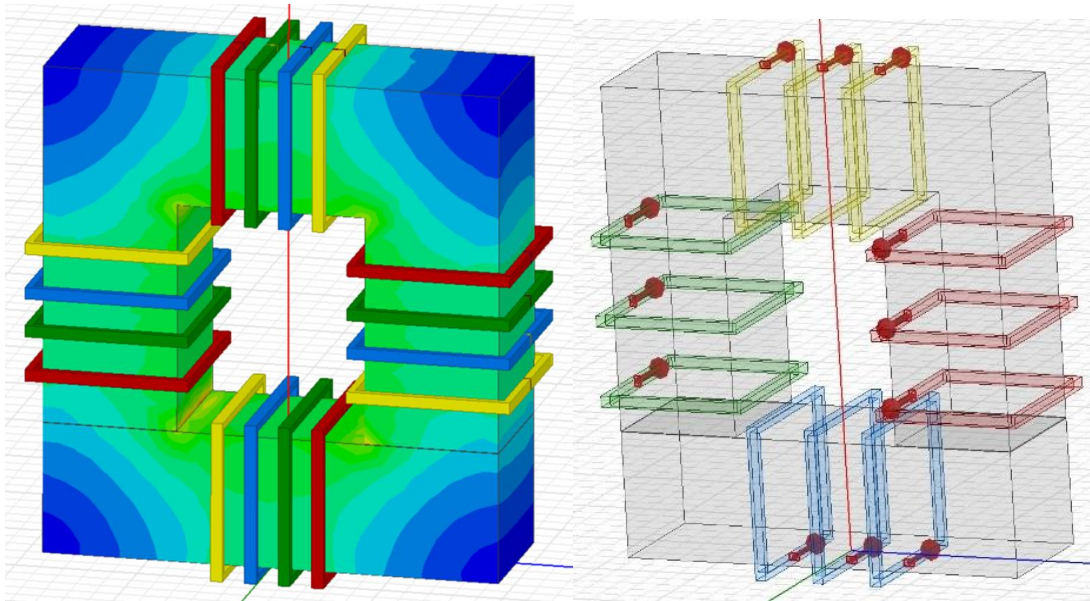


Fig. 5-10. ANSYS Maxwell 3D simulation of the designed core

From the simulation results of Table 1, case B gives the best coupling coefficients. However, it uses more wire for each winding which increases the winding impedance and total loss of the transformer. Since the design constraints are maximizing the coupling coefficients for the fourth winding and at the same time using shorter wire length the winding placement of case C is chosen for this application.

The designed transformer has the core area of  $0.001 \text{ m}^2$  and uses ferrite material with the flux density equal to  $0.21 \text{ T}$  to transfer  $10 \text{ kVA}$  from each winding in the voltage range of  $200\text{-}600 \text{ V}$ . The transformer is built and tested in the lab. The measured leakage inductance from the test set up is  $2.3 \text{ } \mu\text{H}$ , and the magnetizing inductance of the transformer is  $75 \text{ } \mu\text{H}$ . Figure 5-11 shows the built transformer in the lab.

Table 5-4. Coupling Coefficient between the windings for the different case studies

Case A	W1	W2	W3	W4
W1	1	0.93208	0.94208	0.9426
W2	0.93208	1	0.94207	0.94253
W3	0.94208	0.94207	1	0.92272
W4	0.9426	0.94253	0.92272	1
Case B	W1	W2	W3	W4
W1	1	0.99029	0.98688	0.98549
W2	0.99029	1	0.99065	0.98692
W3	0.98688	0.99065	1	0.99013
W4	0.98549	0.98692	0.99013	1
Case C	W1	W2	W3	W4
W1	1	0.92104	0.93076	0.9662
W2	0.92104	1	0.93003	0.96594
W3	0.93076	0.93003	1	0.96992
W4	0.9662	0.96594	0.96992	1
Case D	W1	W2	W3	W4
W1	1	0.93229	0.96829	0.96862
W2	0.93229	1	0.96863	0.96797
W3	0.96829	0.96863	1	0.97094
W4	0.96862	0.96797	0.97094	1



Figure 5-11. Final assembled multi-winding HF transformer

#### **5.4 Running and Test Results**

The last part of this project is the hardware implementation of the converter based on the discussed design parameters. Each of the components is tested separately and then put together in the designed box (Figure 5-12). Finally, after testing the controller board and checking the outputs and routs of the signals, the voltage is applied gradually to the set up (Figure 5-13), and the converter is tested under voltage.

There are some small implementation considerations which could affect the output results of the converter. First of all, each pair of the wires which connect the components of the converter should be twisted together to reduce the interferences. Second, the control circuit must be isolated

from the power circuit. Also, it is important to keep the ribbon cables which are used in routing the control signals as short as it is possible. Furthermore, to get the best performance from the heatsink, it is important to choose a proper thermal paste and put the enough and smooth layer of that on the heatsink. The thickness of the paste layer is suggested to be between 0.06-0.14 mm based on the application.

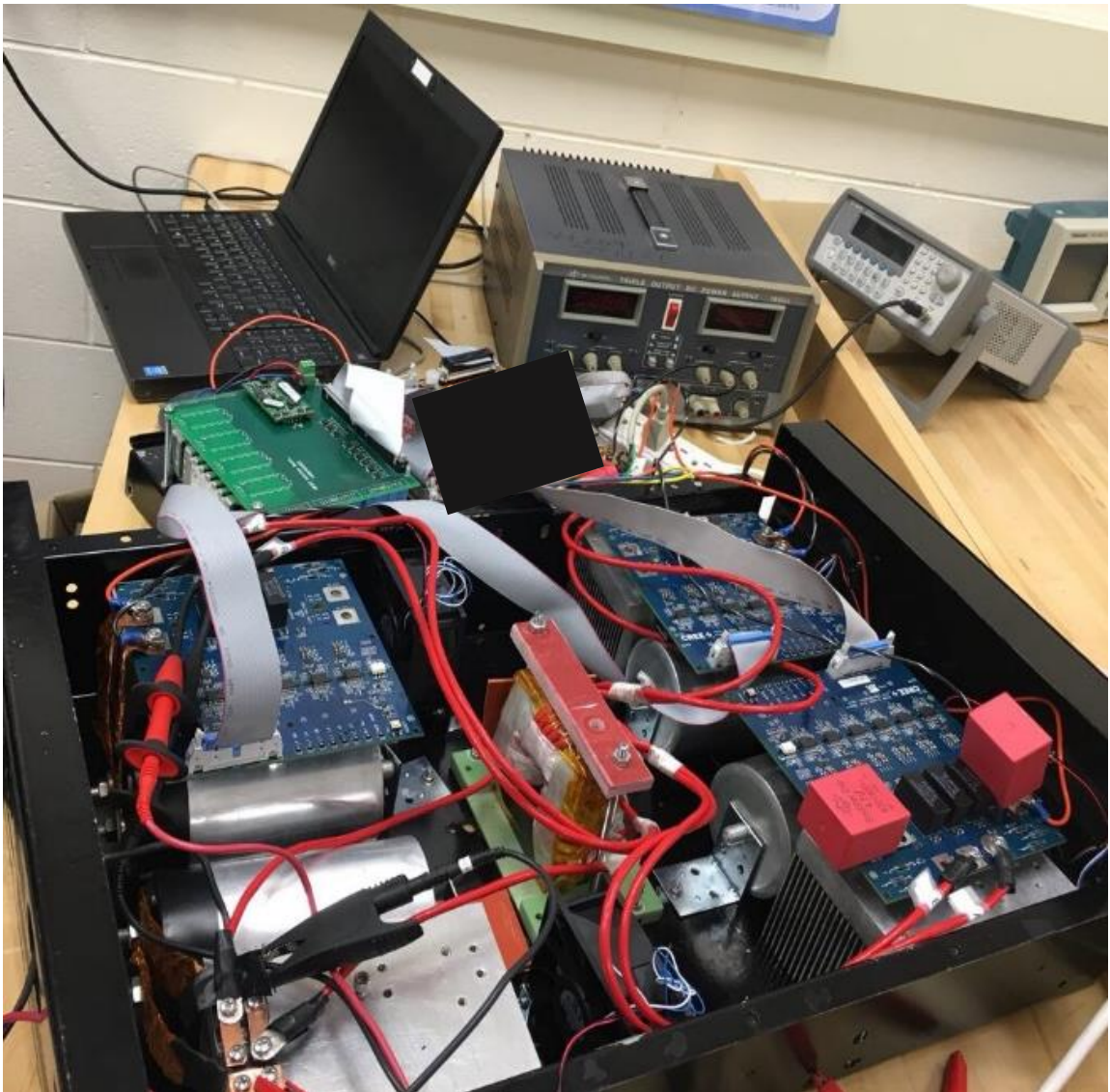


Figure 5-12. Implementation process of the MPSST

The final assembly of the converter is shown in Figure 5-13. Considering 10 kW as the nominal power of this converter the power density of the converter is  $3.2 \text{ w/inch}^3$

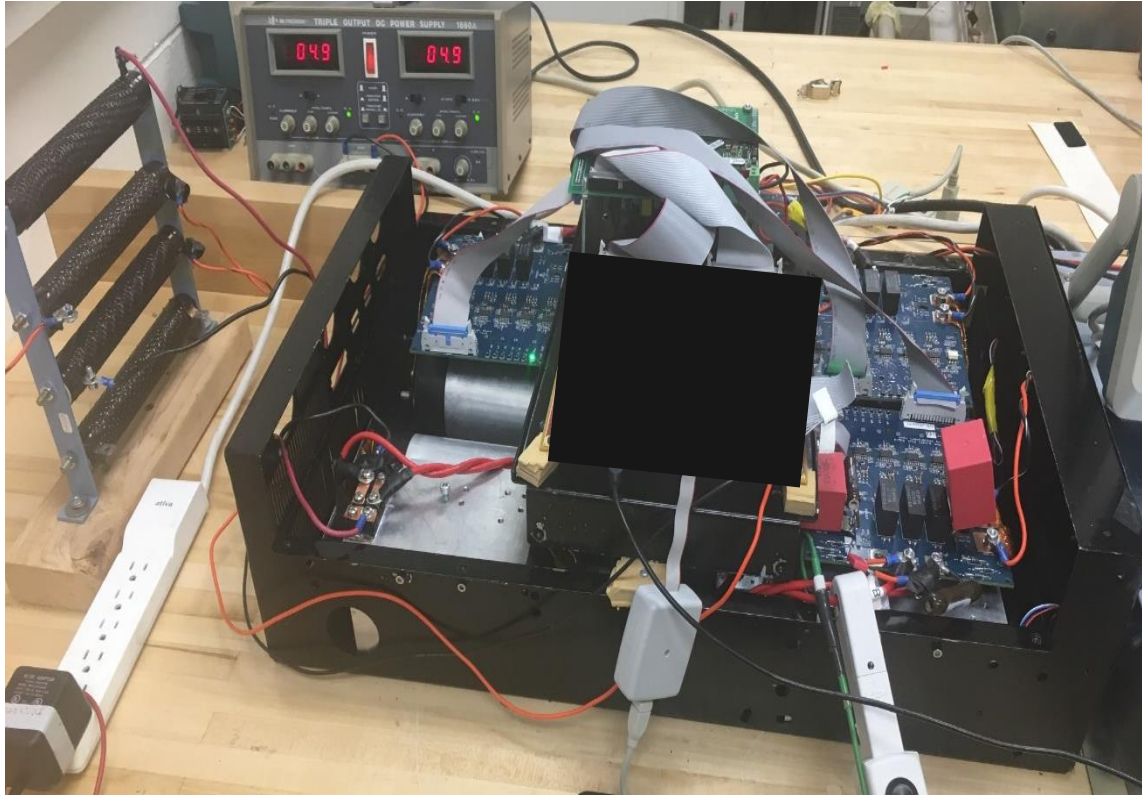


Figure 5-13. Final assembly of the four port solid state transformer

#### 5.4.1 Hardware Test Results

Figure 5-14 and Figure 5-15 shows the test results for running the converter in 100 kHz with different duty cycles. In the first figure,  $D=0.35$  is applied to the H-Bridges. The green curve is the regulated DC voltage at the output of the diode bridge rectifier. The output DC voltage increases by increasing the duty cycle to 0.5 in Figure 5-15 The sensitivity of the method increases by increasing the load and current.

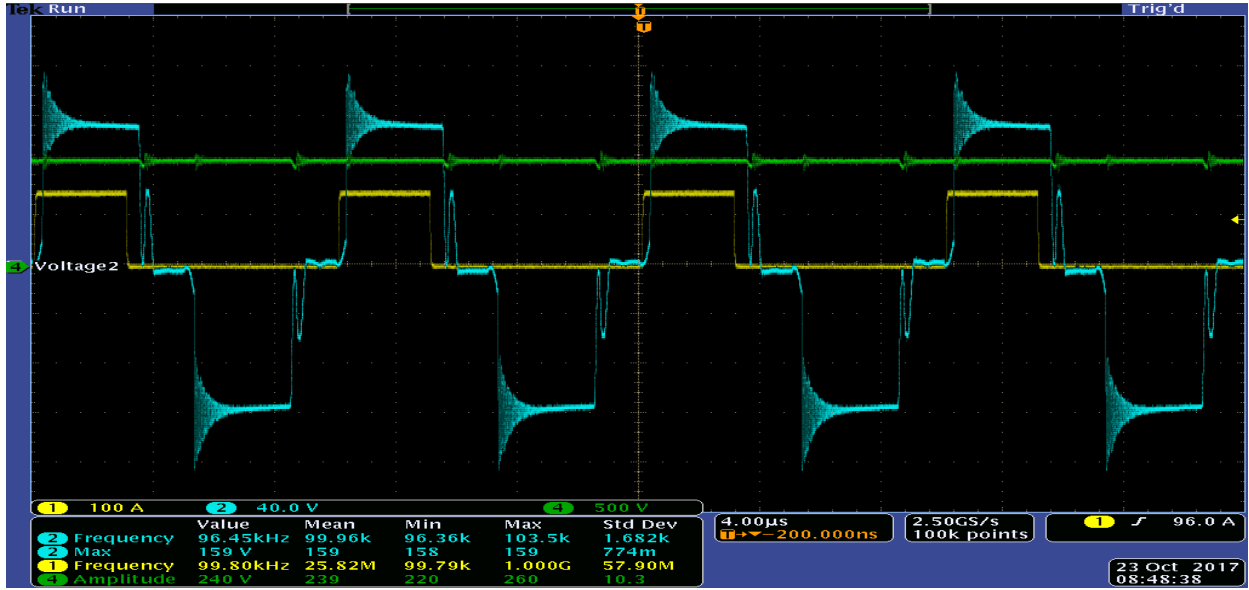


Figure 5-14. MPSST experimental result for  $D=35\%$  and  $f=100\text{ kHz}$

Yellow: gate signal, Blue: AC port voltage, Green: DC output voltage

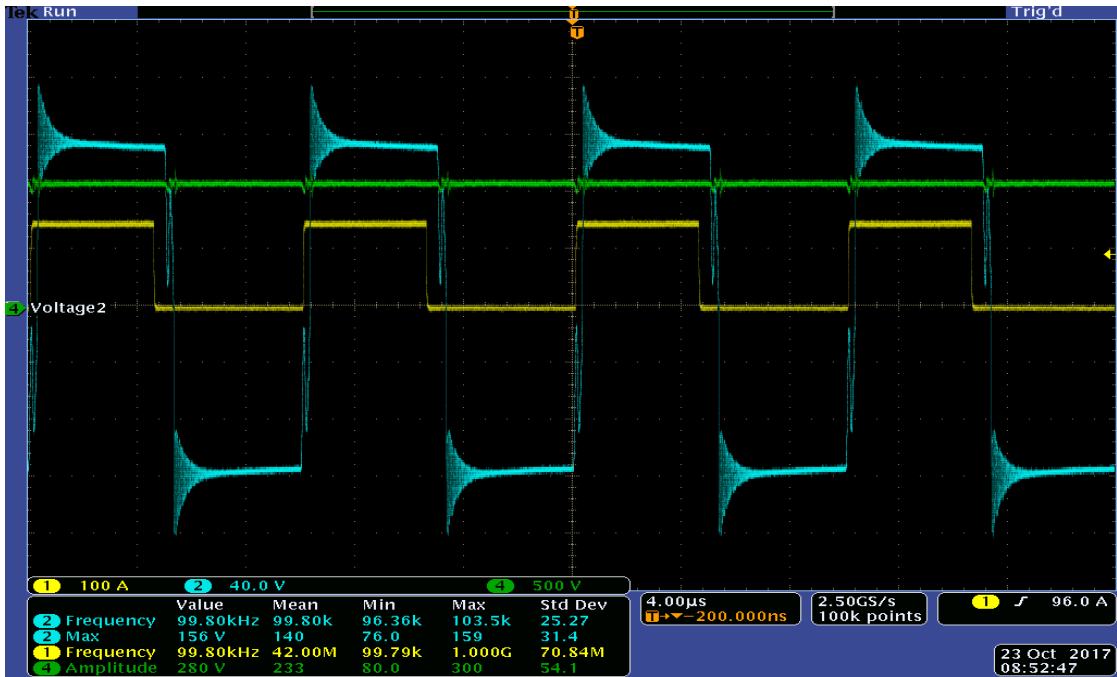


Figure 5-15. MPSST experimental result for  $D=50\%$  and  $f=100\text{ kHz}$

Yellow: gate signal, Blue: AC port voltage, Green: DC output voltage

Figure 5-16 shows the applied shifted gate signals to the three H-Bridge converters. Each set of the signals is fed to one of the H-Bridge converters. Figure 5-17 shows the resulted currents for the different ports. These results verify that the power flow from different ports could be controlled by controlling the phase shifts between the different ports.

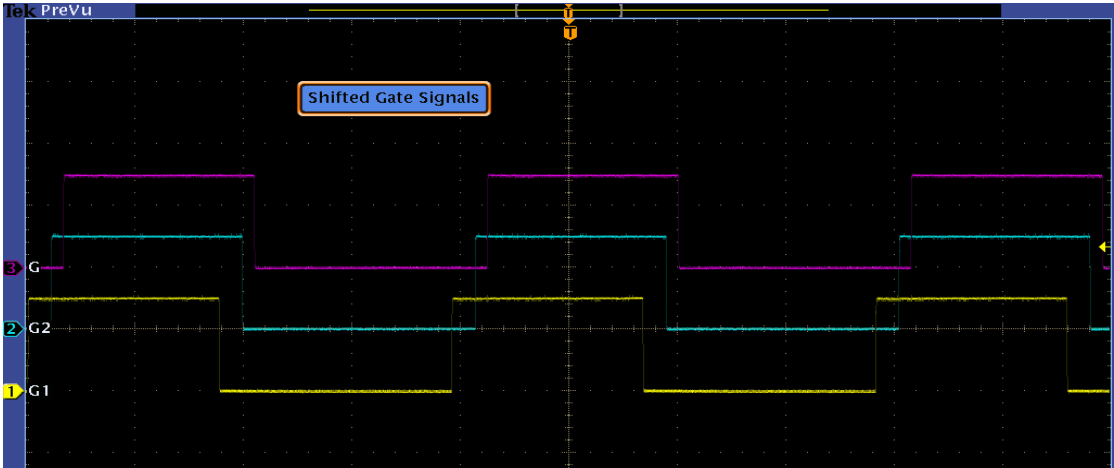


Figure 5-16. Shifted gate signals

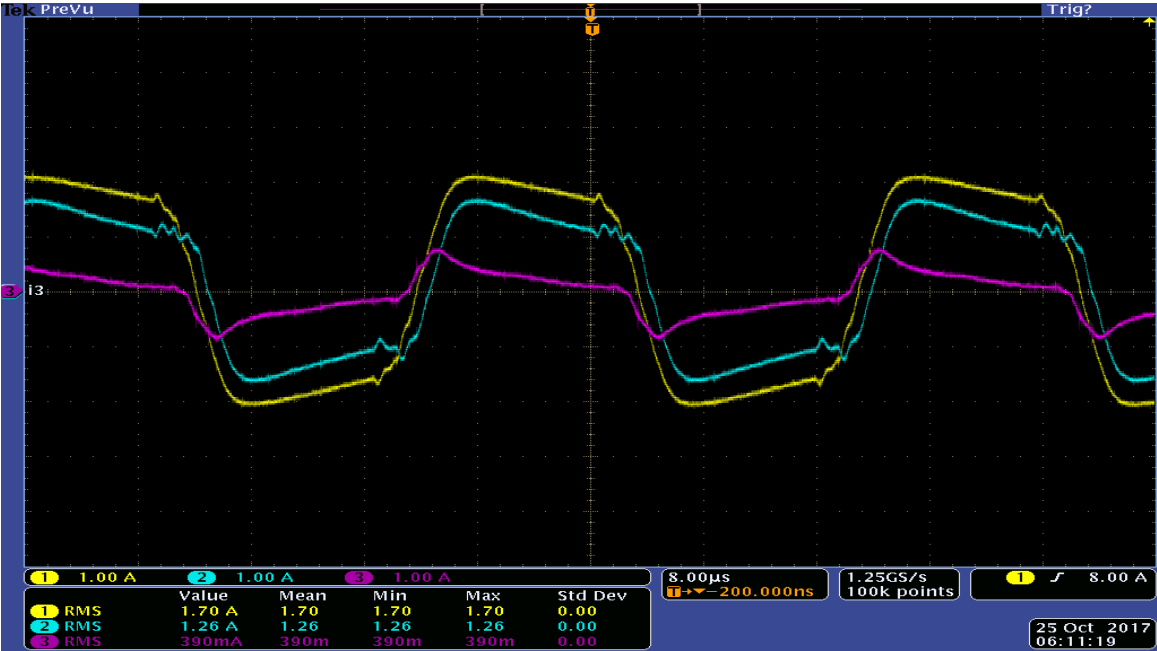


Figure 5-17. Power flow control using phase shift control

The converter is tested at different frequencies. The voltage is increased gradually to prevent any damage from the possible faults.

In Figure 5-14 the output voltage waveform includes a spike in the dead time. Adding extra parallel capacitors directly on the DC ports of the module and snubber circuit, the spike problem is resolved as it is shown in Figure 5-18.

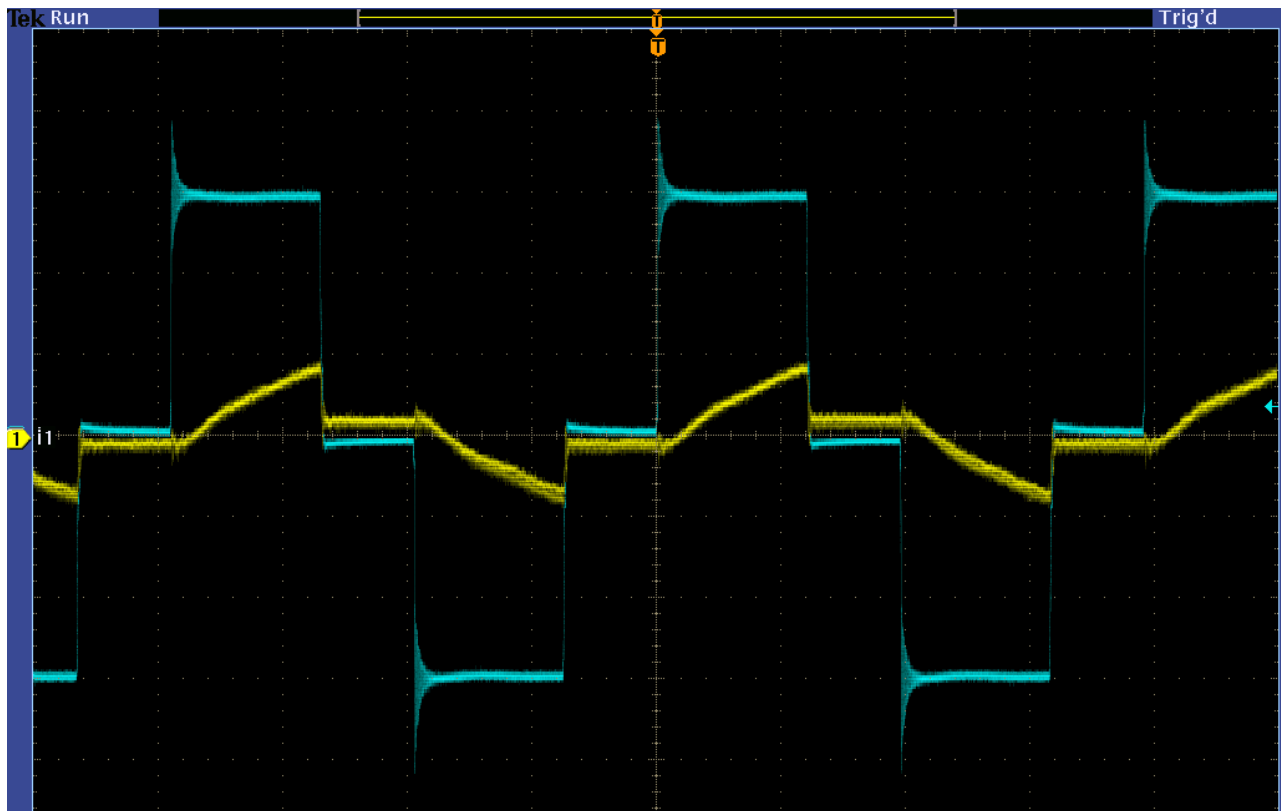


Figure 5-18. Experimental test results by adding snubber circuit and DC capacitors



## CHAPTER 6

### Conclusion

In conclusion, the concept of solid state transformer as an isolated converter which benefits from a combination of power electronic converters and high-frequency transformers is illustrated in this project. The high-frequency design of transformer reduces the size and weight of transformer dramatically in comparison with the conventional transformers. On the other hand, having PE based transformer in the power system benefits the system by providing control and connectivity features to the system using one multi-task converter.

Then a four-port SST topology, including three active bidirectional converters and one diode based unidirectional converter is introduced to be used for fast, modular and isolated utilization of DER/ESS in the power system. This converter is mathematically analyzed, and a two-layer control method is suggested, discussed and simulated to control the multiple parameters of the converter. The control method uses duty cycle control for DC voltage regulation and a modified PSC to control the power flow from the ports. The combination of duty cycle control and PSC is applied to the hardware prototype, and the test results validate the control method. The exchanged power from/to each port is specified through a logical decision-making method which is called pool of power method (PPM). The PPM chart receives the current status of the connected components like SoC of the energy storage, generation capability of RER and the connectivity to the grid and specifies the share of power of each port.

Also, the possible architectures of future efficient PE converter-based distribution systems have been discussed and studied in this project. First, an architecture based on replacing the conventional transformers of the current distribution system with the two port SST is discussed. In such a system SST is used to utilize the RER and ESS in all of the voltage zones of the power system and to monitor and control the system parameters. The drawback of this method of design of power system is the large number of the needed components which increases the investment cost, failure rate and control complexity of the network. Then another configuration for the power distribution is suggested. The main component of this new architecture is MPSST. MPSST provides an isolated, controllable, and modular multi-port node for utilizing different types of elements including, DG, grid, energy storage and the other zones of voltage in the power system. Also, application of HF multi-winding transformer in the MPSST minimizes the size and weight of the whole system dramatically.

Application of Multi-Port Solid State transformer for Volt-VAR control in the new design of distribution system is studied and simulated. The MPSST regulates the voltage by injecting the needed reactive power. Distributed energy resources and energy storages can be plugged directly into the MPSST which allows local generation of reactive and active power to the system for voltage and frequency support. The simulation results verify the capability of the MPSST for supporting the grid locally.

Finally, the whole process of the design and implementation of the MPSST as an isolated power electronic converter including, PCB design, cooling system design, component selection, transformer design and control boards programming is described. ANSYS MAXWELL software is used for optimal designing of the multiport transformer of the MPSST topology. Four different

materials for the HF application of this solid state converter are studied. An FPGA code is developed to program the controller board. Silicon carbide MOSFET modules are chosen to minimize the loss and enable operation in high frequency up to 100kHz. The first prototype of the described topology is built and tested in the lab.

## References

- [1] 2016 US EIA Annual energy outlook US-DOE energy information administration
- [2] D. Boroyevich, I. Cvetković, D. Dong, R. Burgos, F. Wang and F. Lee, "Future Electronic Power Distribution Systems A Contemplative View," Optimization of Electrical and Electronic Equipment (OPTIM), 2010 12th International Conference on, Basov, 2010, pp. 1369-1380.
- [3] Balali MH, Nouri N, Rashidi M, Nasiri A, Otieno W. "A multi-predictor model to estimate solar and wind energy generations, " in Int J Energy Res. 2017.
- [4] M. Rashidi, A. Nasiri and R. Cuzner, "Application of multi-port solid-state transformers for microgrid-based distribution systems," 2016 IEEE International Conference on Renewable Energy Research and Applications (ICRERA), Birmingham, 2016, pp. 605-610
- [5] M. Biberoglu, T. N. Gücin and B. Fincan, "Analyzing the influences of high frequency transformers utilized in parallel resonant converters," 2016 IEEE International Conference on Renewable Energy Research and Applications (ICRERA), Birmingham, 2016, pp. 983-988.
- [6] H. Sepahvand, S. Madhusoodhanan, K. Corzine, S. Bhattacharya and M. Ferdowsi, "Topology selection for medium-voltage three-phase SiC solid-state transformer," 2014 International Conference on Renewable Energy Research and Application (ICRERA), Milwaukee, WI, 2014, pp. 485-489.

- [7] R. M. Cuzner, V. Singh, M. Rashidi and A. Nasiri, "Converter topological and solid state protective device trade-offs for future shipboard MVDC systems," 2015 IEEE Electric Ship Technologies Symposium (ESTS), Alexandria, VA, 2015, pp. 34-39.
- [8] C. D. Bussy-Virat and A. J. Ridley, "Predictions of the solar wind speed by the probability distribution function model," in *Space Weather*, vol. 12, no. 6, pp. 337-353, June 2014.
- [9] J. R. Andrade and R. J. Bessa, "Improving Renewable Energy Forecasting With a Grid of Numerical Weather Predictions," in *IEEE Transactions on Sustainable Energy*, vol. 8, no. 4, pp. 1571-1580, Oct. 2017.
- [10] C. W. T. McLyman, *Transformer and Inductor Design Handbook*. CRC Press, 1964.
- [11] Hengsi Qin and J. W. Kimball, "Ac-ac dual active bridge converter for solid state transformer," 2009 IEEE Energy Conversion Congress and Exposition, San Jose, CA, 2009, pp. 3039-3044.
- [12] R. W. A. A. De Doncker, D. M. Divan and M. H. Kheraluwala, "A three-phase soft-switched high-power-density DC/DC converter for high-power applications," in *IEEE Transactions on Industry Applications*, vol. 27, no. 1, pp. 63-73, Jan/Feb 1991.
- [13] X. She, A. Q. Huang and R. Burgos, "Review of Solid-State Transformer Technologies and Their Application in Power Distribution Systems," in *IEEE Journal of Emerging and Selected Topics in Power Electronics*, vol. 1, no. 3, pp. 186-198, Sept. 2013.

- [14] H. Qin and J. W. Kimball, "Solid-State Transformer Architecture Using AC–AC Dual-Active-Bridge Converter," in *IEEE Transactions on Industrial Electronics*, vol. 60, no. 9, pp. 3720-3730, Sept. 2013.
- [15] Jung, J.-H.; Kim, H.-S.; Ryu, M.-H.; Baek, J.-W., "Design Methodology of Bidirectional CLLC Resonant Converter for High-Frequency Isolation of DC Distribution Systems," in *IEEE Transactions on Power Electronics*, vol.28, no.4, pp.1741-1755, April 2013
- [16] M. S. Agamy and P. K. Jain, "A Variable Frequency Phase-Shift Modulated Three-Level Resonant Single-Stage Power Factor Correction Converter," in *IEEE Transactions on Power Electronics*, vol. 23, no. 5, pp. 2290-2300, Sept. 2008.
- [17] A. Bani-Ahmed, L. Weber, A. Nasiri and H. Hosseini, "Microgrid communications: State of the art and future trends," *Renewable Energy Research and Application (ICRERA)*, 2014 International Conference on, Milwaukee, WI, 2014, pp. 780-785.
- [18] D. Shah and M. L. Crow, "Online Volt-Var Control for Distribution Systems with Solid-State Transformers," in *IEEE Transactions on Power Delivery*, vol. 31, no. 1, pp. 343-350, Feb. 2016.
- [19] E. Z. Abdel-Aziz, J. Ishaq and R. Al-Harthi, "Impact of distributed generators on voltage stability in transmission network," *2015 Saudi Arabia Smart Grid (SASG)*, Jeddah, 2015, pp. 1-7.
- [20] B. Zhao, Q. Song, W. Liu and Y. Sun, "Overview of Dual-Active-Bridge Isolated Bidirectional DC–DC Converter for High-Frequency-Link Power-Conversion System," in *IEEE Transactions on Power Electronics*, vol. 29, no. 8, pp. 4091-4106, Aug. 2014.

- [21] Danwei Liu, Hui Li. A Novel Multiple-Input ZVS Bidirectional DC-DC Converter. 31st Annual Conference of IEEE Industrial Electronics Society, 2005. IECON 2005.
- [22] Y. Du, S. Baek, S. Bhattacharya and A. Q. Huang, "High-voltage high-frequency transformer design for a 7.2kV to 120V/240V 20kVA solid state transformer," IECON 2010 - 36th Annual Conference on IEEE Industrial Electronics Society, Glendale, AZ, 2010, pp. 493-498.
- [23] Colonel WM. T. McLyman Transformer and inductor design Handbook Third Edition, Revised and Expanded Kg Magnetics, Inc. Idyllwild, California, U.S.A, 2004.
- [24] Magnetics Company, Magnetic Cores For Switching Power Supplies Handbook, 2001.
- [25] Ke, L., Yan, G., Yan, S., Wang, Z. and Li, X. (2015), "Optimal Design of Litz Wire Coils With Sandwich Structure Wirelessly Powering an Artificial Anal Sphincter System," *Artificial Organs*, 39: 615–626. doi:10.1111/aor.12433
- [26] Yi, Y., Buttner, U., Fan, Y., and Foulds, I. G. (2015) "Design and optimization of a 3-coil resonance-based wireless power transfer system for biomedical implants," *Int. J. Circ. Theor. Appl.*, 43: 1379–1390. doi: 10.1002/cta.2024.
- [27] L. Liu, X. Ma and J. Sun, "An investigation of the relationship between economic growth and electricity consumption with different industrial structures in different regions in China," *Power Engineering Conference (UPEC), 2013 48th International Universities'*, Dublin, 2013, pp. 1-6.

- [28] D. C. Bohm, "Electricity consumption and economic growth in the European Union: A causality study using panel unit root and cointegration analysis," *2008 5th International Conference on the European Electricity Market*, Lisboa, 2008, pp. 1-6.
- [29] T. H. Ortmeyer and P. Pillay, "Trends in transportation sector technology energy use and greenhouse gas emissions," in *Proceedings of the IEEE*, vol. 89, no. 12, pp. 1837-1847, Dec 2001.
- [30] H. Bai, X. Wang and F. Blaabjerg, "Passivity Enhancement in Renewable Energy Source Based Power Plant With Paralleled Grid-Connected VSIs," in *IEEE Transactions on Industry Applications*, vol. 53, no. 4, pp. 3793-3802, July-Aug. 2017.
- [31] A. Mamen and U. Supatti, "A survey of hybrid energy storage systems applied for intermittent renewable energy systems," *2017 14th International Conference on Electrical Engineering/Electronics, Computer, Telecommunications and Information Technology (ECTI-CON)*, Phuket, 2017, pp. 729-732.
- [32] N. R. Tummuru, M. K. Mishra and S. Srinivas, "Dynamic Energy Management of Renewable Grid Integrated Hybrid Energy Storage System," in *IEEE Transactions on Industrial Electronics*, vol. 62, no. 12, pp. 7728-7737, Dec. 2015.



- [33] G. Omahen, B. Blažič, J. Kosmač, A. Souvent and I. Papič, "Impact of the SmartGrids concept on future distribution system investments in Slovenia," *CIREC 2012 Workshop: Integration of Renewables into the Distribution Grid*, Lisbon, 2012, pp. 1-4.
- [34] B. Zhou and T. Littler, "Local storage meets local demand: a technical solution to future power distribution system," in *IET Generation, Transmission & Distribution*, vol. 10, no. 3, pp. 704-711, 2 18 2016.
- [35] X. She, A. Q. Huang and R. Burgos, "Review of Solid-State Transformer Technologies and Their Application in Power Distribution Systems," in *IEEE Journal of Emerging and Selected Topics in Power Electronics*, vol. 1, no. 3, pp. 186-198, Sept. 2013.
- [36] S. Falcones, R. Ayyanar and X. Mao, "A DC-DC Multiport-Converter-Based Solid-State Transformer Integrating Distributed Generation and Storage," in *IEEE Transactions on Power Electronics*, vol. 28, no. 5, pp. 2192-2203, May 2013
- [37] S. Roy, A. De and S. Bhattacharya, "Multi-port solid state transformer for inter-grid power flow control," *2014 International Power Electronics Conference (IPEC-Hiroshima 2014 - ECCE ASIA)*, Hiroshima, 2014, pp. 3286-3291.

- [38] C. Gu, Z. Zheng, L. Xu, K. Wang and Y. Li, "Modeling and Control of a Multiport Power Electronic Transformer (PET) for Electric Traction Applications," in *IEEE Transactions on Power Electronics*, vol. 31, no. 2, pp. 915-927, Feb. 2016.
- [39] J. L. Brooks, "Solid state transformer concept development," in Naval Material Command. Port Hueneme, CA, USA: Naval construction Battalion Center, 1980.
- [40] M. Rashidi, M. Sabbah, A. Bani-Ahmed, A. Nasiri, MH. Balali "Design and Implementation of a Series Resonant Solid State Transformer" 2017 IEEE Energy Conversion Congress and Exposition (ECCE), Cincinnati, OH, 2017, pp. 1-5.
- [41] G. A. Garvelis, S. N. Manias and G. Kostakis, "A DC-DC boost converter with short circuit protection," *Industrial Electronics, Control and Instrumentation, 1994. IECON '94., 20th International Conference on*, Bologna, 1994, pp. 238-243 vol.1.
- [42] U. Ghisla, I. Kondratiev and R. A. Dougal, "Branch circuit protection for DC systems," *2011 IEEE Electric Ship Technologies Symposium*, Alexandria, VA, 2011, pp. 234-239.
- [43] C. Gould, C. M. Bingham, D. A. Stone and M. P. Foster, "CLL resonant converters with output short-circuit protection," in *IEE Proceedings - Electric Power Applications*, vol. 152, no. 5, pp. 1296-1306, 9 Sept. 2005.

- [44] K. J. Tseng and G. Luo, "Power electronic-based protection for direct-current power distribution in micro-grids," *2014 International Power Electronics Conference (IPEC-Hiroshima 2014 - ECCE ASIA)*, Hiroshima, 2014, pp. 2145-2151.
- [45] W. Fei, Y. Zhang and Z. Lu, "Novel Bridge-Type FCL Based on Self-Turnoff Devices for Three-Phase Power Systems," in *IEEE Transactions on Power Delivery*, vol. 23, no. 4, pp. 2068-2078, Oct. 2008.
- [46] E. Tironi, M. Corti and G. Ubezio, "DC networks including multi-port DC/DC converters: Fault analysis," *2015 IEEE 15th International Conference on Environment and Electrical Engineering (EEEIC)*, Rome, 2015, pp. 1109-1114.
- [47] Woojin Choi and Bo-Hyung Cho, "Topology and control design of converters for short-circuit fault protection in DC microgrids," *IECON 2013 - 39th Annual Conference of the IEEE Industrial Electronics Society*, Vienna, 2013, pp. 1386-1391.
- [48] M. Carminati, S. Grillo, L. Piegari, E. Ragaini and E. Tironi, "Fault protection analysis in low voltage DC microgrids with PV generators," *2015 International Conference on Clean Electrical Power (ICCEP)*, Taormina, 2015, pp. 184-191.

- [49] D. Jovcic and W. Lin, "Multiport High-Power LCL DC Hub for Use in DC Transmission Grids," in *IEEE Transactions on Power Delivery*, vol. 29, no. 2, pp. 760-768, April 2014.
- [50] T. Guillod, F. Krismer, R. Färber, C. M. Franck and J. W. Kolar, "Protection of MV/LV solid-state transformers in the distribution grid," *IECON 2015 - 41st Annual Conference of the IEEE Industrial Electronics Society*, Yokohama, 2015, pp. 003531-003538.
- [51] Woojin Choi and Bo-Hyung Cho, "Topology and control design of converters for short-circuit fault protection in DC microgrids," *IECON 2013 - 39th Annual Conference of the IEEE Industrial Electronics Society*, Vienna, 2013, pp. 1386-1391.
- [52] H. Kakigano, Y. Miura, T. Ise and R. Uchida, "DC micro-grid for super high quality distribution System configuration and control of distributed generations and energy storage devices," 2006 37th IEEE Power Electronics Specialists Conference, Jeju, 2006, pp. 1-7.
- [53] J. P. Vandelac and P. Ziogas, "A novel approach for minimizing high frequency transformer copper losses," 1987 IEEE Power Electronics Specialists Conference, Blacksburg, VA, USA, 1987, pp. 355-367.

- [54] M. Rashidi, A. Bani-Ahmed, A. Nasiri" Application of a Multi-Port Solid State Transformer for Volt-VAR Control in Distribution Systems" 2017 IEEE Power and Energy Society General Meeting, Chicago, IL, 2017.
- [55] J. W. Kolar, G. Ortiz, "Solid State Transformer Concepts in Traction and Smart Grid Applications" 28th Applied Power Electronics Conference and Exposition (APEC 2013):
- [56] Qingshan Wang and D. Liang, "Research on loss reduction of dual active bridge converter over wide load range for solid state transformer application,"2016 Eleventh International Conference on Ecological Vehicles and Renewable Energies (EVER), Monte Carlo,2016, pp. 1-9.
- [57] Chunyang Gu, Zedong Zheng, Yongdong Li. A Power Electronic Transformer (PET) With Multiport Bidirectional Resonant DC-DC Converters for Electric Traction Applications. Transportation Electrification Conference and Expo (ITEC), 2015 IEEE.
- [58] W. L. Malan, D. M. Vilathgamuwa, G. R. Walker and M. Hiller, "A three port resonant solid state transformer with minimized circulating reactive currents in the high frequency link," 2016 IEEE 2nd Annual Southern Power Electronics Conference (SPEC), Auckland, 2016, pp. 1-6.
- [59] R. Gao, X. She, I. Husain and A. Q. Huang, "Solid-State-Transformer-Interfaced Permanent Magnet Wind Turbine Distributed Generation System With Power Management Functions," in IEEE Transactions on Industry Applications, vol. 53, no. 4, pp. 3849-3861, July-Aug. 2017.

- [60] L. F. Costa, G. Buticchi and M. Liserre, "Quad-Active-Bridge DC–DC Converter as Cross-Link for Medium-Voltage Modular Inverters," in *IEEE Transactions on Industry Applications*, vol. 53, no. 2, pp. 1243-1253, March-April 2017.
- [61] Mohammad Rashidi, Abedalsalam Bani-Ahmed, Robabeh Nasiri, Azadeh Mazaheri, Adel Nasiri, "Design and Implementation of a Multi Winding High-Frequency Transformer for MPSST Application" 6th International Conference on Renewable Energy Research and Applications (ICRERA), Nov 2017, San Diego, California, USA.

# APPENDIX A

## PPM method m-file code

```
function [phPg, phDG,phB] = fcn(soc,DG,B,AI)

kPg=0;kDG=0;kB=0;

if soc>0.65

    if AI>DG

        if (AI-DG)>((soc-0.65)*B)

            Pg=AI-DG-((soc-0.65)*B);

            kPg=Pg/AI;kDG=DG/AI;kB=((soc-0.65)*B)/AI;

        else

            kPg=0/AI;kDG=DG/AI;kB=((soc-0.65)*B)/AI;

        end

    else

        kPg=0;kDG=DG/AI;kB=0;

    end

else

    if AI>DG

        kPg=(AI-DG);kDG=DG/AI;kB=0;

    else

        kPg=0;kDG=AI/AI;kB=(AI-DG)/AI;
```

end

end

$$\text{phPg} = -k\text{Pg} * 1/120000;$$

$$\text{phDG} = -k\text{DG} * 1/120000;$$

$$\text{phB} = -k\text{B} * 1/120000;$$



# APPENDIX B

## Transfer Matrix Elements

$$A_{11} = \frac{1}{Z_1 + \left(\frac{1}{Z_2} + \frac{1}{Z_3} + \frac{1}{Z_c}\right)^{-1}}$$

$$A_{12} = -\frac{Z_3 Z_c}{Z_1 Z_2 Z_c + Z_2 Z_3 Z_c + Z_1 Z_2 Z_3 + Z_1 Z_3 Z_c}$$

$$A_{13} = -\frac{Z_2 Z_c}{Z_1 Z_3 Z_c + Z_2 Z_3 Z_c + Z_1 Z_2 Z_3 + Z_1 Z_2 Z_c}$$

$$A_{14} = -\frac{Z_2 Z_3 Z_c}{Z_2 Z_3 Z_c + Z_1 Z_3 Z_c + Z_1 Z_2 Z_3 + Z_1 Z_2 Z_c}$$

$$A_{14} = -\frac{Z_2 Z_3 Z_c}{Z_2 Z_3 Z_c + Z_1 Z_3 Z_c + Z_1 Z_2 Z_3 + Z_1 Z_2 Z_c}$$

$$A_{21} = -\frac{Z_3 Z_c}{Z_1 Z_2 Z_c + Z_1 Z_3 Z_c + Z_1 Z_2 Z_3 + Z_2 Z_3 Z_c}$$

$$A_{22} = \frac{1}{Z_2 + \left(\frac{1}{Z_1} + \frac{1}{Z_3} + \frac{1}{Z_c}\right)^{-1}}$$

$$A_{23} = -\frac{Z_1 Z_c}{Z_2 Z_3 Z_c + Z_1 Z_3 Z_c + Z_1 Z_2 Z_3 + Z_1 Z_2 Z_c}$$

$$A_{24} = -\frac{Z_1 Z_3 Z_c}{Z_2 Z_3 Z_c + Z_1 Z_3 Z_c + Z_1 Z_2 Z_3 + Z_1 Z_2 Z_c}$$

$$A_{31} = -\frac{Z_2 Z_c}{Z_1 Z_3 Z_c + Z_1 Z_2 Z_c + Z_1 Z_2 Z_3 + Z_2 Z_3 Z_c}$$

$$A_{32} = -\frac{Z_1 Z_c}{Z_2 Z_3 Z_c + Z_1 Z_2 Z_c + Z_1 Z_2 Z_3 + Z_1 Z_3 Z_c}$$

$$A_{33} = \frac{1}{Z_3 + \left(\frac{1}{Z_1} + \frac{1}{Z_2} + \frac{1}{Z_c}\right)^{-1}}$$

$$A_{34} = -\frac{Z_1 Z_2 Z_c}{Z_2 Z_3 Z_c + Z_1 Z_2 Z_c + Z_1 Z_2 Z_3 + Z_1 Z_3 Z_c}$$

$$A_{41} = \frac{Z_2 Z_3 Z_c}{Z_1 Z_3 Z_c + Z_1 Z_2 Z_c + Z_1 Z_2 Z_3 + Z_2 Z_3 Z_c}$$

$$A_{42} = \frac{Z_1 Z_3 Z_c}{Z_2 Z_3 Z_c + Z_2 Z_1 Z_c + Z_2 Z_1 Z_3 + Z_1 Z_3 Z_c}$$

$$A_{43} = \frac{Z_2 Z_1 Z_c}{Z_3 Z_1 Z_c + Z_3 Z_2 Z_c + Z_3 Z_2 Z_1 + Z_2 Z_1 Z_c}$$

$$A_{44} = \frac{Z_2 Z_3 Z_c}{Z_1 Z_3 Z_c + Z_1 Z_2 Z_c + Z_1 Z_2 Z_3 + Z_2 Z_3 Z_c}$$

# CURRICULUM VITAE

## **Mohammad (Mo) Rashidi**

Place of Birth: Persian, Hormozgan, Iran

### **Education Background:**

- **Ph.D., Electrical Engineering/Power**, University of Wisconsin Milwaukee, Advisor: Prof. Adel Nasiri. Dissertation title: **Design and Implementation of a Multi-port Solid State Transformer for Flexible DER Integration**-Sep. 2013-Nov. 2017.
- **M.Sc. in Electrical Engineering/Power**, Tehran Polytechnic, Tehran, Iran Thesis title: Assessment of Multilevel Converter Operation in Hybrid Wind/PV/UC System for Feeding Industrial Load Sep.2010–Nov.2012.
- **B.Sc. in Electrical Engineering/Power**, Tehran Polytechnic, Tehran, Iran Thesis title: Modeling and Analysis of Electrical Feeding of Agricultural Water Pump with a Small Wind Turbine Using a Single Phase Induction Motor in PSCAD Software Sep.2005–Aug.2009.

### **Work Experience:**

- **Eaton – Corporate Research & Technology**
  - Power Electronics Engineer Intern, June 2017- August 2017.
    - Test planning for power electronic converters based on standards
    - HF transformer design and test
    - Implementation and testing of H-Bridge HF converter using SiC Mosfet Modules
- **ABB, MVDrives, New Berlin WI.**

Electrical engineering Intern, May 2015- Aug 2015.

- Design and simulation of AC filter for MV Drives

▪ **Rockwell Automation, LVDrives, Mequon WI.**

Electrical engineering Intern, May 2014-Aug 2014.

- Simulation, testing, and post-processing of common mode noises in LV drive system including long cables

**Research Experience:**

- Modeling, simulation and testing of the effect of different cable length for feeding LV drives using ANSYS Q3D and Simplorer.
- Calculating the coupling factor for different winding positions in MPSST using ANSYS MAXWELL 3D simulation.
- Design and Implementation of resonant solid state transformer.
- Design and implementation of a multiport sold state transformer for DER application.
- Using harmonic Spectrum for DC-Source fault Detection at Multilevel Inverters.
- Simulation of 7-level Diode Clamped inverter and 7-level Cascaded Inverter.
- Comparison of Using SVC and STATCOM to Provide Reactive Power for A Grid-Connected Wind Power Plant, Using MATLAB.
- Offering a New Model for Pricing Reserves in Deregulated Electrical Market Considering Security Parameter.
- Modeling Electrical Arc Furnace and Discussion on How to Reduce THD in Arc Furnace.
- Design and simulation of a plant for “Suspension of One Wheel of Car.

### Teaching Experience:

- Teaching assistant and Lab instructor, “Electromechanical Energy Conversion,” UW-Milwaukee. Spring 2014-Spring 2015.

### Computer Skills:

- Modeling and analysis of Control Systems & Power Electronics using **MATLAB Simulink**.
- Modeling and analysis of Control Systems & Power Electronics using **ANSYS Simplorer**.
- Design and Electromagnetic Analysis of Cable and Transformers using **ANSYS Maxwell-Q3D**.
- Altera **FPGA Programming for PE** converters.
- PCB design using PCB123 and **Altium**.
- Power system software **CYME, DIgSILENT, EMTP-RV, PSCAD, Pasha**.
- **OPAL-RT**, Real-time simulator.
- Familiar with **System Advisor Software (SAM)**.
- Microsoft Office, Adobe Photoshop, VISIO, LATEX, etc.

### Publications:

- **Mohammad Rashidi**, Mohamad Sabbah, Abedalsalam Bani-Ahmed, Mohammad Hasan Balali, Adel Nasiri “Design and Implementation of a Series Resonant Solid State Transformer” 2017 IEEE Energy Conversion Congress and Exposition, Cincinnati, Ohio.
- Abedalsalam Bani-Ahmed, **Mohammad Rashidi**, Adel Nasiri “Coordinated Failure Response and Recovery in a Decentralized Microgrid Architecture” 2017 IEEE Energy Conversion Congress and Exposition, Cincinnati, Ohio.

- **Mohammad Rashidi**, Abedalsalam Bani-Ahmed, Robabeh Nasiri, Azadeh Mazaheri, Adel Nasiri, “Design and Implementation of a Multi Winding High-Frequency Transformer for MPSST Application” 6th International Conference on Renewable Energy Research and Applications (ICRERA), Nov 2017, San Diego, California, USA.
- **Mohammad Rashidi**, Abedalsalam Bani-Ahmed, Adel Nasiri, “Application of a Multi-Port Solid State Transformer for Volt-VAR Control in Distribution Systems” IEEE Power and Energy Society General Meeting, Chicago, IL, 2017.
- **Mohammad Rashidi**, Adel Nasiri, Robert M. Cuzner, “Application of Multi-Port Solid State Transformers for Microgrid Based Distribution System” 5th International Conference on Renewable Energy Research and Applications (ICRERA), Nov 2016 Birmingham, UK.
- Robert M. Cuzner, Vikas Singh, **Mohammad Rashidi**, Adel Nasiri “Converter topological and solid-state protective device trade-offs for future shipboard MVDC systems” Electric Ship Technologies Symposium (ESTS), 2015 IEEE
- Narjes Nouri, Mohammad Hasan Balali, **Mohammad Rashidi**, Wilkistar Otieno, Adel Nasiri “A Multi-Predictor Model to Estimate Solar and Wind Energy Generations” Accepted; International Journal of Energy Research (ISI Journal, IF 2.98)
- Abedalsalam Bani-Ahmed, **Mohammad Rashidi**, Adel Nasiri, Hossein Hosseini “Reliability Analysis of a Decentralized Microgrid Control Architecture” Submitted to IEEE Transaction on Smart Grid.
- Abedalsalam Bani-Ahmed, Adel Nasiri, **Mohammad Rashidi**, “Decentralized Resilient Autonomous Control Architecture for Dynamic Microgrids” Submitted to IEEE Transaction on Smart Grid.

- **Mohammad Rashidi**, A. Bani-Ahmed, A. Nasiri, Rob Cuzner" Application of Multi-Port Solid State Transformers for Microgrid Based Distribution Systems" Submitted to IEEE Transactions on Industry Applications
- **Mohammad Rashidi**, A. Bani-Ahmed, A. Nasiri, M. Sabbah "Design and Implementation and Multiport Solid State Transformer" Submitted to IEEE Transactions on Industry Applications.